

GEL DOSIMETRY

**DEVELOPMENT OF A TRANSPARENT AND DEFORMABLE TWO
DIMENSIONAL RADIOCHROMIC GEL DOSIMETER**

by

POURIA ATAELI, B.Eng

A Thesis

Submitted to the School of Graduate Studies

in Partial Fulfillment of the Requirements

for the Degree

Master of Science

McMaster University

© Copyright by POURIA ATAELI, December 2011

Master of Science (2011) McMaster University

(Medical Physics) Hamilton, ON

TITLE: Development of a Transparent and Deformable Two Dimensional Radiochromic Gel Dosimeter

AUTHOR: POURIA ATAEI, B.Eng. (University of Ryerson)

SUPERVISOR: Dr. Kevin Diamond

NUMBER OF PAGES: xvi, 109

Abstract

Radiotherapy is used in many clinics to deliver a sufficient and uniform dose to the cancerous tumours while the dose to normal tissues is minimized. However, there is a possibility of missing the target volume due to patient set up/motion errors, or any fluctuation in treatment delivery. Therefore, accurate dose verification tools are essential to evaluate the delivered dose distribution of the designed treatment plan under realistic treatment conditions.

Current research is focused on developing 3D dose verification tools to record the complex dose distributions for quality assurance purposes and the evaluation of new treatment techniques. New and novel materials and read-out techniques suitable for use in hospitals are desirable. The objective of this research is to fabricate a transparent radiochromic gel dosimeter that may be used as quality assurance tool. Also, the fabricated gel must be analyzed using a simple optical read-out technique.

Gel dosimeters are gels that undergo some chemical changes upon irradiation as a function of absorbed dose. The absorbed dose may be recorded in three dimensions depending on the type of gel dosimeter. Radiochromic gels are dosimeters that change colour upon irradiation. A radiosensitive dye, leucomalachite green (LMG) is dissolved in a matrix material to record the dose distribution in 3D. LMG changes its colour upon irradiation, and has an absorbance band of 629nm.

In this research two different matrix materials were investigated: poly (vinyl alcohol) and gelatin. PVA was studied as the primary agent due to its adjustable mechanical strength

and high transparency. PVA has also been studied to have a low diffusion rate when it was used as the matrix material in Fricke gel dosimeters [41]. Even though PVA had all the desired characteristics, fabricating a PVA based radiochromic dosimeter was not successful. Consequently, gelatin was used as the matrix material to fabricate a gelatin-based radiochromic dosimeter.

Using gelatin, highly transparent radiosensitive gels were successfully fabricated. The absorbencies of the irradiated gels were measured as a function of absorbed dose, using a 1D set up. After, the gels were formed into 5mm thick films and used as two-dimensional dose verification tools. The relationship between absorbance and absorbed dose for 1D measurement was obtained to be $0.00241 \pm 0.00004 \text{ Gy}^{-1}$, and $0.0022 \pm 0.00007 \text{ Gy}^{-1}$ for 2D gels scaled to a thickness of 1 cm.

In all of the experiments the absorbance-dose relationships were similar in slopes, but there was an offset between different batches. The offset was 20% between the different experiments. Moreover, there was less than 5% error associated with the physical set up; the major source of error was due to the production and handling of the mixture, possibly due to the effects of inconsistent heating and UV light exposure.

The 2D gels were used to verify the dose distribution for the purpose of quality assurance. Six different complicated beams were delivered to the gels and their dose distributions were compared to their respective Pinnacle Calculated Planar (PCP) dose maps. The difference was found to be about 35% at worst; however, this error may be reduced by utilizing more sophisticated data processing methods. Nevertheless, the images were quite

similar above 20Gy. Furthermore, the dose distributions recorded by the gels are qualitatively and quantitatively similar to the (PCP) dose map. Although the fabricated gel dosimeters show some promise as future tools for quality assurance purposes, they must go through many more stages of research to be used clinically.

Key words:

Gel Dosimetry, Radiochromic Dosimeter, Radiotherapy, Quality Assurance (QA)
Leucomalachite Green (LMG), Poly(vinyl Alcohol) PVA, Gelatin, Micelle, Two dimensional

Contents

Abstract	iv
Acknowledgment	ix
List of Tables	x
List of Figures	xi
Acronyms	xv
Nomenclature	xvi
1. Introduction	1
1.1 Where does gel dosimetry fit in the clinic?	2
1.2 Radiotherapy	5
1.3 Gel Dosimeters	7
1.3.1 Fricke Gel Dosimeter	8
1.3.2 Polymer Gel Dosimeter:	9
1.3.3 Radiochromic Gel Dosimeter	12
1.4 Thesis proposal	16
2. Radiochromic Gel Dosimetry Methodology	18
2.1 Fabrication	19
2.1.1 PVA-based dosimeters	20
2.1.2 Gelatin-based Dosimeters	22
2.2 Irradiation	25
2.3 Optical Measurements	26
2.3.1 Linear Transmission Apparatus	28
2.3.2 CCD Camera Apparatus	30
2.4 Data Processing and Analysis	32
2.4.1 De-noising Filter	33
2.4.2 Image Registration	36
3. Characterization of Potential Dosimeters	47
3.1 PVA based Dosimeter	47
3.1.1 Selecting a Formulation	48
3.1.2 Dose Response	50

3.1.3	PVA-based Cryogel dosimeter.....	63
3.2	Gelatin-based Dosimeter.....	65
3.2.1	Determination of the formulation.....	66
3.2.2	Dose Response	69
3.3	Discussion	72
4.	2D optical Measurements.....	74
4.1	Dose Response Measurements.....	75
4.2	IMRT field analysis	79
4.3	Discussion	96
5.	Summary	100
5.1	Conclusion	100
5.2	Future Research.....	104
	References.....	106

Acknowledgment

This research would not have been possible without the help of many people. First, I have to thank my supervisor, Dr. Kevin Diamond for his amazing support, encouragement and significant guidance during the course of this research; without his knowledge and assistance this study would not have been successful. I must also record my gratitude to Dr. Orest Ostapiak and Dr. Marcin Wierzbicki for their supervision, advice, and guidance from the very early stage of this research. I would also like to voice my appreciation to Mark Weston for his invaluable assistance and guidance in the lab. Deepest gratitude are also due to people from Electrical and Computer Engineering, Mohammad Reza Dadkhah, Bahram Marami, and Mahdy Nabaee who were abundantly helpful and offered invaluable assistance. I must also voice my appreciation to the radiation therapist team, Richard Hung and Crystal Ho for their assistance. I would also like to express my gratitude to my beloved family for their love and support. My special thanks go to Azadeh Tasbaz for her endless support through this research. Finally, an honourable mention goes to Mohammad Talebi and Siavash Rahimian for teaching me many new things during these years.

List of Tables

Table 1.1	Different monomers used through history of development of polymer gel dosimeter and their MRI dose	10
Table 2.1	Chemicals used in the fabrication of the in-house radiochromic gel dosimeter.....	19
Table 2.2	Concentrations of LMG, CCl ₄ and DMSO leading to highest dose sensitivity.....	20
Table 2.3	Summary of chemical concentrations used in the gelatin based gel dosimeter.....	22
Table 3.1	Different types of errors to be investigated.....	53
Table 3.2	Summary of experiments.....	62
Table 3.3	Optical density summary for different chemical concentration.....	69
Table 3.4	Summary of optical density for 14 experiments.....	70
Table 3.5	Summary of stability data over time.....	72
Table 4.1	Summary of mean absorbance and standard deviation at each dose level for multiple experiments	78
Table 4.2	SNR values for different dose ranges.....	92
Table 4.3	Overall SNR value for measured dose maps.....	92
Table 4.4	Mean ratio of the measured image to the PCP image, the associated error represents the standard deviation	95

List of Figures

Figure 1.1	The steps involved in a gel dosimetry Quality Assurance process.....4
Figure 1.2	Multileaf collimators are set to contour the tumour volume with a margin of 1-2 cm6
Figure 1.3	Creation of a fluence map by combining three radiation fields with different MLC settings.....7
Figure 1.4	Molecular Structure of colourless LMG.....15
Figure 2.1	Steps involved in investigating the in-house radiochromic gel.....19
Figure 2.2	Illustration of MG and LMG within the micelle (a) Pre-irradiation (b) Post-irradiation.....24
Figure 2.3	Irradiation set up for (a) Cuvettes for 1D measurement, (b) 5 mm thick gel for 2D dose distribution.....26
Figure 2.4	Absorbance Vs Wavelength, The optical density is calculated from 619-639nm.....27
Figure 2.5	Picture of in-house linear optical scanner, a white light source is used as the light source, a cage is used to hold the samples and a spectrum analyzer to obtain the intensity of transmitted light.....29
Figure 2.6	The intensity of transmitted light pre and post irradiation. The decrease in intensity at 629 nm corresponds to increase in absorption from LMG.....29
Figure 2.7	Picture of in-house 2D optical scanner, a red light surface in a light tight box CCD with lens on top.....31
Figure 2.8	The absorbance must be zero above visible spectrum. (A)The offset shown is a result of sources of uncertainties (B) it is adjusted back to zero.....32
Figure 2.9	$x(n)$ is the original signal, $c(n)$ is the average of two neighbouring pairs and, $d(n)$ is the average of their differences.34

Figure 2.10	The transfer function for (a) decomposition of the signal (b) reconstructing the signal.....	34
Figure 2.11	Decomposition is repeated three times.....	35
Figure 2.12	Four level wavelet transform for (a) a signal without noise (b) with random noise.....	36
Figure 2.13	The matching points selected on the measured and PCP images.....	39
Figure 2.14	Midpoint discretization of the PCP image.....	41
Figure 2.15	Transforming the midpoint discretization of the PCP image on the measured image.....	42
Figure 2.16	Each transformed point is surrounded by 4 points.....	43
Figure 2.17	The Transformed and non-transformed grid.....	44
Figure 3.1	Different concentrations of LMG and CCl ₄ in DMSO.....	48
Figure 3.2	Absorbance vs Wavelength with different LMG concentrations (a) 7.5 mM (b) 5.5mM (c) 12mM.....	49-50
Figure 3.3	Dose response experiments: the 6 rows represent different sample batches which and the 7 columns corresponds to different amount of radiation	51
Figure 3.4	Absorbance at 629 nm for 4 different test groups.....	52
Figure 3.5	(a) Absorbance with/out the filter, samples were self-referenced (b) absorbance with/out neutral density filter; samples are being referenced to a single reference sample. (c) Absorbance vs Dye concentration combining the data.....	54-55
Figure 3.6	Six set of samples made from two different batches, 3 sets from each batch.....	56
Figure 3.7	Three sets of samples were prepared from each of the two batches (A, B). The optical intensity was measured three times. The error bars represents the uncertainty corresponding to optical intensity measurement. Regression lines are for two different batches of LMG and DMSO mixtures.....	57

Figure 3.8	Dose-response curve when CCl ₄ alone kept as the only variable. Two different batches are prepared from the same LMG and DMSO stock. The error bars are the standard deviation of 9 data points measured at each level.....59
Figure 3.9	Dose response under 3 different conditions: in (a) and (c) everything is kept under same condition; (b) CCl ₄ is the only variable, and (d) LMG and CCl ₄ are both variable.....60-61
Figure 3.10	Dose-response of the six experiments combined. 13 batches, 36 sets and 108 data points. This represents the entire body of data for LMG and CCl ₄ dissolved in DMSO.....62
Figure 3.11	Dose response of gelatin dosimeters with different concentrations of LMG: (a) 0.38 mM;(b) 1 mM; (c) 1.5mM.....67-68
Figure 3.12	Effect of different concentrations of SDS on radiosensitivity.....68
Figure 3.13	Absorbance Vs dose. LMG 037mM, CHCl ₃ 80mM, SDS 50mM, CCl ₃ COOH 5mM, gelatine 5.5% by weight and water 92% by weight.....70
Figure 3.14	Change in the optical density over time at different dose levels. The experiment was repeated two times and each graph represents different experiment. (a) Experiment #1, (b) Experiment #2.....71
Figure 4.1	The Intensity of transmitted (a) Pre-irradiation, and (b) Post-Irradiation at each pixel. The x- and y-axis are pixels and the colour wash is the intensity of transmitted red light.....74-75
Figure 4.2	2D maps of absorbance measured at each pixel(1024x1392) for (a)80Gy, (b)60Gy, and (c)40Gy.....76-77
Figure 4.3	Average absorbance vs. dose for the 2D gels. The error bars are smaller than the plotted points and so are not shown.....78
Figure 4.4	Pinnacle Calculated Planar dose map of Beam#6. The x- and y-axis represent the field size in mm.....79
Figure 4.5	Different stages of signal processing: (a) Measured absorbance normalized to 0.093, (b) Passage through the De-Noising filter; (c) The transformation matrix is applied and resolution adjusted; (d) Pinnacle Calculated Planar dose map normalized to 80Gy.....80-82

Figure 4.6	The selected points on the measured image (Panel a), and the corresponding points on the PCP image (panel b). The points were chosen manually.....82
Figure 4.7	The transformed grid on the measured image.....83
Figure 4.8	Different stages of data processing for six different IMRT fields. (a) Raw absorbance map, the absorbance was computed at each pixel. (b) The images were De-noised through wavelet transform and noise reduction, (c) The measured images were mapped onto the PCP image and down-sampled; (d) PCP image.....84-87
Figure 4.9	Repeated measurements for beam 2,3 and 4. (a) Raw absorbance map, the absorbance was computed at each pixel. (b) The images were De-noised through wavelet transform and noise reduction, (c) The measured images were mapped onto the PCP image and down-sampled; (d) PCP image.....88-89
Figure 4.10	(a) The ratio of the measured to the PCP image at each pixel (Experiment 1) (b) The ratio of the measured to PCP images at each pixel for replicate measurements of beams 2,3 and 4.....94-95

Acronyms

CCD	Charged Coupled Device
CHCl ₃	Chloroform
CCl ₃ COOH	Trichloroacetic acid
CCl ₄	Carbon tetrachloride
DMSO	Dimethyl sulfoxide
EBRT	External beam radiation therapy
IMRT	Intensity modulated radiotherapy
LMG	Leucomalachite green
MLCs	Multileaf collimators
MU	Monitor Units
MRI	Magnetic Resonance Imaging (MRI)
MAGIC	Methacrylic acid, ascorbic acid, gelatin and copper
PCP	Pinnacle Calculated Planar
PVA	Poly(vinyl alcohol)
QA	Quality assurance
SDS	Sodium dodecyl sulphate
SNR	Signal to noise ratio

Nomenclature

$\Delta[\text{Fe}^{3+}]$	Concentration of Ferric ions
$G(\text{Fe}^{3+})$	Chemical yield of Fe^{3+} (ions produced per 100 eV)
$N_A \cdot e$	Number of Joules per electron volt
$\Delta\text{OD}(x)$	Optical density
E	Extinction coefficient in $[\text{M}^{-1}\text{cm}^{-1}]$
C	Concentration of absorbing molecule in $[\text{M}]$
L	Optical path length in $[\text{cm}]$
SNR	Ratio of the expected pixel value with the error
A_T	Pinnacle Calculated Planar Dose value
$ \Delta A $	Error (the absolute difference in normalized absorbance of the measured image to the Normalized value of Pinnacle Calculated Planar dose map)

1. Introduction

The aim of radiotherapy is to deliver a uniform high dose of radiation to a tumour while sparing the surrounding healthy tissues. To reduce the risk of damaging the surrounding healthy tissue, it is of utmost importance to verify the 3D dose distribution prior to the start of treatment. Complementary to recent advancement in radiotherapy delivery such as IMRT, brachytherapy and radiosurgery, many dosimetry techniques are also being investigated to verify these dose distributions. In turn, gel dosimeters have appeared as one of the candidates for this purpose [1]. One of the most important applications of gel dosimeters in radiation therapy quality assurance is the verification of dose distribution. Gel dosimetry is slowly making its way into routine clinical use, although more research is needed in this field. [3]

Gel dosimeters are radiosensitive materials that, upon irradiation, undergo changes in their chemical structure as a function of absorbed radiation dose. These types of dosimeters have advantages over one-dimensional dosimeters such as ion-chambers or two-dimensional dosimeters such as radiosensitive films. The absorbed radiation dose distribution may be recorded in three-dimensions depending on the type of gel dosimeter used. The verification of dose distribution is desirable in situations with complex dose distributions such as stereotactic radio-surgery or intensity modulated radiotherapy (IMRT). Furthermore, gel dosimeters may be modified to be soft-tissue equivalent, and depending on the application, their physical properties may be modified.

In this chapter, first the clinical use of gel dosimetry is discussed. In section 1.2, basics of radiotherapy and IMRT are reviewed. In section 1.3, the advancement of gel dosimeters through history is being reviewed. And lastly in section 1.4 is the thesis proposal.

1.1 Where does gel dosimetry fit in the clinic?

Radiotherapy is used to deliver an adequate and uniform dose to the cancerous tumours in order to obtain tumour control, while minimizing complications by reducing the dose to normal tissues. Over the past several years, this has been achieved by the development of three dimensional radiation therapy techniques such as Intensity Modulated Radiation Therapy (IMRT). Using IMRT, the 3D dose distribution can be conformed the specific target volume; however, due to patient set up errors or any fluctuation in treatment delivery, the possibility of missing the target increases [1]. Consequently, the verification of 3D dose distribution is essential to the effective delivery of radiation therapy. The advancement in modern radiotherapy has therefore shifted the focus of dosimetry from dose determination to verifying the deliverable dose distribution, where dosimeters must be able to measure the dose not only at a point, but rather in a three dimensional space. Therefore, gel dosimeters, which inherently are three-dimensional dosimeters, may have an advantage over the traditional dosimeters such as ion chambers and films in applications of radiotherapy dosimetry. Since the dose distribution may be recorded in 3D, gel dosimeters play a role in validating the commissioning of a treatment planning system. They may also be used as an “end-to-end” tool.

Even though gel dosimeters have the potential for high resolution, tissue equivalent 3D dosimetry, they are not being used clinically due to two problems: 1) The original polymer gels are difficult to prepare in the clinical environment; 2) Access to simple read-out techniques is limited. Therefore, the aims of gel dosimetry research are to develop gels that may be made in clinics easily, and also to develop more convenient read-out techniques. The development of radiochromic gels, along with the development of optical imaging for read-out, have made their routine use more suitable. Even with such advancements, gel dosimeters are not used in everyday clinical practice [3].

A suitable approach to verify that the treatment planning and delivery process is working well is to fabricate a tissue equivalent dosimeter and deliver the planned radiation to it. This approach was examined by Oldham *et al.* [4], where they used radiochromic gels to verify the 3D dose distribution. The advantage of radiochromic gels is the simple read-out techniques that are used. The irradiated volume changes colour, allowing one to measure the change in absorbance via simple transmission measurements or optical CT scanning. Hence, radiochromic gel dosimeters may be an easy to use tool for quality assurance of the radiotherapy process. The steps involved in a potential gel dosimetry quality assurance (QA) process are summarized in figure 1.1.

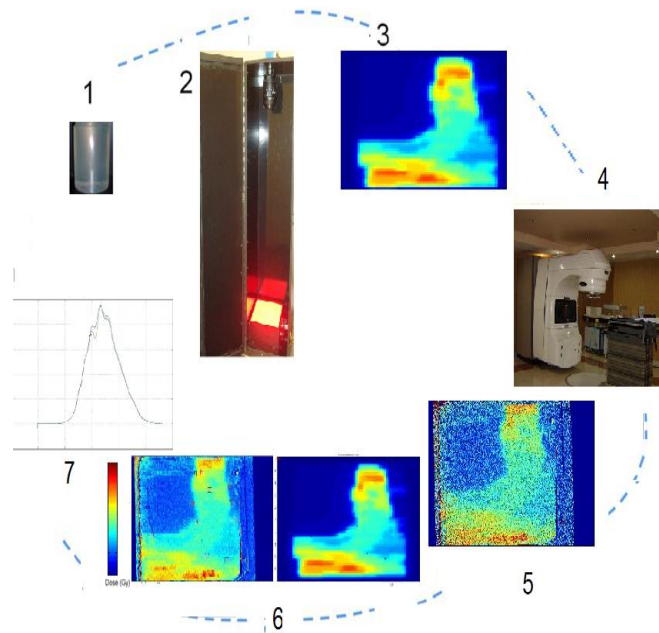


Figure 1.1 The steps involved in a gel dosimetry Quality Assurance process

As shown in figure 1.1, step one is the preparation of the gel dosimeter by the physics team. Step two, the pre-irradiated gel dosimeter is imaged and analyzed. In step three a treatment plan is designed. In step four, therapists set up the linear accelerator, adjust the gel phantom, and deliver the treatment plan. Subsequently in step five the irradiated gel dosimeter is imaged and analyzed again. In steps six and seven the data are registered and evaluated by the physicist.

Quality assurance is related to all procedures that ensure the accuracy of the medical prescription and safe delivery of dose to the target volume. Based on International Organisation for Standardisation (ISO 1995), as well as the British Standards Institutes (BSI): “Quality Assurance (QA) is defined as all those planned and systematic actions

necessary to provide adequate confidence that a structure, system or component will perform satisfactorily in service, or will satisfy given requirements for quality.”

Thus, the aim of quality assurance is to produce and maintain consistent and continuing quality in treatment. Implementing a quality assurance programme should minimize errors and accidents.

1.2 Radiotherapy

Historically there are three main types of radiation therapy differing in the position of the radiation source.

- External beam radiation therapy
- Brachytherapy
- Systemic radio-isotope therapy

In external beam radiation therapy (EBRT), the radiation is transmitted through the air to the patient; in brachytherapy the radioactive source is sealed and placed precisely in or near the treatment volume; and in systemic radioisotope therapy the radio-isotopes are given by infusion or ingestion.

External beam radiation therapy has been revolutionized since the introduction of computed tomography imaging into treatment planning. Over the past twenty years there has been an interest in advancement of radiotherapy; moreover IMRT is a

significant development in conformal radiotherapy. IMRT was first introduced in 1982 by Brahme *et al.* and its clinical use is now wide-spread [4, 5].

Conformal radiation therapy refers to a type of radiotherapy where the radiation beams are shaped to match the shape of the tumour. Using the CT image of the tumour, physicians contour the tumour volume and add a margin of 1 – 2 cm to account for subclinical disease and setup errors. IMRT is an extension of conformal radiation therapy, which allows for modulating of the intensity of the radiation beams. This is typically achieved by using multileaf collimators (MLCs) that provide a spatial resolution of 1 cm or better (Figure 1.2).

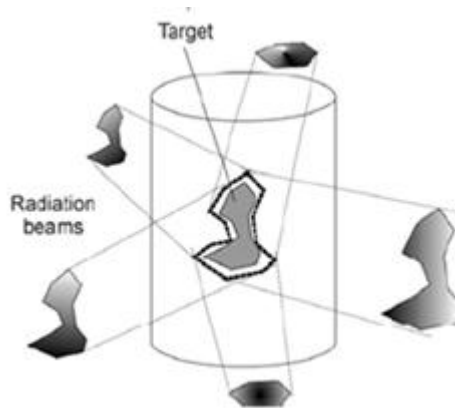


Figure 1.2 Multileaf collimators are set to expose the tumour volume with a margin of 1-2 cm

The dose distribution may be improved further by modulating the fluence of each beam. Different fluence patterns may be obtained by utilizing various layers of materials in the beam to modify the transmission in different part of the beam. Using MLCs allows the fluence to be varied by shielding different parts of the beam at different times; this results

in a fluence intensity map such as shown in figure 1.3 [3]. These fluence maps, when delivered, result in a highly conformal dose distribution.

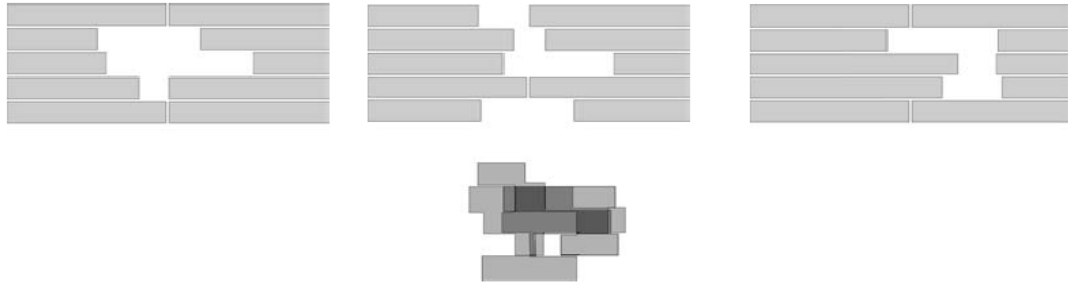


Figure 1.3 Creation of a fluence map by combining three radiation fields with different MLC settings [3]

These highly conformal dose distributions, produced with complex radiation fields, should undergo regular QA involving a 3D measurement technique. Consequently, it is desirable to develop a verification tool to confirm that the delivered dose matches up exactly with the planned treatment in 3D. Such a clinical dosimeter should be tissue equivalent; have high sensitivity, accuracy, and spatial resolution; and be easy to use. A good candidate is the radiochromic gel dosimeter, which is the main focus of this research.

1.3 Gel Dosimeters

The use of radiosensitive gel dosimeters was first studied by Day and Stein in 1950. They observed the absorbed dose by experimenting on gels that contained dyes that changed colour upon irradiation [6]. In their study, methylene blue and phenol-indo-2:6-

dichlorophenol were used as the chemical dyes that bleached upon irradiation. Moreover, gelatin or agar was used as the gelling agent in which the dye was dissolved. It was further investigated that the change in colour was due to the change in chemical structure of the dye, after being exposed to radiation. “Almost all the change finally observed in the dye was due indirectly to energy absorbed in the rest of the aqueous system.” [6]. A Few years after, in 1957, Andrew *et al.* used a chloral hydrate-agar gel to measure the depth-dose and investigate the nature of colour change[7]. The dose measurement was obtained through determining the HCl formed using electrical conductivity and pH analysis. It was also demonstrated that the chemical reaction that resulted in colour change was undoubtedly indirect, through free radicals produced from water during irradiation [7]. In this section three types of gel dosimeters, Fricke, Polymer and Radiochromic gel dosimeters are introduced and discussed in detail.

1.3.1 Fricke Gel Dosimeter

Most of radiation sensitive gels currently in use are a result of the development of Fricke gel dosimetry. In 1984 Gore *et al.* [8] proposed that adding a gel matrix to the traditional Fricke dosimeter and reading the system with Magnetic Resonance Imaging (MRI) would allow it to be used for three-dimensional radiation dosimetry. The gel matrix was used to fix the geometric information opening the door for Fricke gel dosimetry.

The absorbed dose is recorded as a chemical change, as Ferrous (Fe^{2+}) ions get converted to Ferric (Fe^{3+}). The absorbed dose distribution is read-out by measuring the spin-lattice and spin-spin relaxation rates (R1 and R2) and compared to a calibration. Fricke solution is an acidic oxygenated aqueous solution of ferrous ions where, upon irradiation, water

decomposes and resultant hydrogen atoms react with oxygen to produce highly reactive radicals [9]:

Different reactions then result in conversion of ferrous ions to ferric ions; this number of ferric ions is dependent on the delivered dose of radiation. Moreover, it is dependent on the energy that is absorbed by the Fricke solution. The concentration of Ferric ions is obtained by the following equation:

$$\Delta[Fe^{3+}] = \frac{D \times G \times (Fe^{3+}) \times 10\rho}{N_A \times e} \quad (1.1)$$

where D is the dose, G is the chemical yield of Fe^{3+} (ions produced per 100 eV), ρ is the density, and e represents number of Joules per electron volt.

Using gelatin or agarose as a matrix to hold the ferric solution led gel dosimeters to be the first real 3-D QA tool, with tissue equivalent properties over a wide range of photon energies. Later studies showed that Fricke gel dosimeters were subject to ion diffusion, which result in a loss of spatial fidelity. Even though different gelling matrices were investigated, diffusion continued to be a significant problem in the advancement of the gel dosimetry [10].

1.3.2 Polymer Gel Dosimeter:

Polymer gel dosimeters are produced from radiation sensitive chemicals that undergo polymerization upon irradiation. In order to preserve the 3D spatial information of the absorbed dose and hold the produced polymer structure in place, monomers are dissolved in a gelling matrix. Such monomers crosslink to form polymers upon irradiation. Water

molecules are dissociated into highly reactive species when irradiated: the radiolytic products of water, mostly e^-_{aq} , react with the monomers and initiate the cross-linking. Therefore, the spatial information of the absorbed dose is recorded through polymerization of the monomers in the gelling matrix.

Through the history of polymer gel dosimeters different chemical compositions, gelling agents, and radiation sensitive monomers have been investigated. The summary of different monomers used is given in Table 1.1 [11].

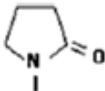
Monomer	Functional group
AAm/Bis	$\begin{array}{c} \text{O} \\ \\ -\text{C}-\text{NH}_2 \end{array}$
Acrylic acid (AAc)	$\begin{array}{c} \text{O} \\ \\ -\text{C}-\text{OH} \end{array}$
Methacrylic acid (Mac)	$\begin{array}{c} \text{O} \\ \\ -\text{C}-\text{OH} \\ \\ \text{CH}_3 \end{array}$
1-Vinyl-2-pyrrolidone (VP)	
2-Hydroxyethyl-acrylate (HEA)	$\begin{array}{c} \text{O} \\ \\ -\text{C}-\text{OCH}_2\text{CH}_2\text{OH} \end{array}$
2-Hydroxyethyl-methacrylate (HEMA)	$\begin{array}{c} \text{O} \\ \\ -\text{C}-\text{OCH}_2\text{CH}_2\text{OH} \\ \\ \text{CH}_3 \end{array}$
<i>N</i> -Iso-propylacrylamide (NIPAM)/Bis (Bis)	$\begin{array}{c} \text{O} \\ \\ -\text{C}-\text{NH}-\text{HC}-\text{CH}_3 \\ \\ \text{CH}_3 \end{array}$

Table 1.1 Different monomers used through history of development of polymer gel dosimeter and their MRI dose sensitivity [11]

Polymer gel dosimeters were first introduced in 1954 by Alexander *et al.* [12], where the effect of radiation on polymethylmethacrylate was investigated. Later in 1958 Hoecker and Watkins [13] discussed that radiation induces polymerization in liquids. Subsequently in 1961 Boni *et al.* used polyacrylamide as a gamma dosimeter [14]. Much later in 1992, Kennan *et al.*[15] performed a study on an irradiated aqueous solution of N,N'-methylene-bis-acrylamide and agarose. In the same year Maryanski *et al.* [16] proposed a new gel formulation based on polymerization of acrylamide (AAM) and Bis monomers in an aqueous agarose matrix. This formulation was later given the acronym of BANANA due to use of chemical components (Bis, AAM, nitrous oxide and agarose). Later Maryanski *et al.* changed the formulation by replacing Agarose with gelatin, which then given the acronym BANG (Bis, AAM, Nitrogen and Gelatin) [17].

Even though the polymer-type gel dosimeters do not have the diffusion problem associated with the Fricke gels, oxygen inhibits the polymerization reactions. Hence, they must be manufactured in an oxygen-free environment or have the oxygen removed using scavengers. This is certainly a significant limitation in introducing these types of dosimeters into the clinic. De Deene *et al.* investigated the accuracy of the polymer gel dosimeter systems for verification of conformal radiotherapy treatments [18], and showed that oxygen inhibition can have a significant effect on the accuracy.

In 2001, Fong *et al.* reported a new formulation of a polymer gel dosimeter known as MAGIC (methacrylic acid, ascorbic acid, gelatin and copper). These gels are considered to be a new class of “normoxic” polymer gels, where oxygen is removed using

scavengers [19]. This advancement has the advantage of producing MAGIC gel dosimeters on the benchtop in any laboratory.

The absorbed doses are readout utilizing different techniques, most commonly MRI and optical CT. In research by Maryanski *et al.*, the relaxation rate R1 was found to change upon polymerization [20]. An alternative read-out technique is optical computed tomography, optical-CT, which was first introduced by Gore *et al.* in 1996 [21]. Transparent, unirradiated gels become increasingly opaque due to increased density of radiation-induced polymerization.

1.3.3 Radiochromic Gel Dosimeter

Both Fricke and Polymer gels have their advantages and disadvantages. Even though Fricke gels have high reproducibility and can be prepared easily, they suffer from ion diffusion. On the other hand, polymer gels are relatively stable and have high sensitivity to radiation, but they are hard to prepare as they must be fabricated in an oxygen free environment [22]. Therefore, a gel dosimeter that does not suffer diffusion problems, could be prepared easily in the laboratory, and also could be analyzed with a simple read-out technique is of great interest.

Advanced technology in radiotherapy requires more accurate, less expensive, and faster tools to verify the designed treatment plans. As discussed earlier, one of the best candidates for verifying the 3D dose distributions are gel dosimeters. However, one of the major obstacles with the mentioned gel dosimeters involves their read-out techniques. MRI scanners are one of the most widely used pieces of equipment for the purpose of

reading the 3D dose distribution in the gel phantoms. However, MRI access is challenging at many clinical sites. Therefore alternative scanning techniques, which are more accessible and easier to use, is a focus of current research. Recently there have been many studies conducted to develop optical CT scanning. Optical scanners are more accessible; therefore the introduction of these scanners stimulated the development of 3D radiochromic dosimeters. These dosimeters change colour where exposed to radiation, and remain transparent elsewhere. Transparent dosimeters suffer less from light scattering as compared to the polymer gels.

The molecular structure of the leuco dyes used in many radiochromic dosimeters change upon irradiation. This change shifts the optical absorption spectrum of the dye from the near ultraviolet into the visible range. The leuco dye or other starting structure is colourless, yet, upon irradiation and structural change it becomes coloured. The colour change is the result of structural changes that may be caused by: 1) direct absorption of penetrating radiation; 2) a reduction of pH level by releasing H⁺ ions caused by the absorption of the radiation either by the medium or by an added activator; 3) the action of free radicals generated by the absorption of the radiation either by the medium or by an added free radical initiator [23]. Therefore, leuco dyes may be photochromic dyes, radiochromic dyes, pH indicating dyes, and radiographic dyes.

The first radiochromic dosimeter was studied by Day and Stein in 1950. They studied methylene blue, a coloured dye that bleaches upon irradiation. They also observed that certain dyes change colour upon irradiation [6]. In 1957 Andrew *et al.*[7] used a chloralhydrate-agar gel to examine the nature of the colour change. They observed that the dose

may be determined by measuring the amount of HCl formed. Further investigations showed that the chemical reaction responsible for the change was through free radicals produced from water.

In 1958 Armstrong *et al.* [24] used leuco Triarylmethane as a colourless dye that became coloured after irradiation. They also employed chlorinated halocarbons such as chloroform, carbon tetrachloride, and trichloroethylene, along with an acid-base indicator such as bromocresol purple or phenol red. It was shown that, upon irradiation, water-saturated chlorinated hydrocarbons released hydrochloric acid, resulting in change in pH of the system. Even though these systems could detect doses as low as 50 – 600 cGy there were some disadvantages involved with chloroform systems [23]. Due to the chain reaction nature of these systems when initiated by radiation, the acid yield was dose-rate and energy dependent. These systems could be improved by using an appropriate stabilizer, but this resulted in a decrease in the sensitivity of the system. The sensitivity decrease led them to investigate a chemical dosimeter that depends on the oxidation of a dye by radiolysis products of water. After water molecules are exposed to radiation, highly reactive radicals are formed. A suitable base chemical, susceptible to oxidation by free radicals to a dye form, was required. Leuco dyes met these criteria.

In 2000 Bero *et al.* suggested a modified version of the Fricke gel system[23]. This radiochromic Fricke gel dosimeter was a modification of an earlier radiochromic system developed by Gupta *et al.* [25]. They investigated a new formulation described as FXG (Ferrous sulphate Xylenol Orange) in which gelatin gels are loaded with a modified Fricke solution that has pale orange colour; after irradiation the colour changes to purple.

A new class of radiochromic dosimeter was introduced in 2003: an optically clear polyurethane matrix formulated with a halogenated hydrocarbon free radical initiator and Leuco dye, called PRESAGE [26,27,28]. The advantage of PRESAGE is its transparent matrix allowing much simpler read-out to analyze the 3D dose distribution. The PRESAGE dosimeter was developed in parallel with an optical CT scanner and the two are sold together as a system.

PRESAGE is a polyurethane based radiochromic dosimeter loaded with Leucomalachite green (LMG) dye and halogenated hydrocarbon free radical initiator. Upon irradiation, the halogenated hydrocarbons dissociate to highly reactive free radicals. These free radicals react with the leuco dye and oxidize it to its dye form. The concentration of the dye is dose dependent and can be measured using a simple light transmission measurement. Since the shift in the absorption of LMG is due to oxidation of the leuco dye, the dosimeter must be prepared carefully.

Figure 1.4 represents the original molecular structure of LMG. The C-H bond is broken upon irradiation, resulting in a change in the molecular structure of the colourless LMG leuco dye.

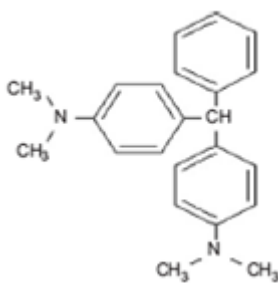


Figure1.4 Molecular Structure of Colourless LMG [31]

1.4 Thesis proposal

Advanced radiotherapy techniques conform high doses to tumours while minimizing the dose to normal tissues. Although the recent advancement in three dimensional conformal radiation therapy techniques has led to improved tumour control, there is still possibility of missing the target volume [3]. Hence, accurate quality assurance tools are essential to verify the three dimensional dose distributions of the complex treatment plans.

Gel dosimeters are gels that are sensitive to radiation; moreover, they undergo some measurable chemical changes as a function of absorbed dose. The absorbed dose may be recorded in three dimensions depending on the type of gel dosimeter.

Current research is focused on developing 3D dose verification tools to record the complex dose distributions for quality assurance purposes and the evaluation of new treatment techniques. New and novel materials and read-out techniques suitable for use in clinics are desirable. The objective of this research is to fabricate a transparent and deformable radiochromic gel dosimeter that may be used as quality assurance tool; moreover, fabricating an inexpensive gel dosimeter in a clinical environment that may be analyzed using a simple optical read-out technique is of great interest. In this research two different gelling agents were investigated. First, poly(vinyl-alcohol) (PVA) was investigated followed by gelatin. The advantage of PVA is its ability to mimic the mechanical properties of tissues. On the other hand, gelatin is a proven matrix material that will also take the shape of the container it is set in. However, its mechanical properties are inferior to PVA. Unlike PRESAGE, where polyurethane is used as the

matrix material, softer matrix materials were investigated in this research. PVA is a matrix material with adjustable mechanical properties; this leads to fabricating dosimeters that may be shaped into any desired organs or tissues, while their mechanical properties are also mimicked. Dosimeters that mimic human organs are useful research tools to investigate the dose distribution accumulated in those organs over a large number of treatments and delivery conditions (*e.g.* intrafraction organ motion and deformation).

After choosing gelatin as the desired gelling matrix, the research was performed in two stages. First the dose-response of the gels was characterized. The absorbance of the irradiated gels was measured as a function of absorbed dose, using a 1D set up. Later, 5mm thick 2D gels were fabricated and used as two-dimensional dose verification tools. In chapter two of this thesis, the methods with which the gels were fabricated, read, and analyzed are described in detail. In chapter three, the results for the 1D measurements are shown and discussed. In chapter four, the results for the 2D gel dosimeter used as a quality assurance tool are illustrated and discussed. Chapter 5 summarizes the research and suggests possible future directions.

2. Radiochromic Gel Dosimetry Methodology

The radiochromic gels studied in this research change colour upon irradiation due to the oxidation of a leuco dye by halogen radicals. In PRESAGE, a commercially available product, the halogen free radical initiator and the leuco dye are dissolved in a polyurethane based matrix [27]. In research by Jordan *et al.* [29] and a recent paper by Vandecasteele *et al.* [30] the leuco dye and the free radical initiators are dissolved in gelatin gel.

This research was divided in two phases. The objective of phase one was to investigate the effect of radiation on a leuco dye and initiator suspended in two different gelling matrices, PVA and gelatin, and obtain the chemical concentrations that led to the desired level of radiosensitivity. The gels were formed in cuvettes to facilitate 1D optical measurements to characterize the samples over a wide range of dose levels. The objective of phase two was to fabricate two-dimensional radiochromic gel dosimeters to be used as quality assurance tools, and verify the 2D dose distribution for IMRT fields. In phase two, the gels were formed in 5 mm thick aluminum moulds

Analyzing the radiochromic gel dosimeters involves four steps, as shown in figure 2.1. First, the gels are fabricated; second, the gels are irradiated under well controlled conditions; third, after the colour change, the gels are scanned utilizing an appropriate read-out technique; finally, the acquired data are analyzed. In this chapter the fabrication

method is discussed first, then the radiation technique is reviewed, and in the last section the readout technique and data processing methods are discussed in detail.

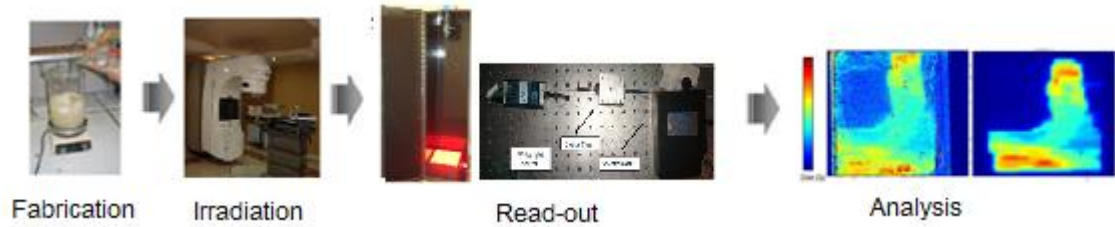


Figure 2.1 Steps involved in investigating the in-house radiochromic gel

2.1 Fabrication

Two different matrix materials were investigated; first, transparent poly(vinyl alcohol) (PVA) (Sigma-Aldrich, St. Louis, USA) and then gelatin (Sigma-Aldrich, St. Louis, USA). The effects of changing carbon tetrachloride (CCl₄) and chloroform (CHCl₃) concentrations, free radical initiators that induce oxidation of the colourless dye upon irradiation, were also studied. Table 2.1 shows the chemicals that were used to fabricate the radiochromic gel dosimeters.

	Solvent	Radiosensitive dye	Free-radical initiator	Surfactant	Others
PVA Based	DMSO + Water	LMG	CCl ₄	None	
Gelatin Based	Water	LMG	CCl ₄ and CHCl ₃	SDS	CCl ₃ COOH

Table 2.1. Chemicals used in the fabrication of the in-house radiochromic gel dosimeter. DMSO (Dimethyl sulfoxide), SDS (Sodium dodecyl sulphate)

2.1.1 PVA-based dosimeters

As shown in Table 2.1 the PVA-based dosimeters were fabricated using three main components: the matrix complex (PVA, DMSO and water), radiosensitive dye (LMG), and free radical initiator (CCl₄).

In order to use a simple optical read-out technique the gels must be transparent. Transparency reduces any error caused by photon scattering in the dosimeter.

Fabrication of transparent PVA based dosimeters was performed in two steps. First, PVA was dissolved in DMSO (Sigma-Aldrich, St. Louis, USA) and water; LMG (Sigma-Aldrich, St. Louis, USA) and CCl₄ (Sigma-Aldrich, St. Louis, USA) were added as the mixture cooled. Second, the mixture was poured into moulds and put through freeze-thaw cycles. Cooling the PVA mixture below -20° C causes the molecules of PVA to crystallize. The mechanical properties are adjustable by varying the number of freeze-thaw cycles [32]. In order to obtain the highest dose sensitivity of the gel dosimeter, different chemical concentrations of LMG, CCl₄, and DMSO were studied. Table 2.2 shows the concentration of LMG, CCl₄ and DMSO that resulted in the highest radiosensitivity of the dosimeter before being dissolved in the PVA matrix.

	Molar concentration (M)	% (w/w)
LMG	0.12	0.35
CCl ₄	2.82	34.6
DMSO	10	65.05

Table 2.2 Concentrations of LMG, CCl₄ and DMSO leading to highest dose sensitivity obtained by trial and error. %(w/w) refers to percentage weight of the chemical to the overall weigh of compound. DMSO (Dimethyl sulfoxide).

The desired stiffness of PVA was obtained by mixing 10% PVA by weight with water and DMSO, keeping the liquid ratio at 20/80 by weight, and stirring the mixture at 100 - 120° C for 90 - 120 minutes under normal atmospheric pressure. After lowering the temperature to 50°C the mixture was left for 20 minutes until all the bubbles came to the surface, where they may be scraped off easily. After removing the bubbles the mixture was cast on a metal plate and kept in a freezer for 12 hours at -80°C. After the PVA underwent crystallization it was left at room temperature for 12 hours. 2 mm thick transparent PVA cryogels were prepared following the above procedure, using a single freeze-thaw cycle; however, the mechanical strength of PVA cryogel sheets could be enhanced by increasing the number of freeze/thaw cycles. [33]

Different water/DMSO ratio led to a change in light transmittance; the maximum light transmittance was achieved by keeping the ratio at 20/80 by weight. The transparent gel has very small regular pores with the size of 1 µm, which are distributed homogeneously and densely. On the other hand the translucent gel has many irregular pores with size of 3 µm.

There were some complications when adding LMG to the PVA mixture: LMG is sensitive to heat; it will change colour when the temperature is too high. If it is added at a lower temperature, the PVA mixture thickens, making it difficult to dissolve LMG homogeneously. Also, the boiling point of CCl₄ is 76.7°C and it must be added to the matrix material at a lower temperature. Once PVA hydrogel cools to 50°C, a solution containing the LMG and CCl₄ dissolved in DMSO was added. The hydrogel was stirred

for an additional 30 minutes, after which it was poured into cuvettes or moulds for freeze-thaw cycling.

2.1.2 Gelatin-based Dosimeters

As shown in Table 2.1 the gelatin-based dosimeters were fabricated using five main components: the matrix complex (gelatin and water), radiosensitive dye (LMG), free radical initiator (CCl₄ or CHCl₃) (Sigma-Aldrich, St. Louis, USA), trichloroacetic acid (CCl₃COOH) (Sigma-Aldrich, St. Louis, USA), and surfactant Sodium dodecyl sulphate (SDS) (Sigma-Aldrich, St. Louis, USA).

These are the same components for a gelatin based matrix suggested by Vandecasteele *et al.* in 2010. The formulation is similar to the PVA dosimeter, except gelatin is substituted for the PVA and DMSO. Using gelatin as the matrix was first purposed by Jordan *et al.*[29] However, the composition used in this research is identical to Vandecasteele. The difference between Vandecasteele’s and Jordan’s formulation is the choice of surfactant (Sodium dodecyl sulphate *versus* Triton x-100).

Different concentrations of CHCl₃, CCl₃COOH and LMG were studied; however the highest radiosensitivity was achieved using the values given in table 2.3.

	Molar Concentration (mM)	% (w/W)
LMG	0.38	0.01
CHCl ₃	80	1.21
CCl ₃ COOH	5	0.06
SDS	50	1.34
Gelatin		5.55
Water		91.83

Table 2.3 Summary of chemical concentrations used in the gelatin based gel dosimeter.SDS (Sodium dodecyl sulphate)

The free radical initiators used with gelatin were halogenated carbon atoms that are divided into two subgroups: acidic halocarbon CCl_3COOH , and neutral halocarbons CHCl_3 and CCl_4 . These free radical initiators improve the effect of radiation sensitivity by forming highly reactive species such as $\text{OH}\cdot$, $\text{H}_2\text{O}_2\cdot$ and $\text{Cl}\cdot$, which oxidize LMG to its chromatic form.

The surfactant, SDS, was used since it is believed to bind very strongly with gelatin below a certain pH threshold, where the gelatin molecules are positively charged [33]. Binding with gelatin leads to less diffusion of micelles in the gel [30]. Micelles are aggregates of surfactant molecules dispersed in a liquid and are formed when the concentration of surfactant exceeds a certain threshold [34]. Water insoluble molecules are encapsulated within the micelle core. In the presence of a surfactant the mutual interaction between dye and surfactant also increases. This leads to the appearance of a stronger absorption band [33]. Bielska *et al.* suggested that a positively charged dye molecule will interact with surfactant molecules like SDS to limit the diffusion of dye molecules outside the micelle [35], as shown in figure 2.2. The radiation induced MG+ dye, the chromatic structure of LMG, is also more soluble in SDS micelles than in the surrounding water, leading to less diffusion of the dye and a more stable post irradiation dose distribution. The greater amount of bonds with the surfactant, the stronger an absorption band can be produced.

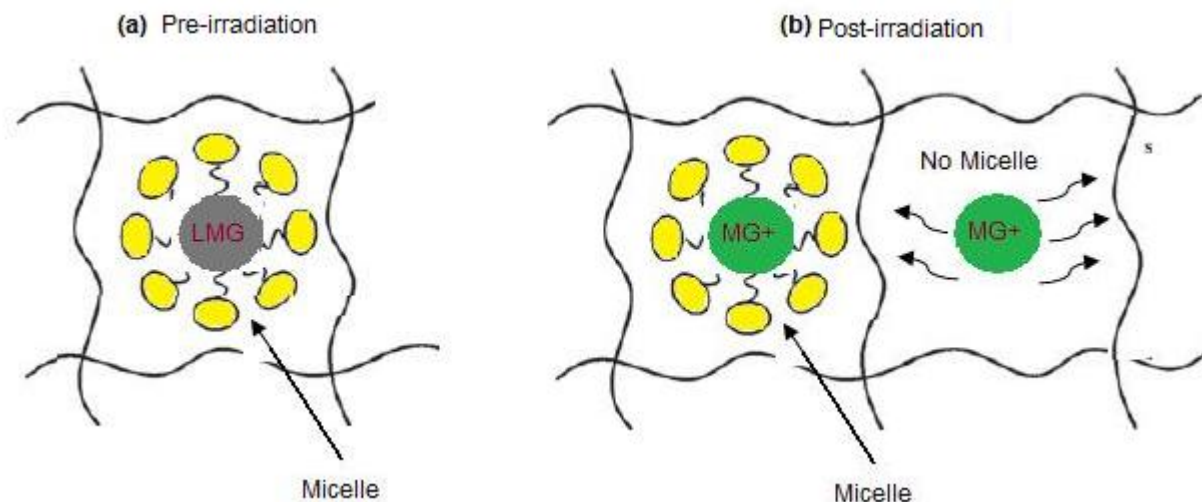


Figure 2.2 Illustration of MG and LMG within the micelle (a) Pre-irradiation (b) Post-irradiation

For consistency, the gelatin formulation was fabricated in three parallel steps. In each step a different mixture was prepared and later they were all mixed together. Mix_A was prepared by heating up 37% (weight of water/total weight (w/W)) water by total weight to 75°C. Gelatin, which accounts for 5.55% of total weight of the compound, was slowly added to water. The mixture was stirred for 10 minutes and then the temperature was slowly raised to 90°C. After stirring the mixture for 30 minutes the temperature was slowly reduced back to 75°C and stirred for another 20 minutes. Mix_B was prepared at the same time. 0.38 mM LMG (0.01% w/W) was dissolved into 80 mM CHCl₃ (1.21% w/W). Since CHCl₃_LMG is sensitive to light, the container was fully covered with aluminum foil. Meanwhile, 50mM SDS (1.34% w/W) and 5mM CCl₃COOH (0.06% w/W) was dissolved in 54.83% (w/W) water and stirred for 10 minutes at room temperature (Mix_C). While reducing the temperature of Mix_A to 40°C, Mix_B and

Mix_C were combined and stirred for 20 minutes. Later, Mix_B + Mix_C was added to Mix_A at 40°C and stirred until the mixture cooled to room temperature.

At this point, the completed gel was poured into plastic cuvettes for 1D measurements or in 5 mm thick aluminum moulds for 2D analysis. In both cases, either cuvettes or metal plates were kept in a refrigerator at 4° C for 6 hours. The metal plates were made in-house and have interior dimensions of 15 X 15 cm² with 5 mm thickness. Since the gelatin tended to stick to the metal plates, a thin transparent film was attached to the inner surfaces of the metal plates; this would also reduce any distortions caused by surface scratches on the metal plate. The transparent films were changed every time the gels were made.

2.2 Irradiation

Radiation was produced using a Varian 2100iX linac delivering 6MV photons at 400 monitor units per minute. Radiation was delivered to the cuvettes in phase one using a 20 x 20 cm² open field. The cuvettes were placed in a water bath to try to achieve electronic equilibrium throughout. The water bath was set up so that the middle height of the cuvettes was located at isocentre height (SSD= 97 cm, d =3 cm shown in figure 2.3 (a)).

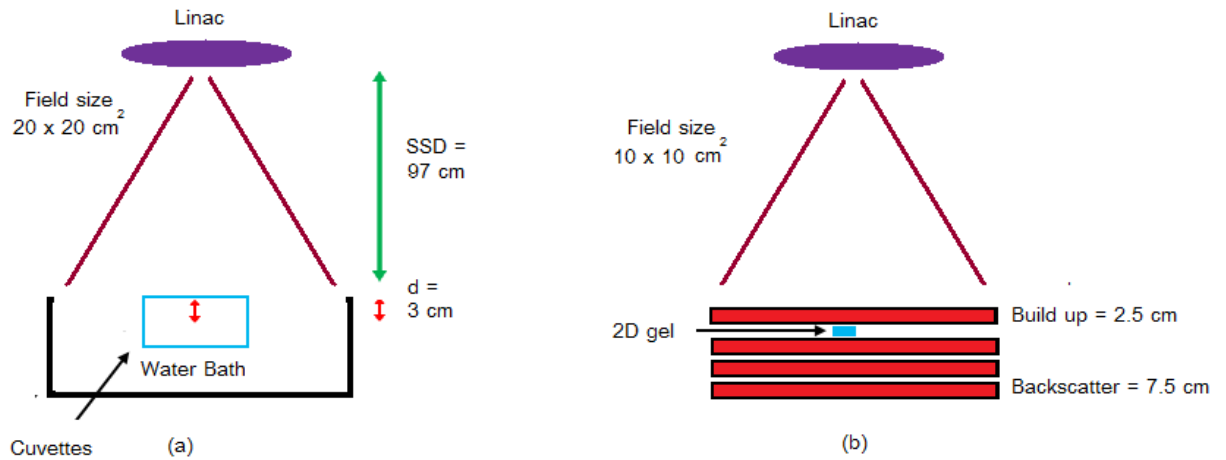


Figure 2.3 Irradiation set up for (a) Cuvettes for 1D measurement, (b) 5 mm thick gels for 2D dose distribution.

The second phase was divided in two different stages. In stage one, the 2D films were characterized using 10×10 open fields; in stage two, six different IMRT treatment beams were used to deliver radiation. 5cm of polystyrene was used for build-up and backscatter for characterization. Even though it is not 100% accurate (polystyrene has a slightly higher electron density than water), it was approximated that each Monitor Unit (MU) corresponded to 1 cGy. In the second stage of phase two, 2.5cm of polystyrene was used as build up for the IMRT fields, and 7.5 cm used for backscatter (figure 2.3 panel (b)). The measured dose distributions for the IMRT fields were compared to the dose calculated by a treatment planning system (Pinnacle 8.0m).

2.3 Optical Measurements

The irradiated leuco dye turns a green colour with an absorption peak at 629nm. Since only the irradiated samples absorb at 629nm, the attenuation profiles of unirradiated and

irradiated samples were analyzed at that specific wavelength. The change in optical density of samples post irradiation directly correlates with the absorbed dose. However, in order to have more accurate results, the change in optical density was calculated over the range of 619 – 639 nm, where the intensity drops to 90% of its peak value (figure 2.4). Hence, using Beer-Lambert law:

$$\Delta OD(x) = -\log_{10} \left(\frac{Intensity_{Irradiated}(\lambda=619-639nm)}{Intensity_{un-Irradiated}(\lambda=619-639nm)} \right) = \epsilon c L \quad (2.1)$$

the optical density $\Delta OD(x)$ over the range of 619-639nm was obtained. ϵ is the extinction coefficient in $[M^{-1}cm^{-1}]$, c is the concentration of absorbing molecule in $[M]$ and L is the optical path length in $[cm]$. The change in optical density obtained from the above equation is only valid in the absence of light scattering and reflections [36]. To translate the change in optical density to the absorbed dose, a calibration curve must also be computed. The intensity in wavelength band of 619 – 639 nm is computed by averaging it over the bandwidth.

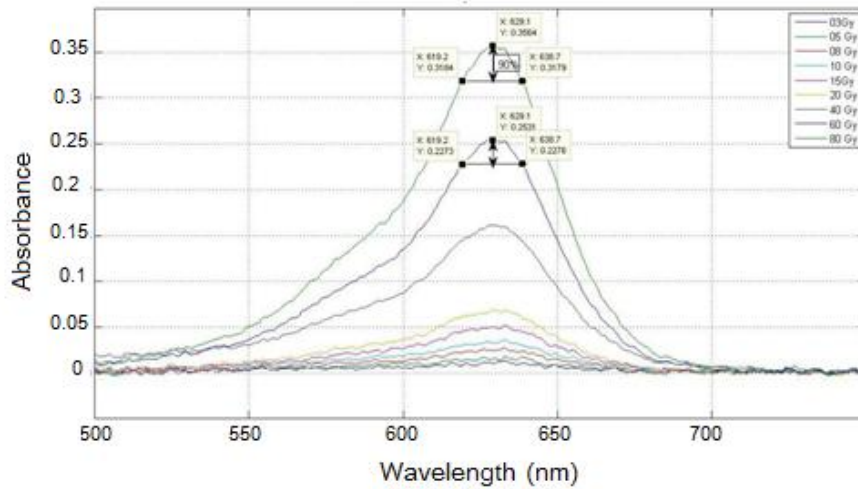


Figure 2.4 Absorbance Vs Wavelength, The optical density is calculated from 619-639nm

As mentioned earlier, this research was conducted in two phases: In phase one the radiochromic gel material was characterized; in phase two, the two dimensional radiochromic gels were studied as possible quality assurance tools. Therefore, different read-out techniques were needed for each of the phases. In phase one, a simple 1D transmission measurement was used. In phase two, a CCD camera was mounted above a red lamp so that the entire 2D gel could be imaged at once. Both techniques measured the change in optical density. Hence, equation 2.1 was used for both techniques.

2.3.1 Linear Transmission Apparatus

All cuvettes were taken out of the refrigerator 1 hour before pre-irradiation read-out to reach room temperature. The cuvettes were placed in a cuvette holder and analyzed before and after irradiation using a transmission apparatus. The measurement set up comprised two optical fibres, a white light source(Ocean Optics) , optical cage, and a spectrometer as shown in figure 2.5. An Ocean Optics LS-1 white light source was coupled to the optical cage using one of the optical fibres. A spectrometer (Ocean Optics HR4000) was coupled to the opposite side of the optical cage to detect the intensity of the light transmitted through the samples; moreover, the integration time of the spectrometer was set to 4000 μ s to maximize the dynamic range of the signal. A neutral density filter was used to avoid saturation of the spectrometer. The spectrometer was connected to a computer and controlled using the OOIBASE software package.

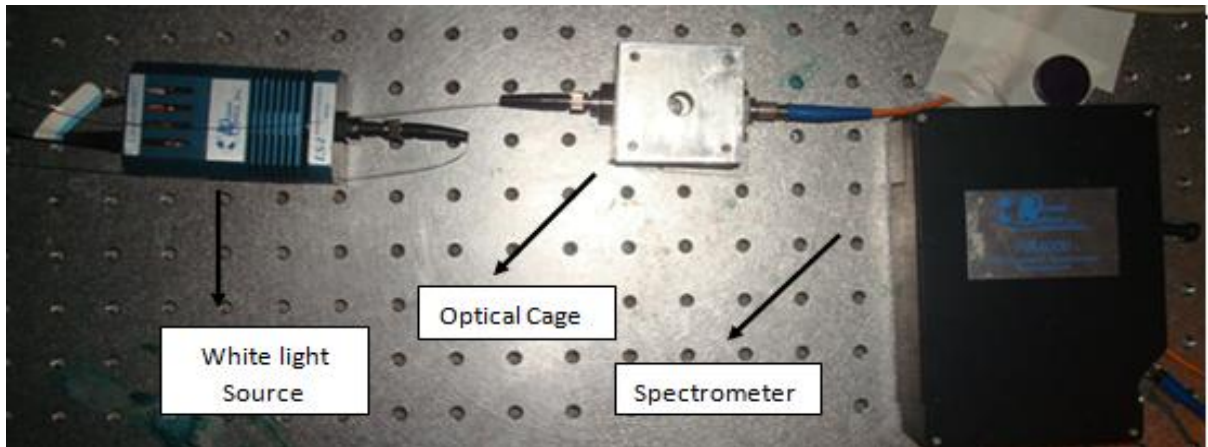


Figure 2.5 Picture of in-house linear optical scanner, a white light source is used as the light source, a cage is used to hold the samples and a spectrum analyzer to obtain the intensity of transmitted light.

The measured spectra were later exported and analyzed in Matlab. Figure 2.6 shows the intensity of transmitted light through the gelatin based radiochromic dosimeters before and after irradiation.

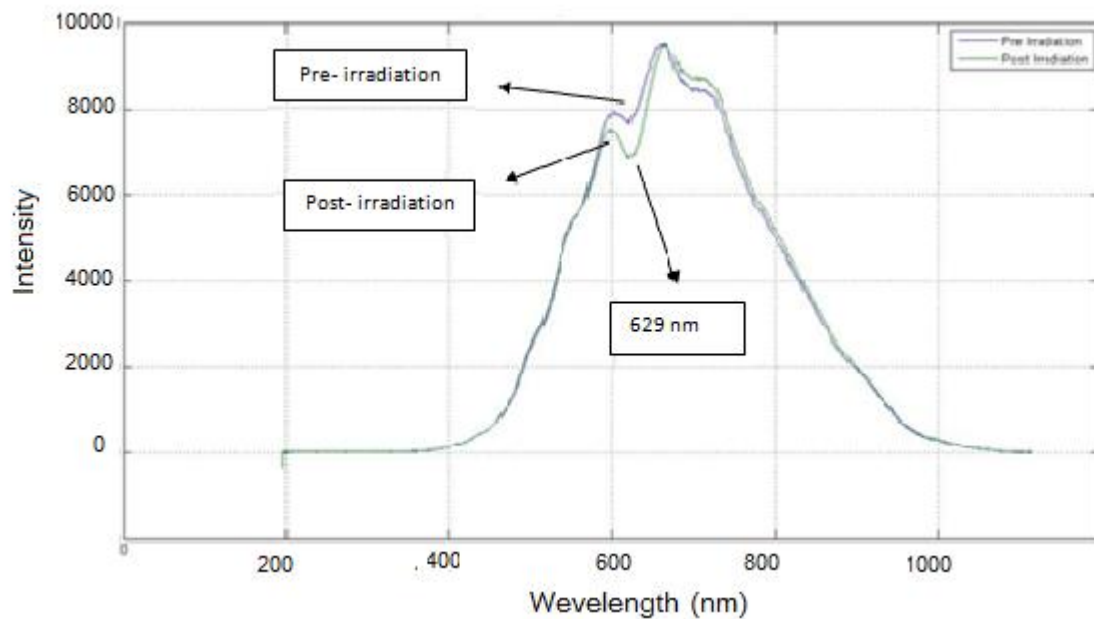


Figure 2.6 The intensity of transmitted light pre and post irradiation. The decrease in intensity at 629 nm corresponds to increase in absorption from LMG

The accuracy in the measured intensity of transmitted white light may also be affected by any variations in the output intensity of the white light source. These were minimized by turning it on 30 minutes prior to measurements.

2.3.2 CCD Camera Apparatus

The metal plates were taken out of the refrigerator 60 minutes before read out in order to reach room temperature. Once they were at room temperature, the clear gel dosimeters were carefully removed using the transparent films.

The transparent films have dimensions of $14.5 \times 14.5 \text{ cm}^2$, which is slightly smaller than the dimensions of the plates. The sides of the gels must be cut in order for the gels to fall exactly in the centre of the film. Therefore the gels were cut to $13.5 \times 13.5 \text{ cm}^2$. This resulted in a frame with a 0.5 cm edge at each side. Marking one side of the frame, the gels were placed exactly on the same location in the centre of a red light surface by registering to a point marked on the frame.

The diffusive red light surface had adjustable intensity. The red light source and a CCD camera were housed in a light tight box. The CCD's lens was focused on a plane at the centre of the gel as shown in figure 2.7.



Figure 2.7 Picture of in-house 2D optical scanner, a red light surface in a light tight box with a lens-coupled CCD on top.

The images captured by the CCD were transferred to a computer and analyzed using Matlab. The images were 1024 X 1328 with pixel values that corresponded to the intensity of the transmitted light. Since both pre and post irradiated gels sat exactly at the same spot on the red light surface, the Beer-Lambert equation was used to calculate the change in optical density at each point.

2.4 Data Processing and Analysis

The data processing technique involved in the first phase of this research was relatively simple, since everything is one dimensional.

The optical density was calculated from the pre- and post- irradiation transmission measurements using Beer Lambert equation (eq. 2.1). The optical density sometimes had a small offset that will be discussed in chapter 3. Since the change in optical density should be zero in certain regions of the measured spectrum, the data were normalized to zero in these regions and that factor applied to the entire spectrum. This normalization is shown in figure 2.8.

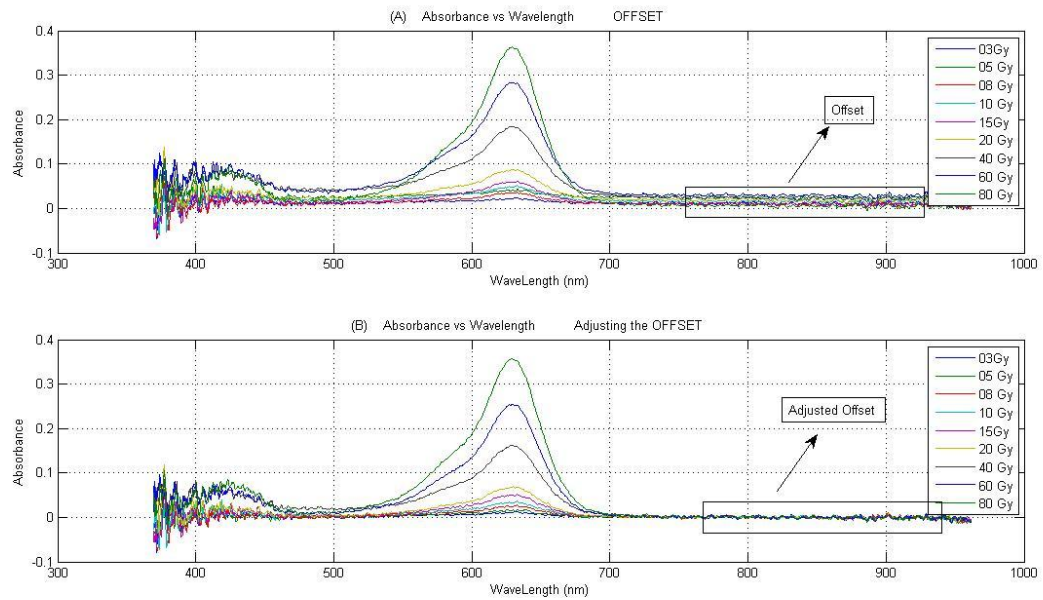


Figure 2.8 The Absorbance must be zero above visible spectrum. (A)The offset shown is a result of sources of uncertainties (B) it is adjusted back to zero.

In phase two of this research, more complex data processing techniques were required.

Here, the pre- and post irradiation images of the 2D gels were captured with the CCD

camera and the absorbance was calculated at each pixel. The captured images were also noisy. The absorbance images were smoothed using a de-noising filter. The measured image must also be compared with a Pinnacle Calculated Planar (PCP) dose-map image; hence, both images must have same sizes and placed accurately on top of each other. This way, the images may be compared point by point. Since the captured image is rotated and stretched in comparison with the PCP image, the measured image must be mapped onto the PCP image.

2.4.1 De-noising Filter

To remove the high frequency noise of the images, a built-in de-noising Matlab function was used. “*wdencmp*” is a Matlab function that performs the de-noising process of a signal using wavelets. In the wavelet transform, the image is decomposed into different coefficients [37]. The function zeros coefficients below a certain threshold. The transform is inverted after thresholding. In the wavelet, or Haar transform, the original signal, $x(n)$ is decomposed into two components: 1) the average of two neighbouring pair of data $c(n)$, and 2) the average of their differences $d(n)$ (shown in figure 2.9).

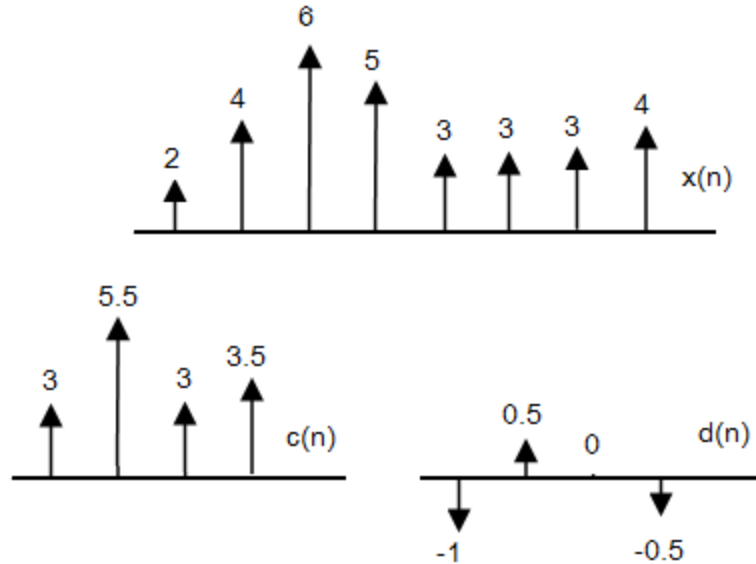


Figure 2.9 $x(n)$ is the original signal, $c(n)$ is the average of two neighbouring pairs and, $d(n)$ is the average of their differences.

As shown in figure 2.9, a signal with eight points is decomposed into two signals with four points each.

$$c(n) = \frac{1}{2} [x(2n) + x(2n + 1)] \quad (2.2a)$$

$$d(n) = \frac{1}{2} [x(2n) - x(2n + 1)] \quad (2.2b)$$

Consequently, $x(n)$ may be re-constructed if $c(n)$ and $d(n)$ are passed through an inverse transfer function. Figure 2.10 shows the transfer function for both cases.

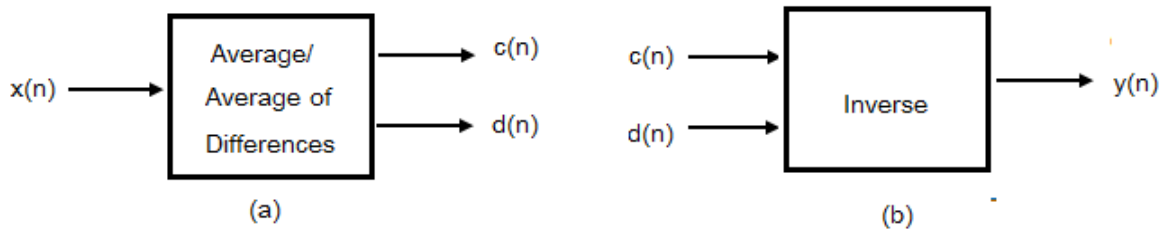


Figure 2.10 The transfer function for (a) decomposition of the signal (b) reconstructing the signal

The signal, $y(n)$, is reconstructed as follow:

$$y(2n) = c(n) + d(n) \quad (2.3a)$$

$$y(2n + 1) = c(n) - d(n) \quad (2.3b)$$

For an eight-point signal the decomposition may be repeated three times as shown in figure 2.11.

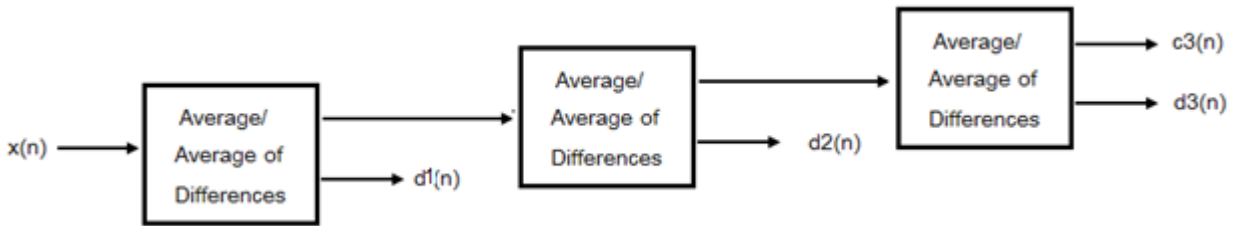


Figure 2.11 Decomposition is repeated three times

The three stages of the wavelet transform shown in figure 2.9 are represented as follows:

$$c_3(n) = [3.75]$$

$$d_3(n) = [0.5]$$

$$d_2(n) = [-1.25, -0.25]$$

$$d_1(n) = [-1, 0.5, 0, -0.5]$$

Any noisy signal may go through a wavelet transform to be decomposed into smaller signals for an effective noise reduction. If a noisy signal with 1024 points is considered, the noise may be removed by transferring the signal through a multistage wavelet transform to get smaller coefficients. The coefficients are then set to zero if they are below a certain threshold [38].

Figure 2.12 shows a 1024 point signal with and without noise, as well as their four level wavelet representations.

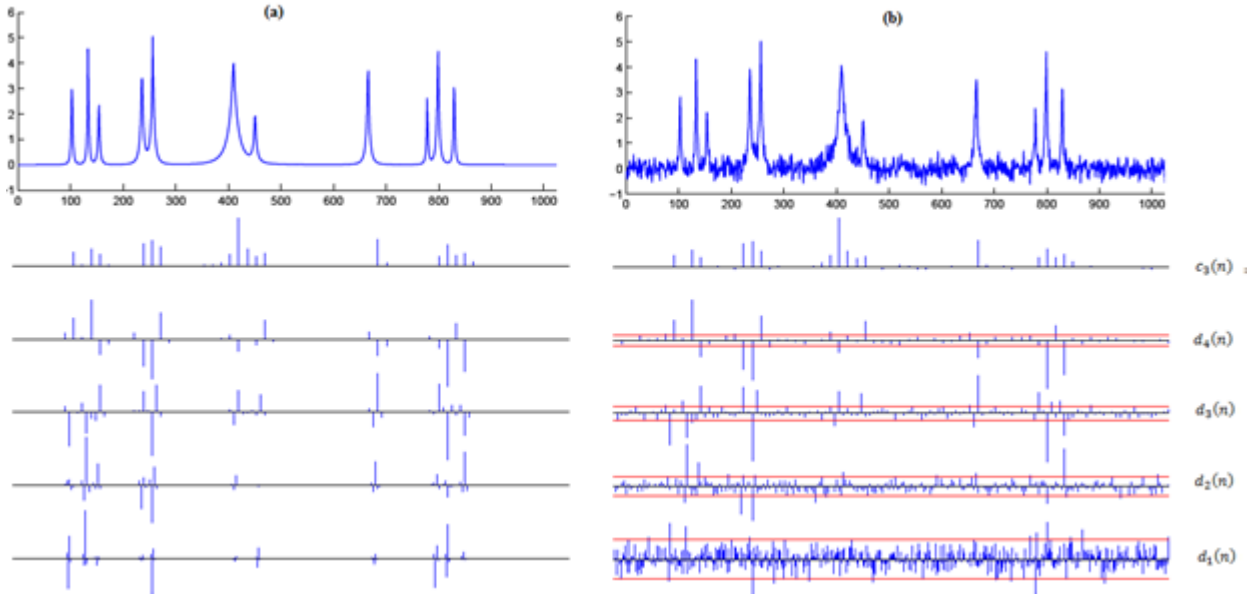


Figure 2.12 Four level wavelet transform for (a) a signal without noise (b) with random noise [38]

As shown in figure 2.12 (b), the values within the red lines, which corresponds to the noise in the signal, must be set to zero. Once the noise is removed the original signal is recovered using equation 2.3a and 2.3b.

In the de-noising process, the signal was transformed, thresholded and inverse-transformed. Filtering the noise may also affect the edges and the high dose gradient regions of the actual image.

2.4.2 Image Registration

Image registration was performed in three steps: first the transformation matrix was constructed, second, an address grid was constructed for the measured image; and third,

the grid was translated onto the PCP image using the transformation matrix, and then the corresponding colour value at each pixel was computed.

2.4.2.1 Transformation Matrix

In order to compare the measured with the PCP image, both images must be located exactly on top of each other; this would allow pixel by pixel comparison. Therefore, after de-noising the de-noised image, it was passed through a transformation matrix to be mapped onto the PCP image.

The types of geometric transformations that may be associated with the measured images were translation, rotation, scaling, and shear. Affine transformation is a transformation that involves all mentioned transformations.

Rotation

For rotation by an angle θ the following rotation matrix may be used:

$$\begin{bmatrix} x' \\ y' \end{bmatrix} = \begin{bmatrix} \cos\theta & -\sin\theta \\ \sin\theta & \cos\theta \end{bmatrix} \begin{bmatrix} x \\ y \end{bmatrix} \quad (2.4a)$$

Where x' and y' are the rotated points (PCP Image), θ is the angle of rotation (counter clockwise about the origin), and x and y are the primary points (Measured Image) to be rotated.

Therefore,

$$x' = x \cos\theta - y \sin\theta$$

$$y' = x \sin\theta + y \cos\theta$$

Scaling

On the other hand the scaling matrix is as follows:

$$\begin{bmatrix} x' \\ y' \end{bmatrix} = \begin{bmatrix} a & 0 \\ 0 & b \end{bmatrix} \begin{bmatrix} x \\ y \end{bmatrix} \quad (2.4b)$$

where a is the horizontal and b is the vertical stretch. Therefore,

$$x' = ax$$

$$y' = by$$

Shear

There was also sheer mapping parallel to x or parallel to y

$$\begin{bmatrix} x' \\ y' \end{bmatrix} = \begin{bmatrix} 1 & k_x \\ k_y & 1 \end{bmatrix} \begin{bmatrix} x \\ y \end{bmatrix} \quad (2.4c)$$

$$x' = x + y k_x$$

$$y' = y + x k_y$$

Translation

For translation operator another dimension must be added to the matrix, which is as follows:

$$\begin{bmatrix} x' \\ y' \\ 1 \end{bmatrix} = \begin{bmatrix} 1 & 0 & t_x \\ 0 & 1 & t_y \\ 0 & 0 & 1 \end{bmatrix} \begin{bmatrix} x \\ y \\ 1 \end{bmatrix} \quad (2.4d)$$

where t_x is the horizontal translation and t_y is the vertical translation. Therefore,

$$x' = x + t_x$$

$$y' = y + t_y$$

Combining the matrices yields the affine transformation matrix:

$$\begin{bmatrix} x' \\ y' \\ 1 \end{bmatrix} = \begin{bmatrix} a_{11} & a_{12} & t_x \\ a_{21} & a_{22} & t_y \\ 0 & 0 & 1 \end{bmatrix} \begin{bmatrix} x \\ y \\ 1 \end{bmatrix} \quad (2f)$$

$$x' = (a_{11}x + a_{12}y) + t_x$$

$$y' = (a_{21}x + a_{22}y) + t_y$$

To construct the transformation matrix, ten points were chosen on the PCP image. These ten points were matched with ten other points on the measured image. Figure 2.13 shows the matching points.

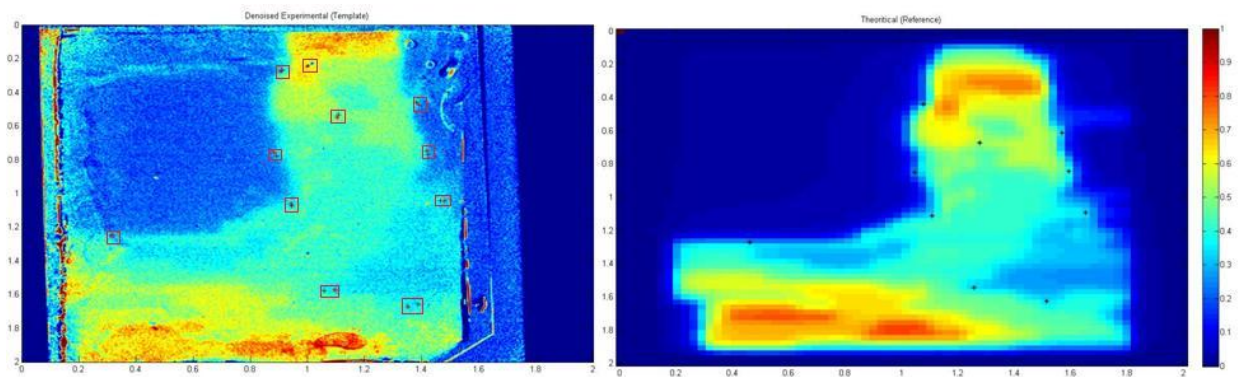


Figure 2.13 The matching points selected on the measured and PCP images.

Even though three points were required to construct the transformation matrix, ten points were chosen to obtain more accurate results. Since these points were chosen manually, human error may be reduced by choosing more points.

2.4.2.2 Constructing the address grid

Every image is made of pixels. Pixels are the smallest addressable elements in each image, which hold the attributes of the image. The address of each pixel is the coordinate that the pixel is positioned. The colour information of the image is stored at each pixel. Every image has two significant pieces of information: 1) the intensity of each pixel, 2) the address of each pixel. Whenever an image goes through transformation, the coordinate of its pixels go through transformation. In order to register the image the coordinate of its pixels must be obtained and later be transformed. Therefore, an address grid was constructed to represent the coordinate of each pixel.

The grid was built in a way that each squares of the grid holds one pixel. The reason the grid is constructed is to have an imaginary address for each pixel. The centre of each square on the grid corresponds to the address of that pixel. This method is called midpoint discretization of the image [39]. The coordinate of each pixel is represented by a dot in the centre of each square on the grid. Figure 2.14 shows the midpoint discretization of the PCP image.

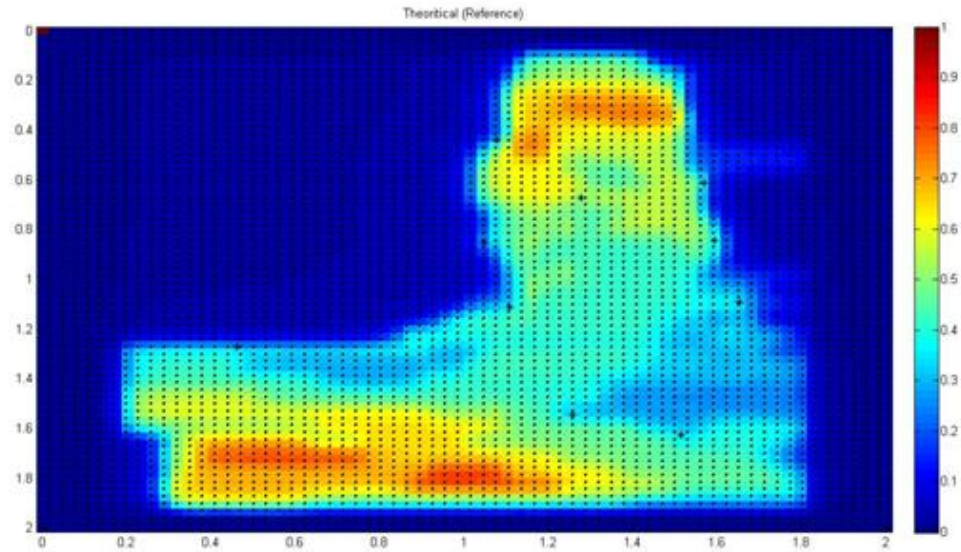


Figure 2.14 midpoint discretization of the PCP image

As shown in figure 2.14, the black dots in the centre of each colour pixel represent the address of each pixel. When an image go through transformation all these address dots would also go through a transformation. Therefore, the midpoint coordinates go through the previously obtained transformation matrix to obtain the address grid for the transformed image. Figure 2.15 represents the transformed grid on the measured image.

In figure 2.15, the midpoint discretized grid was transformed by multiplying the coordinates of each midpoint by the transformation matrix.

Once the address grid was transformed, the colour value at each pixel was interpolated from the grid.

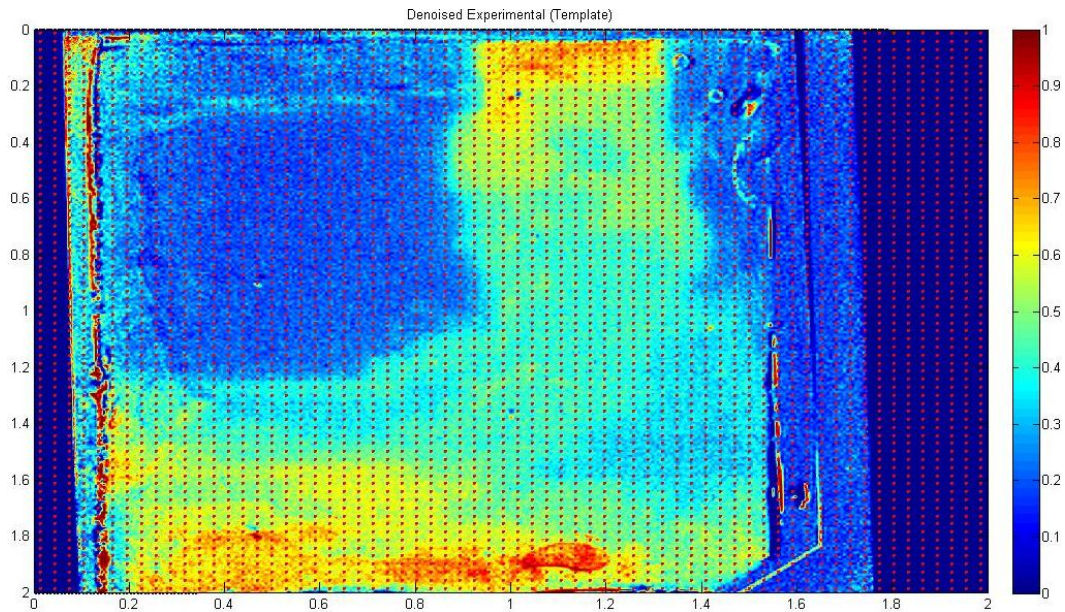


Figure 2.15 transforming the midpoint discretization of the PCP image on the measured image

2.4.2.3 Interpolating the colour value at each pixel

As mentioned earlier, each image has two significant pieces of information: 1) the coordinates of each pixel, 2) the value at each pixel. The coordinates of the pixels go through transformation when the images go through transformation. Now the question is how to interpolate the colour value at each transformed coordinates? Bilinear interpolation is a resampling technique used to extract the most accurate value of each pixel.

Whenever an image is mapped, the pixel coordinate of the reference image is mapped onto the measured image, and then the colour attributes at each pixel is computed. If both transformed and non-transformed grids are positioned on top of each other, each of the transformed midpoints is surrounded by four points of the non-transformed grid.

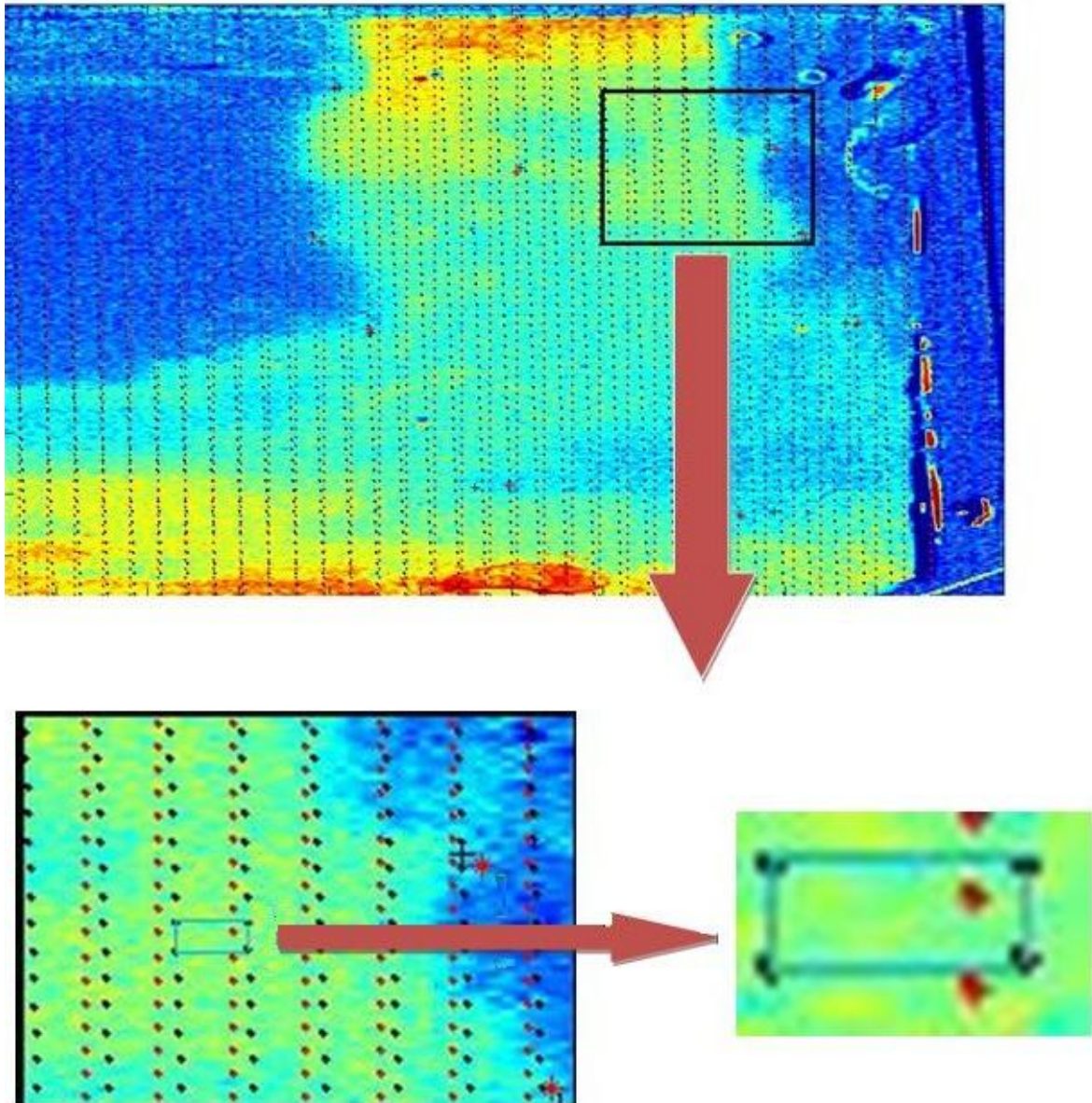


Figure 2.16 Each transformed point is surrounded by 4 points

In figure 2.16, the red dots are the transformed coordinates and the black dots are just the non-transformed mid-points. Each black dot is positioned in the centre of a different pixel. In order to compute the colour attributes of the translated pixel, the colour attributes of the four surrounding pixels must be used. The most accurate method to extract a value from the four surrounding points is to compute a weighted average of the four points.

Figure 2.17 illustrates an example of the transformed and non-transformed grids on any given image. The red dots correspond to the non-transformed midpoints, and green dots correspond to the transformed midpoints.

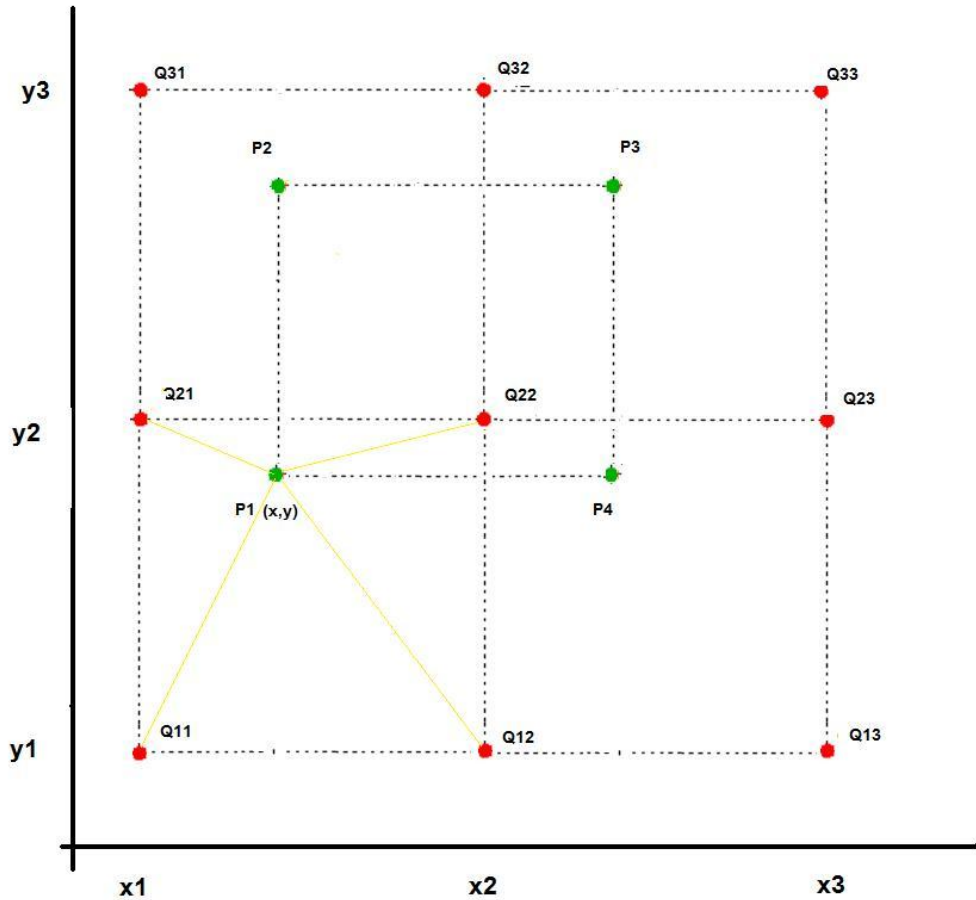


Figure 2.17 The Transformed and non-transformed grid

Since P1 is surrounded by Q11-Q22, the colour information which must be allocated to P1 must be a combination of the colour information in the surrounding four dots. Since the P1 is closer to Q21, then Q21 must have a large offset on the colour assigned to P1. The colour information of the new dot must be extracted from the surrounding dots;

however, each dot would have a different weight due to their distance to the newly transformed dot. To extract the colour value at P1 from Q11-22, the weight distance of each surrounding dots must be obtained. This method of interpolation is called bilinear interpolation [39]. If P1 is exactly located in the centre of surrounding dots, then the colour information at P1 could be simply calculated by just averaging the colour value at each of the surrounding dots. Since P1 is not located in the centre, a weighted average must be computed. The colour attributes $f(x,y)$ at point p is calculated using the following equation:

$$\begin{aligned}
 f(x,y) &\approx f(Q_{11}) \frac{(x_2 - x)(y_2 - y)}{(x_2 - x_1)(y_2 - y_1)} \\
 &+ f(Q_{21}) \frac{(x - x_1)(y_2 - y)}{(x_2 - x_1)(y_2 - y_1)} \\
 &+ f(Q_{12}) \frac{(x_2 - x)(y - y_1)}{(x_2 - x_1)(y_2 - y_1)} \\
 &+ f(Q_{22}) \frac{(x - x_1)(y - y_1)}{(x_2 - x_1)(y_2 - y_1)} \\
 f(x,y) &\approx [1 - x \quad x] \begin{bmatrix} f(x_1, y_1) & f(x_2, y_1) \\ f(x_1, y_2) & f(x_2, y_2) \end{bmatrix} \begin{bmatrix} 1 - y \\ y \end{bmatrix} \quad (2f)
 \end{aligned}$$

Where x and y are the coordinates of point P and x_1, x_2, y_1 and y_2 are the coordinates of the four surrounding points.

In summary, to register the measured image onto the PCP image, a transformation matrix was computed. Then, the address grid of the PCP image was constructed and transformed

using the transformation matrix. Later, the colour attributes of each translated pixel was extracted from its surrounding, non-transformed, pixels.

3. Characterization of Potential Dosimeters

There are many combinations of radiochromic chemicals and matrix materials suggested by the literature. The preliminary work in this project focused on selecting the combination that would satisfy the desired physical properties and radiosensitivity. Phase one of this research is discussed in this chapter. In section 3.1, transparent PVA is evaluated for use as a dosimeter; in section 3.2, the gelatin based dosimeters are studied. Since gelatin was chosen as the matrix material for 2D studies, it was fully characterized.

3.1 PVA based Dosimeter

Poly(vinyl alcohol) was the first candidate matrix material to be investigated due to its superior mechanical properties and excellent transparency. In the first step, four different PVA solvents were studied: Dimethyl sulfoxide (DMSO), Acetone, Ethylene glycol, and Glycerine. Each of these solvents led to clear and transparent dosimeters [40]. The literature suggests that DMSO results in gels with higher light transmittance and tensile strength, therefore DMSO was used as the main solvent [32]. DMSO is a polar solvent that dissolves both polar and non polar compounds well. A transparent PVA cryogel with adjustable mechanical properties was successfully fabricated using PVA and DMSO, unfortunately the formulation was found to be insensitive to radiation. Various other solvents were investigated to replace DMSO but unfortunately none of them led to the desired level of transparency.

The investigation of PVA based dosimeters was performed in two stages: first, producing the transparent gel; and second, selecting the concentrations of the radiosensitive dye and other chemicals. In section 3.1.1, fabrication of the transparent PVA gels, as well as the chemical concentrations leading to the best radiosensitivity are investigated. In section 3.1.2, the dose response of the chosen chemical concentration is demonstrated. In section 3.1.3, the complications related to the PVA based dosimeter are discussed.

3.1.1 Selecting a Formulation

42 different combinations of LMG and free radical initiator (CCl₄) in DMSO were prepared, spanning a broad range of concentrations. Figure 3.1 shows how the samples were arranged during irradiation: each row represents a single LMG concentration and different CCl₄ concentrations.

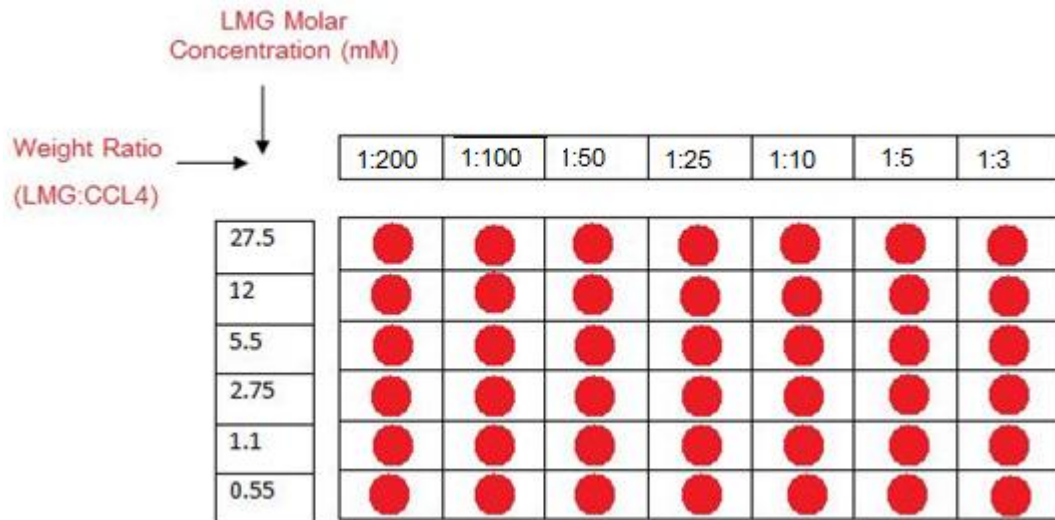
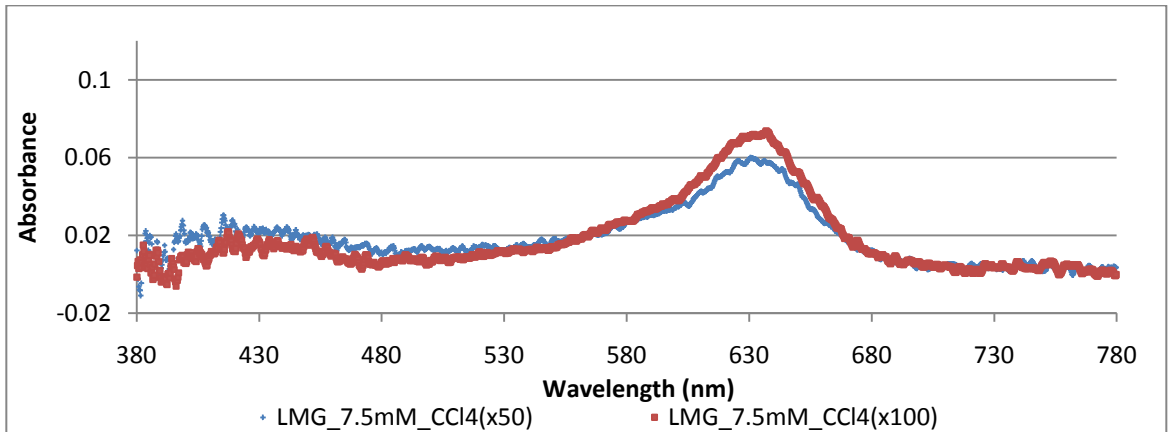


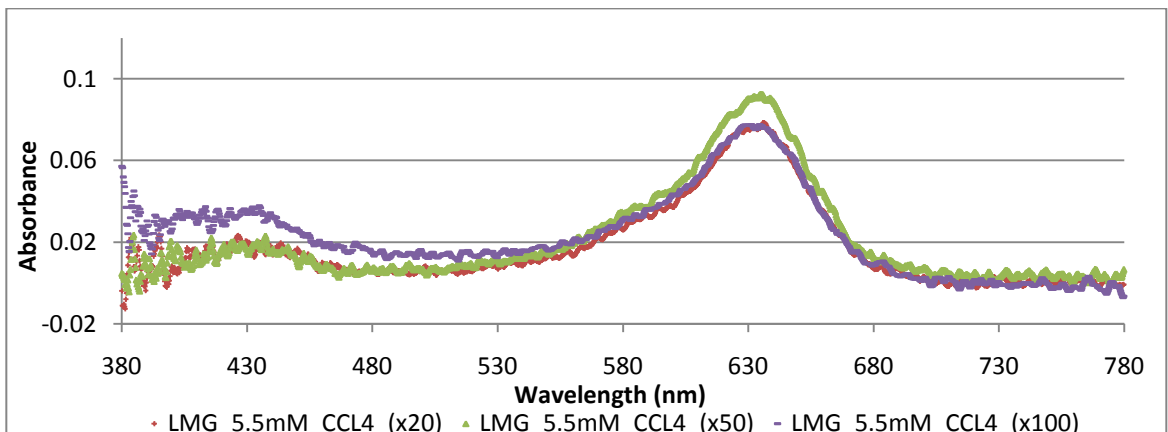
Figure 3.1 Different concentrations of LMG and CCl₄ in DMSO.

Different weight ratios of CCl₄ to LMG were exposed to 300 MU of 6 MV photons (delivered at 400 MU/min). The highest radiosensitivity was obtained in the range of 5.5 -

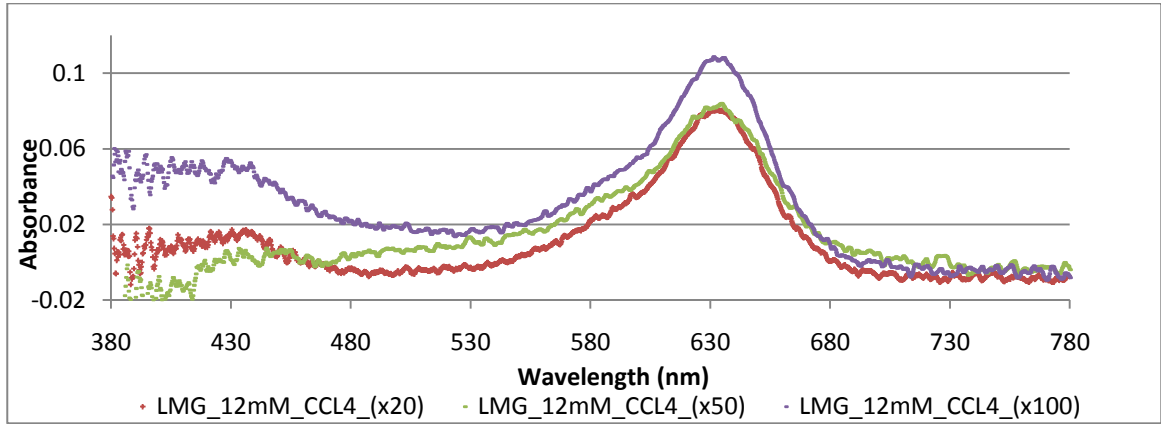
12 mM of LMG. Further experiments focused on this range found that 12 mM of LMG with 2.8M CCl₄ (x100 by weight) led to highest radiosensitivity. Figure 3.2 shows the absorbance for LMG concentrations of 5.5, 7.5 and 12 mM. The maximum absorbance was 0.15, as shown in panel C.



(a)



(b)



(c)

Figure 3.2 Absorbance vs Wavelength with different LMG concentrations (a) 7.5 mM (b) 5.5mM (c) 12mM. Different weight ratios of CCl₄ are also used. Different graphs represent CCl₄ ratios.

3.1.2 Dose Response

Once the concentrations of LMG and CCl₄ were chosen, the mixture was exposed to different doses of radiation to investigate the radiosensitivity of the compound and obtain a dose-response curve over a wide range of radiation dose. The same 6x7 cuvette holder shown in figure 3.1 was used to hold 42 test tubes with diameter of 1 cm. In figure 3.3, the 7 different columns represent different dose levels and each row represents a different batch of samples (A-F). Each independently prepared batch was exposed to seven different amounts of 6MV radiation (300, 400, 500, 600, 800, 1000, 1200 MU). The cuvette holder was placed in a water bath to achieve electronic equilibrium. The container was set up in a way so that the isocenter height was located at the midpoint of the cuvettes. Radiation was delivered using a 20x20 open field at dose rate of 400 MU/minute. This set up was used every time the samples were irradiated.

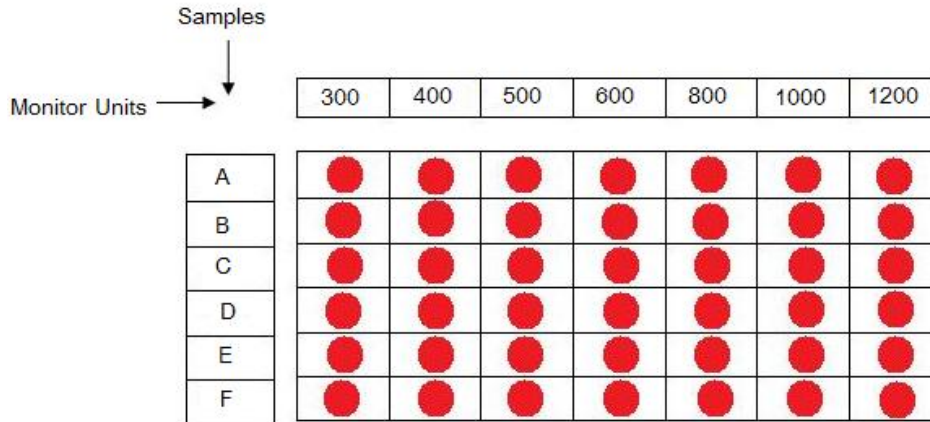


Figure3.3 Dose response experiments: the 6 rows represent different sample batches and the 7 columns corresponds to different amount of radiation

The 6 different batches of DMSO and LMG were made from dissolving 84mg of LMG in 14mL of DMSO, and distributed evenly among 7 cuvettes. This is equivalent to having 12 mg LMG in 2 mL DMSO in each cuvette. 0.75mL of CCl₄ was also added to each cuvette. This process was repeated six times in order to make identical samples from 6 different batches. The samples were measured pre and post irradiation. The intensity of the transmitted light was captured over the range of 380 - 750 nm. The pre-irradiation measurements were used as references for the post-irradiation optical density measurements. Self referencing each sample reduces any sources of uncertainties caused by surface scratches or unclean spots on the surface of each cuvette. The absorbance at 629 nm was calculated by averaging the absorbance over the range of 619 – 639 nm, where the absorbance reaches 90% of its peak value. The absorbed dose in Gray (Gy) may also be estimated from the Monitor Units (MU) by applying an exposure factor.

Since the light is being transmitted through the cuvettes 3cm below the surface, the correction factor corresponding to 3cm depth, $CF= 1.117 \text{ cGy/MU}$, can be used.

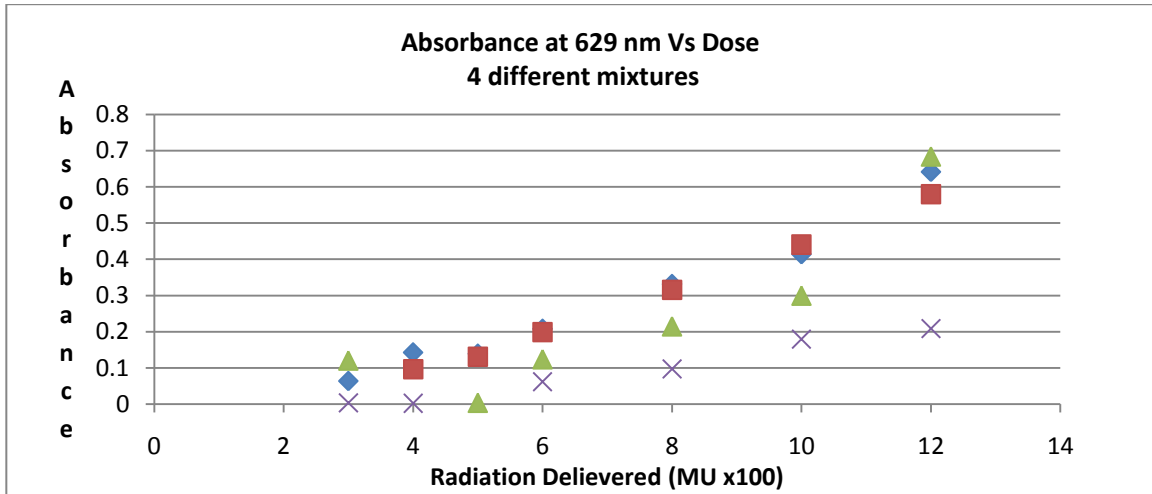


Figure 3.4 Absorbance at 629 nm for 4 different test groups.

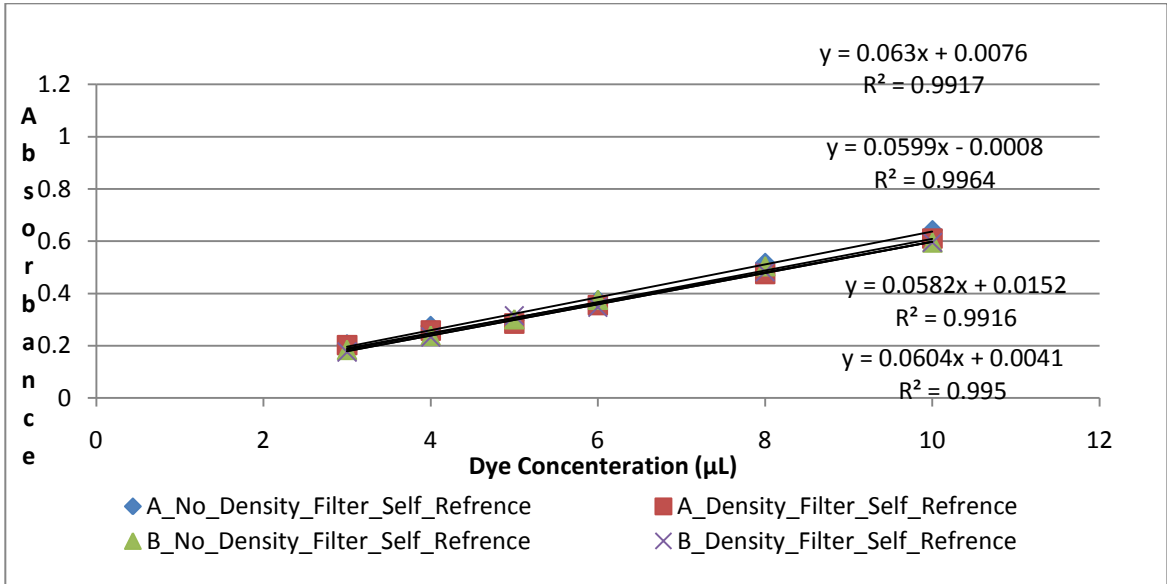
As shown in figure 3.4, the obtained data were not consistent, suggesting there must be various sources of uncertainties. Due to variations in the calculated optical densities, they were not reliable and the sources of uncertainty were investigated. Two main sources of error were found: 1) uncertainties preparing the samples; 2) error in the read-out technique. The first source of error is referred to as “chemical”, and the second source is referred to as “physical”. Details about each of the mentioned sources are summarized in Table 3.1.

The fluctuation of the output power of the white light source was examined by splitting 5% of the light from the source to monitor the output during measurements. An optical power meter (Newport SX503) was connected to the splitter using an optical fibre.

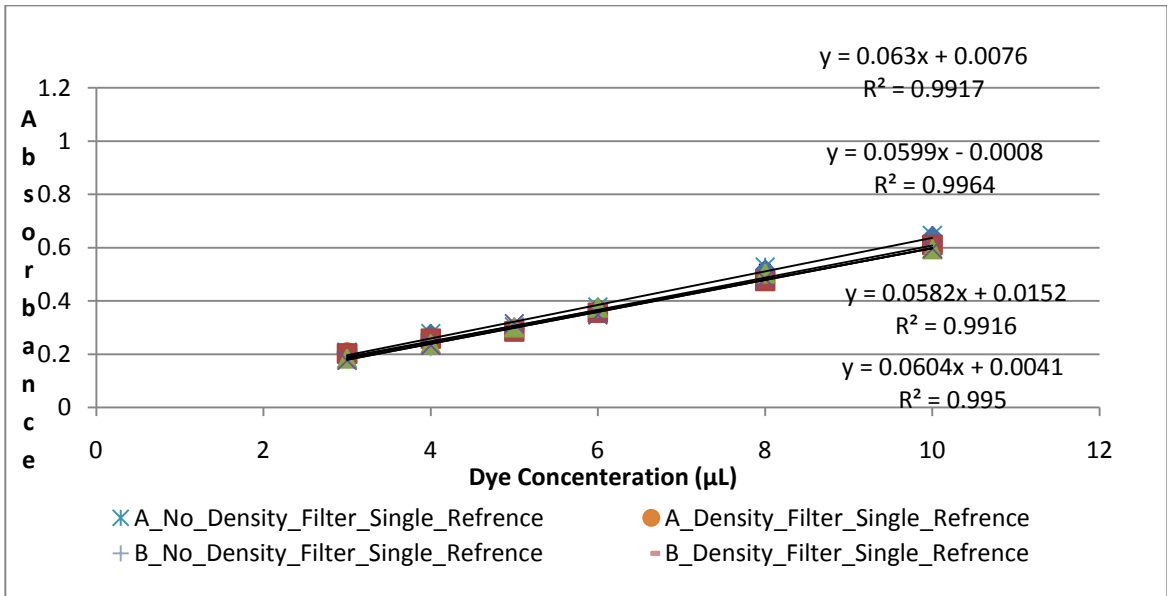
Sources of Uncertainty			
Chemical	LMG not being dissolved uniformly in DMSO	LMG not being distributed evenly among the samples	Vaporization of CCl ₄ while preparing the samples
Physical	Fluctuation in output power of the white light source	Unclean spots/scratches on the surface of the cuvettes	

Table 3.1 Different types of errors to be investigated

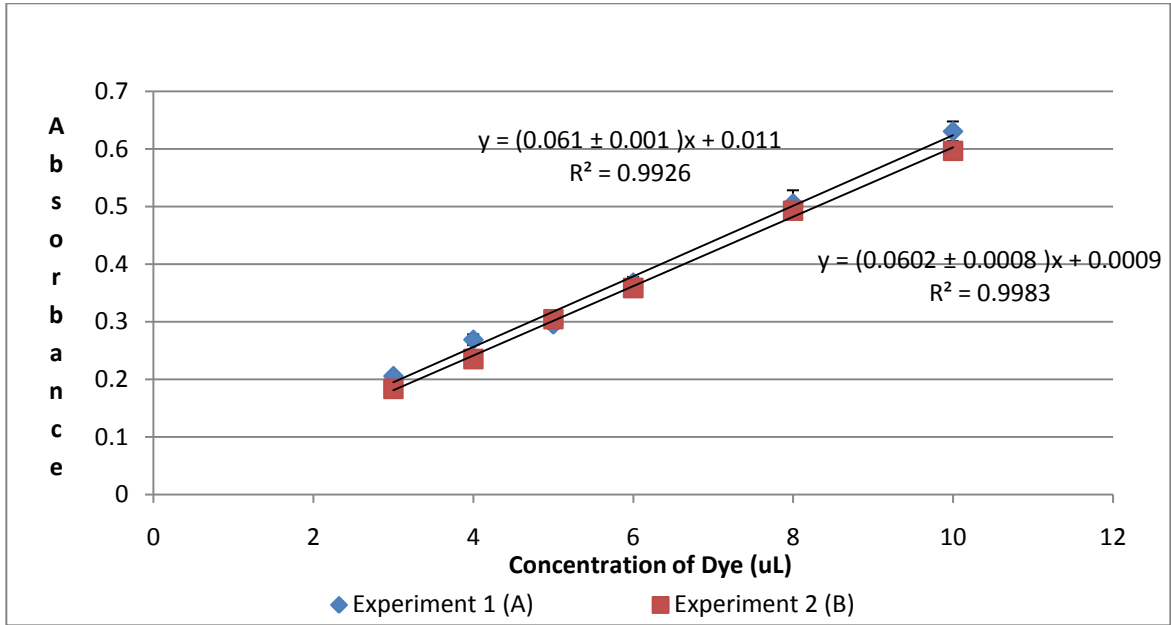
To investigate the physical error only, the error associated with sample preparation was minimized by adding a known concentration of blue dye to cuvettes filled with water. The intensity of the transmitted light through the samples and the output power of the source were recorded. Subsequently, different volumes of blue dye (3, 4, 5, 6, 8, 10 and 12 μL) were added to the cuvettes and their optical densities, as well as the output power of the source, were again recorded. The intensity of the transmitted light and output power, before and after adding the dye, were measured under two different conditions: having a neutral density filter in front of the light source, and having no filter. The effect of self-referencing was also examined by comparing the absorbance calculated using different references. This experiment was repeated two times. Figure 3.5 (a) represents the absorbance with/without the filter while the samples are being self-referenced and (b) represents the absorbance with/without the filter while the samples are being referenced to a single reference sample.



(a)



(b)



(c)

Figure 3.5 (a) Absorbance with/out the filter, samples are self-referenced (b) absorbance with/out neutral density filter; samples are being referenced to a single reference sample. (c) Absorbance vs Dye concentration combining the data

As shown in figure 3.5 the obtained absorbance curves are consistent. The graph on panel (C) shows the regression line for both experiments. The error bars show the deviation in absorbance with and without the neutral density filter, as well as self and single referencing. This deviation is very small for both experiments, less than 2% difference in the slopes. This suggests that imperfections on the cuvettes do not constitute a significant source of error. The output power of the light source was also examined over time. The optical power of the light source remained unchanged during the measurement. It is measured to be $3.146 \pm 0.002 \mu\text{W}$ with no filter and $2.465 \pm 0.001 \mu\text{W}$ when the filter was added. The physical sources of uncertainty were examined; none of them introduced errors of the magnitude seen in the preliminary LMG experiments (figure 3.4). The sources of chemical uncertainties were first examined by investigating leuco-malachite green. Since different concentrations of LMG are made from dilutions of the

LMG/DMSO solution, it is possible that LMG may not have been uniformly dissolved in the DMSO. To test this, the desired mass of LMG was dissolved in the DMSO and stirred for 20 minutes.

Two different batches of LMG_DMSO mixtures with exact masses of LMG in DMSO were prepared under the exact same conditions. Three sets of samples were prepared from each batch as shown in figure 3.6.

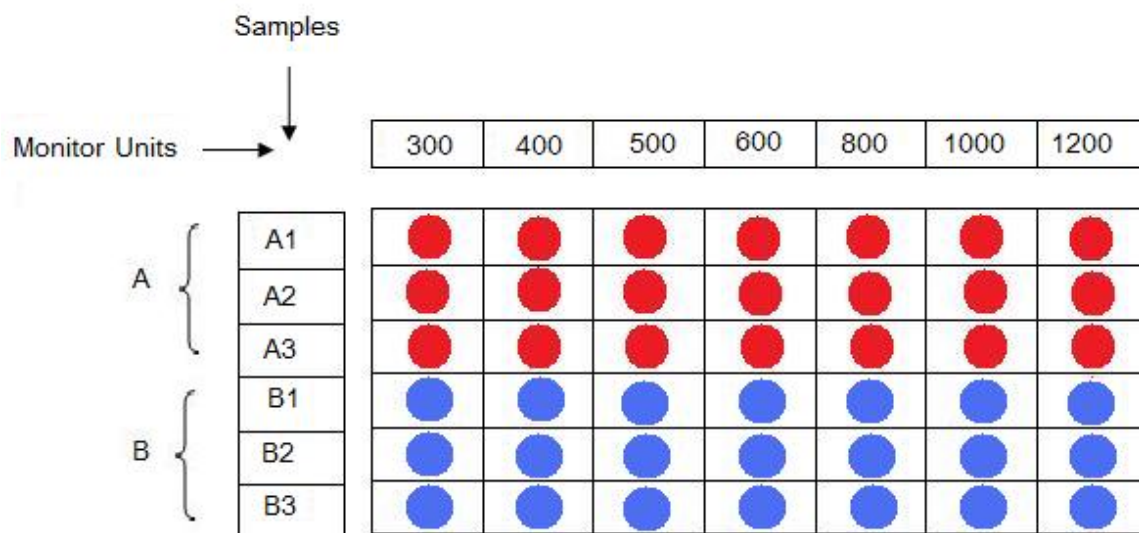


Figure 3.6 Six set of samples made from two different batches, 3 sets from each batch

To make each of the batches, 300mg of LMG was dissolved in 50 mL of DMSO. After, 18.75 mL of CCl₄ was added to each batch. The mixtures were covered with aluminum foil to keep them in a dark environment, and stirred for 10 minutes at room temperature. Each of the two batches was used to fill 21 test tubes equally. The pre and post irradiation transmitted light intensity was measured three times for each sample to reduce

any sources of uncertainty from the set-up. Figure 3.7 shows the dose-response for this series of measurements.

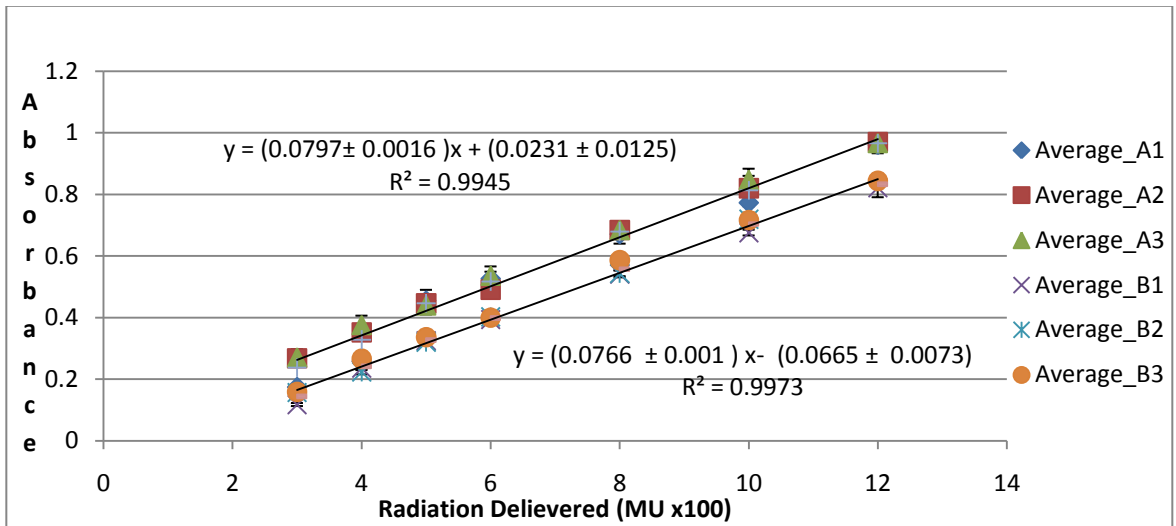


Figure 3.7 Three sets of samples were prepared from each of the two batches (A, B). The optical intensity was measured three times. The error bars represents the uncertainty corresponding to optical intensity measurement. Regression lines are for two different batches of LMG and DMSO mixtures

Even though the dose-response varied between the two different batches, the three sets made from each batch were quite consistent with each other. The error bars show the uncertainty in the calculated absorbance. The regression line for each batch of samples was calculated and is included in Figure 3.7. For each batch there are nine data points at every level of delivered radiation. The nine data points were averaged and the standard deviation calculated using equation 3.1.

$$\sigma^2 = \sqrt{\frac{1}{N} \sum_{i=1}^N (x_i - \mu)^2} \quad (3.1)$$

where N is the number of data points, μ is the mean at each dose level, and x_i is any absorbance value. The standard deviation for each batch was less than 2%. This suggests that a single stock of LMG in DMSO should yield a reproducible dose response.

Even though the uncertainty on preparation of the samples within one batch was reduced, the inter-batch difference was still large. This issue was investigated further by repeating the experiment with various modifications. First, the effect of changing CCl_4 alone was examined. Two batches were prepared from the same mixture of LMG and DMSO, and CCl_4 was added to each batch individually. 300mg of LMG was stirred in 500mL of DMSO for 20 minutes at room temperature; the mixture was then poured into two different sealed containers. Later, CCl_4 was added to each of the sealed containers and stirred for ten minutes. The whole experiment was performed in a dark room with no external sources of light to reduce the effects of stray light on the signal. Furthermore, to prevent activation of the LMG, all containers used to make the solutions were covered with aluminum foil. Figure 3.8 shows the dose-response curve when CCl_4 alone was the only variable.

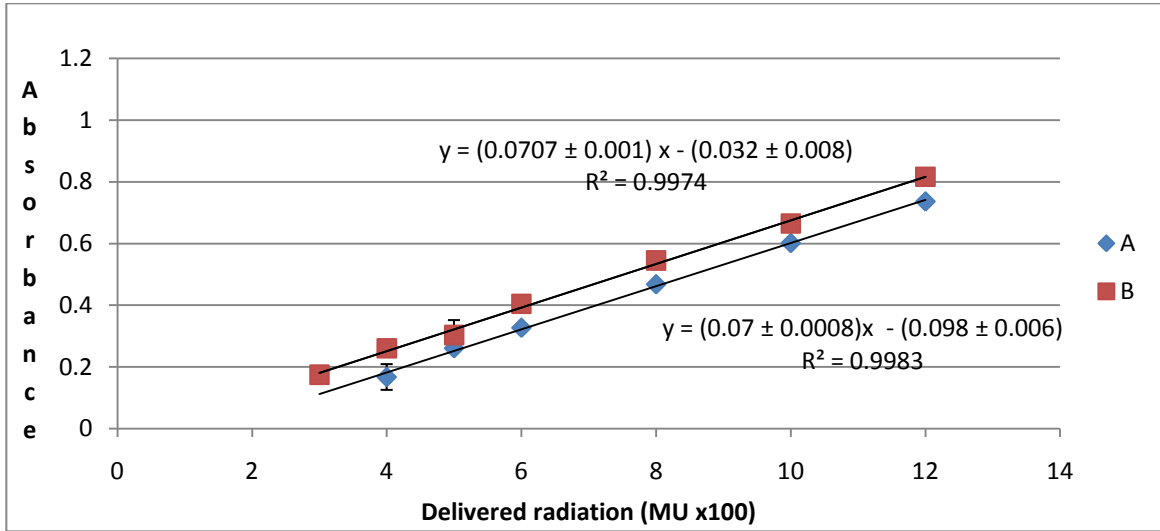
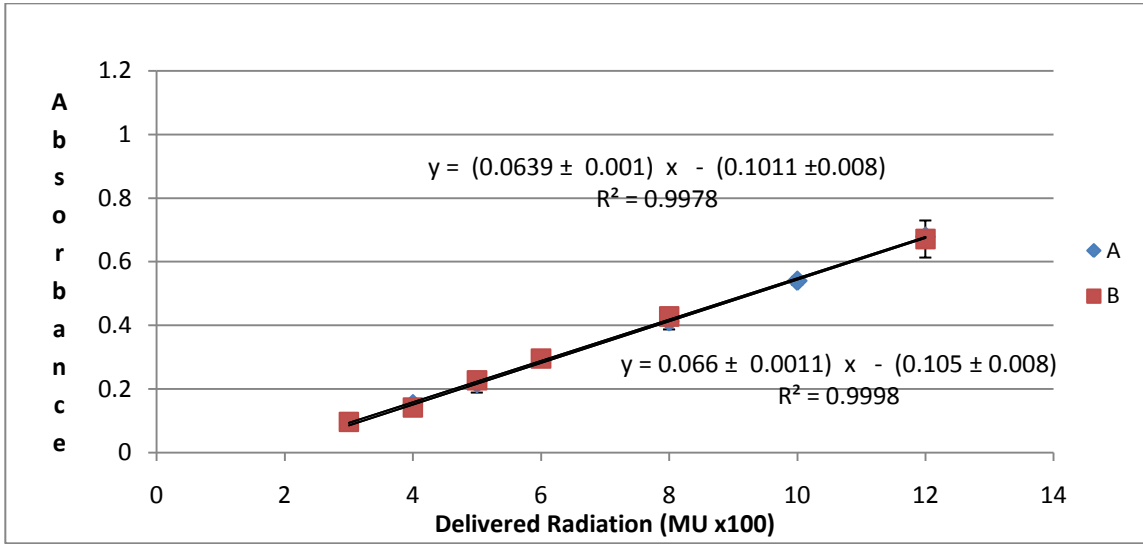
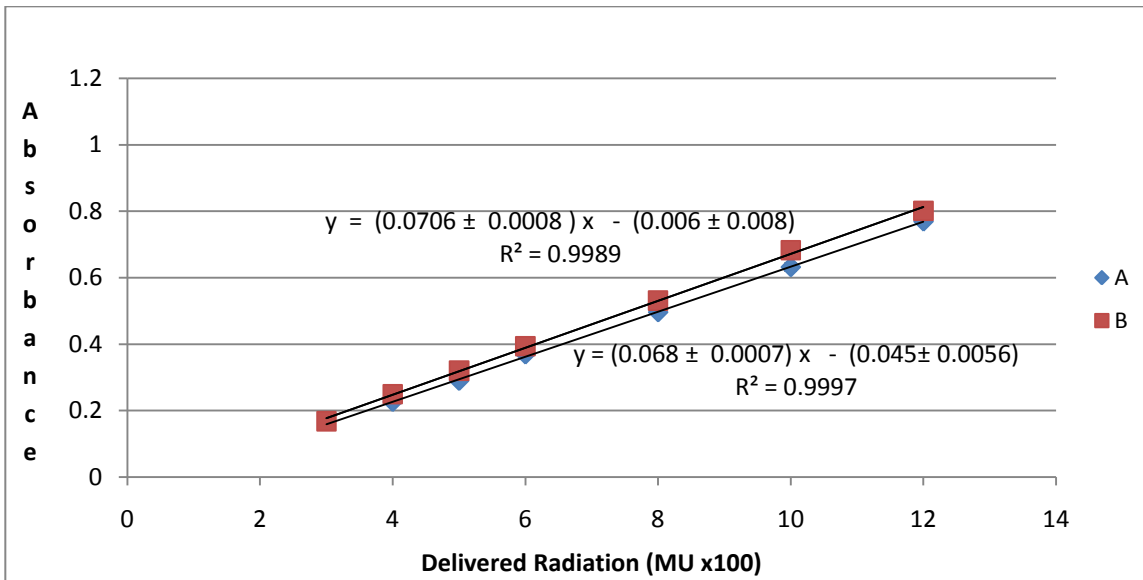


Figure 3.8 Dose-response curve when CCl₄ alone kept as the only variable. Two different batches are prepared from the same LMG and DMSO stock. The error bars are the standard deviation of 9 data points measured at each level.

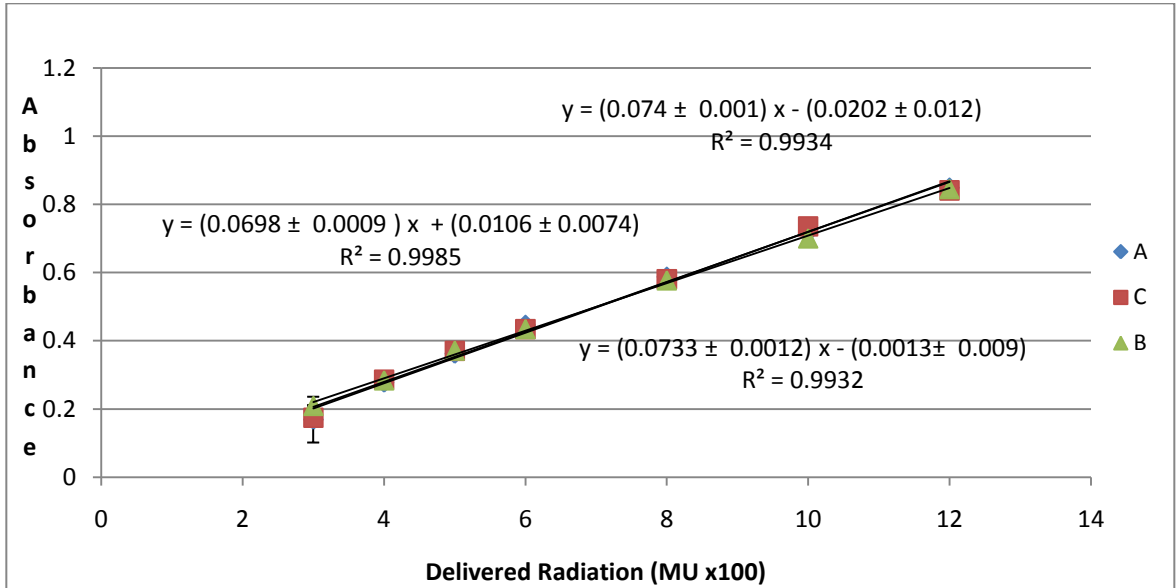
As seen in figure 3.8, the uncertainty within the same batch is less than 1%, similar to Figure 3.7. However, there is still separation between the two groups. The experiment was carried out six times, choosing either CCl₄ or LMG as the variable. Figure 3.9 and Figure 3.9 (b) show the experiments when CCl₄ is kept as the only variable. Figure 3.8 and Figure 3.9 (d) illustrate the dose response for the experiments in which both LMG and CCl₄ were chosen as the variables. Figures 3.9 (a) and (c) show the dose response when LMG and CCl₄ were both dissolved in DMSO in a single batch.



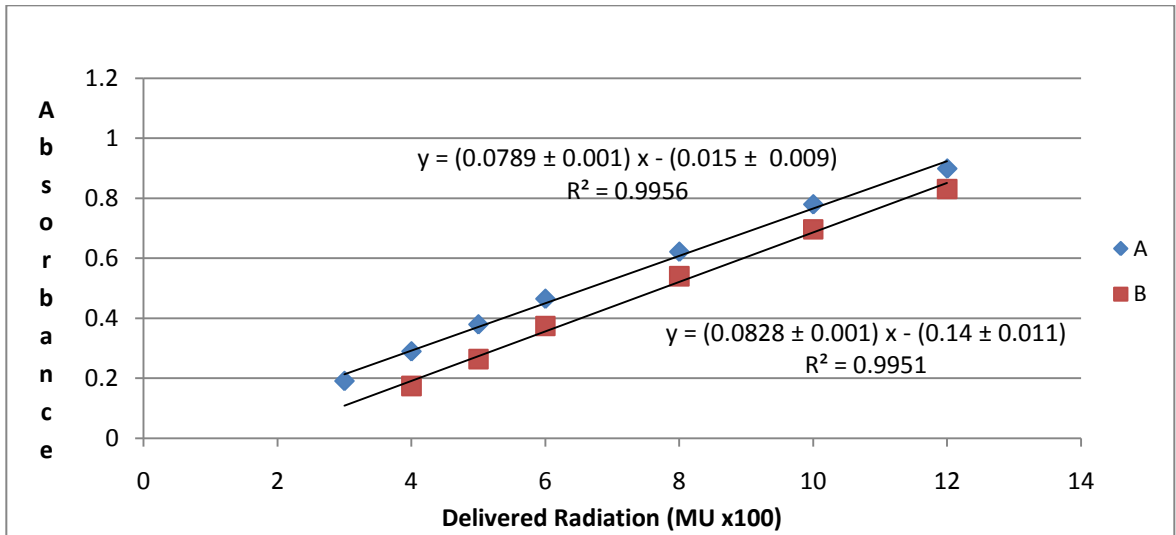
(a)



(b)



(C)



(d)

Figure 3.9 Dose response under 3 different conditions: in (a) and (c) everything is kept under same condition; (b) CCl4 is the only variable, and (d) LMG and CCl4 are both variable

As seen in figures 3.7 – 3.9, there is always less than 2% uncertainty in the slope within the samples made from one single batch. However, when different batches are compared with each other the error is greater, and thus there are some reproducibility issues. Table 3.2 summarizes the data obtained in all 6 experiments.

		Slope (x 10^{-5} cGy^{-1})	Y-intercept
1	A	0.0766 ± 0.0012	$- 0.0665 \pm 0.007$
	B	0.0797 ± 0.0016	0.0231 ± 0.012
2	A	0.0707 ± 0.0011	$- 0.0321 \pm 0.008$
	B	0.0701 ± 0.0008	$- 0.0981 \pm 0.006$
3	A	0.0639 ± 0.0011	$- 0.1011 \pm 0.008$
	B	0.0660 ± 0.0011	$- 0.1052 \pm 0.008$
4	A	0.0706 ± 0.0008	$- 0.0063 \pm 0.008$
	B	0.0680 ± 0.0007	$- 0.0451 \pm 0.006$
5	A	0.0742 ± 0.0010	$- 0.0202 \pm 0.012$
	B	0.0698 ± 0.0009	0.0106 ± 0.0074
	C	0.0733 ± 0.0012	$- 0.0013 \pm 0.009$
6	A	0.0789 ± 0.0011	-0.0154 ± 0.009
	B	0.0828 ± 0.0012	-0.1402 ± 0.011

Table 3.2 Summary of 6 experiments

In these six experiments, 13 different batches were investigated. Each batch has three sets of samples, and each sample was measured three times. Therefore, at each level of radiation delivered there are almost 110 data points. Figure 3.10 shows the combined data of the six experiments.

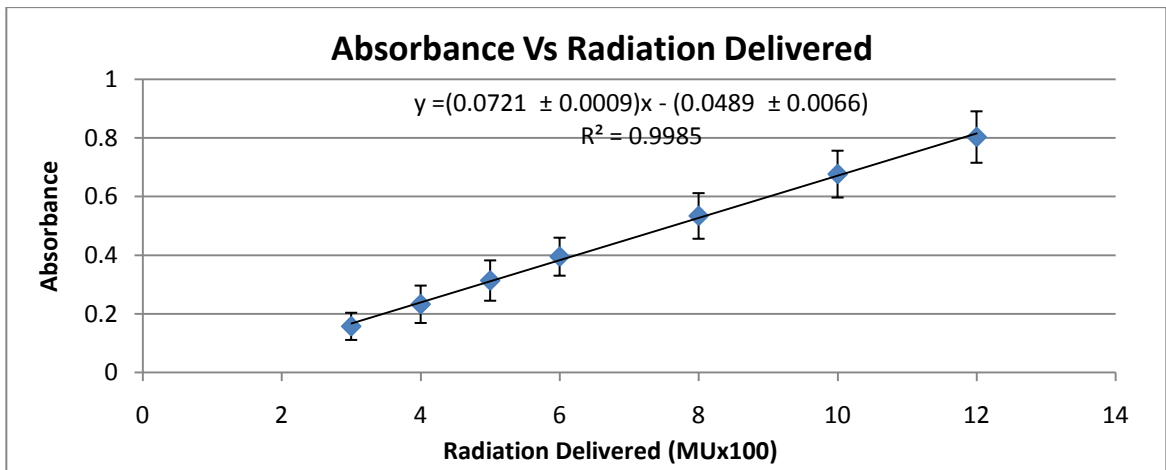


Figure 3.10 Dose-response of the six experiments combined. 13 batches, 36 sets and 108 data points. This represents the entire body of data for LMG and CCl4 dissolved in DMSO. The error bars represent the standard deviation in 110 data points.

As it is shown in table 3.2, the uncertainty on the slope and hence the dose sensitivity is 1.3%. However the uncertainty between different batches is 20%. This suggests that the relationship between the absorbance and absorbed dose is reasonably accurate as there is only 1.3% error on the slope of the regression line. The 13% uncertainty in reproducibility is definitely due to a chemical source of error.

Even though all the experiments were performed under the same conditions, dark environment, and same temperature and atmospheric pressure, large variations in optical density were observed. Samples were moved between different rooms, which may have affected the LMG. Even though the samples were covered with a black sheet when moving between different rooms, it is possible they were exposed to some UV light when being set up for radiation. . Worst case, there was less than 5% uncertainty associated with the physical measurement set up; ; therefore, the major deviation in the results was due to the chemistry of the mixture, likely related to the LMG.

3.1.3 PVA-based Cryogel dosimeter

At this stage, transparent PVA based radiochromic gels must be fabricated by mixing the selected combination of radiosensitive chemicals (LMG and CCl₄ in DMSO) with transparent PVA to produce the dosimeter. Once the transparent PVA mixture was prepared and cooled to 50 °C, the radiosensitive formulation (LMG and CCl₄ in DMSO) was added and the combination stirred for an additional 30 minutes. The mixture was dispensed into cuvettes and frozen over night at -80 °C; subsequently they were thawed for three hours prior to irradiation.

All of the gels were exposed to a relatively high amount of radiation (8000 MU) but unfortunately none of them changed colour. This experiment was repeated to verify that the PVA cryogels were not radiosensitive.

At this point the non-radiosensitivity of the PVA cryogels was studied. First, the effect of DMSO was investigated by replacing DMSO with water. PVA was dissolved in water at 100 - 120 °C for 90 - 120 minutes, the temperature reduced to 50°C, and the LMG/CCl₄ solution added. The samples were frozen overnight at -80°C and thawed for three hours prior to irradiation. The gels were exposed to 6000 MU and a colour change was observed. This suggests that the presence of DMSO in the crystallized matrix may have inhibited the oxidation of LMG to its chromatic form.

The effect of PVA crystallization was also examined by irradiating the hydrogels after refrigeration rather than freezing. The samples were kept in a refrigerator at 4°C and taken out one hour prior irradiation. These samples changed colour at high dose (6000 – 8000MU), suggesting that the combination of PVA and DMSO may be interacting with the LMG somehow during the crystallization process.

Next, PVA is taken out of the picture and thus the radiosensitive mixture (LMG and CCl₄ in DMSO) was frozen at -80°C overnight and thawed three hours prior to irradiation. Once again the samples changed colour after irradiation at 300MU, suggesting that the freezing of LMG and CCl₄ in DMSO alone does not inhibit radiosensitivity.

These measurements suggested that crystallization of PVA in the presence of DMSO prevented LMG oxidation when being exposed to radiation. An alternative method of crystallizing LMG-loaded transparent PVA is a main focus of future research.

Since presence of DMSO in the cryogel inhibited colour change, three other solvents that lead to transparent gels were examined. Acetone, ethylene glycol, and glycerine all yield transparent PVA cryogels; therefore the same fabrication process was used substituting these solvents for DMSO. Even though transparent PVA gels were fabricated using these solvents, they were not able to hold other chemicals. As soon as the gels reached room temperature, the water and radiosensitive chemicals were released. Therefore, none of the solvents were good choices to replace DMSO.

At this point it was decided to examine another water soluble matrix material that leads to a transparent gel. After reviewing the literature, gelatin was determined to be the best candidate for use as an alternative matrix material.

3.2 Gelatin-based Dosimeter

Gelatin was the second matrix material to be investigated. The idea behind radiochromic gel dosimeters is their ability to transmit light as well as their ability to change colour upon irradiation. The most important feature of these types of dosimeters is that the phantom and the detector are the same material. Also, since more than 90% of the gelatin based dosimeter is water, the dosimeters are close to tissue equivalent. This provides the convenience of a direct comparison of dose to calculation in tissue without the application of a density correction.

Unlike the PVA dosimeters, micelles are used in gelatin dosimeters. Micelles, which are aggregates of surfactant molecules, are formed when a variety of different molecules including detergents were added to water. In the preparation of the micelle gel dosimeters, different combinations of chemicals were investigated to determine the highest transparency and greatest radiochromic effect. Once the desired chemical combination was chosen, the dose response of the dosimeter was examined. The gelatin based dosimeters were responsive at high doses of radiation. Measuring the dose response in cuvettes, it was observed that there was a non-linear response at low doses (below 10 Gy). Even though there was a non-linear response below 10 Gy, it may be resolved by pre-irradiating the samples to that dose.

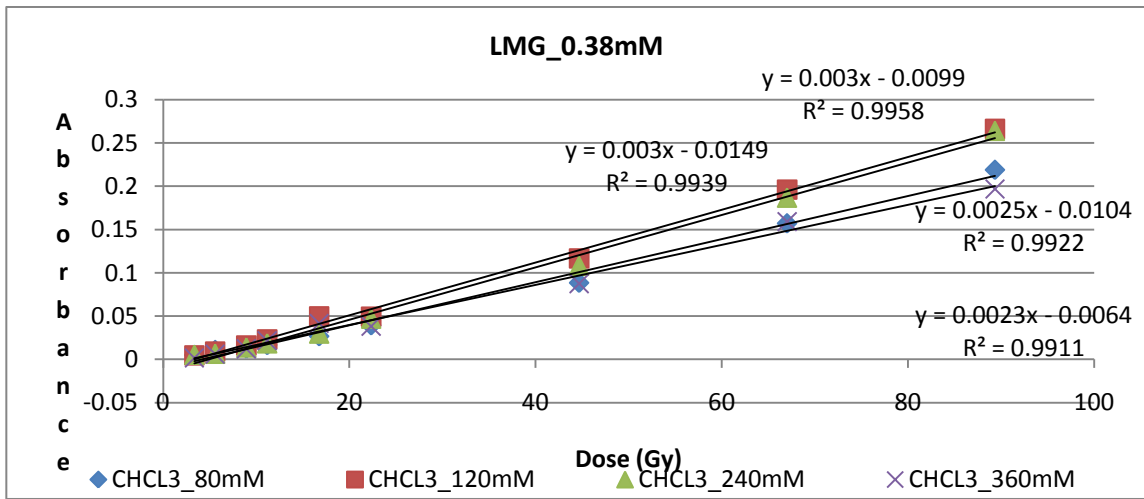
Besides replacing the matrix material, the free radical initiator was also replaced. Acidic halocarbon CCl_3COOH and neutral halocarbon CHCl_3 were used as the free radical initiators. Also, Sodium dodecyl sulfate (SDS), which is a detergent, was used as surfactant.

In section 3.2.1, the chemical concentration that led to a satisfying radiosensitivity was determined. In section 3.2.2, the dose response of the chosen formulation was studied.

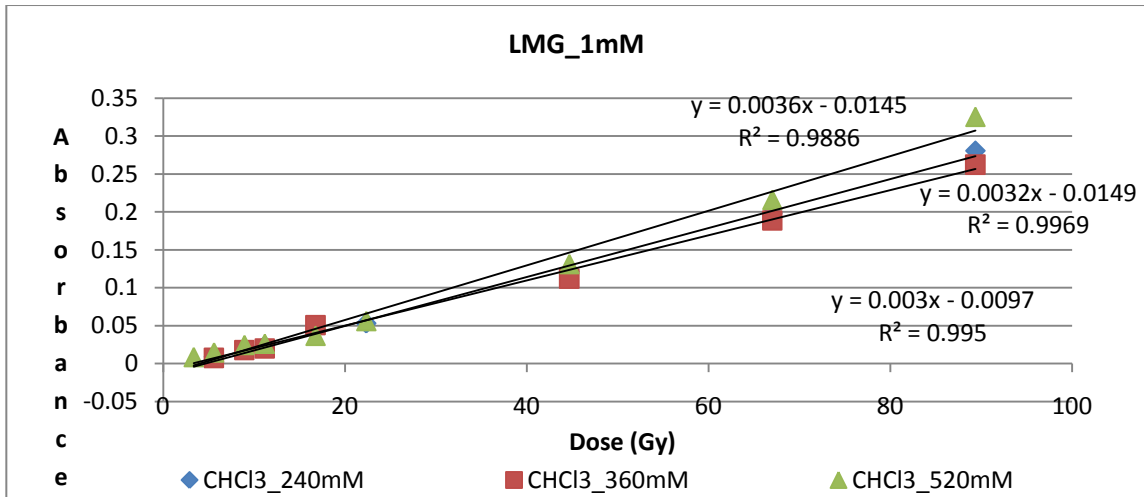
3.2.1 Determination of the formulation

Three different concentrations of LMG were examined at various concentrations of CHCl_3 (Figure 3.11 shows the dose-response curve for different concentrations of LMG). Since the radiation was delivered using a $20 \times 20 \text{ cm}^2$ open field, and the optical density measured at a depth of 3cm, Monitor Units were translated to Gray by multiplying it by

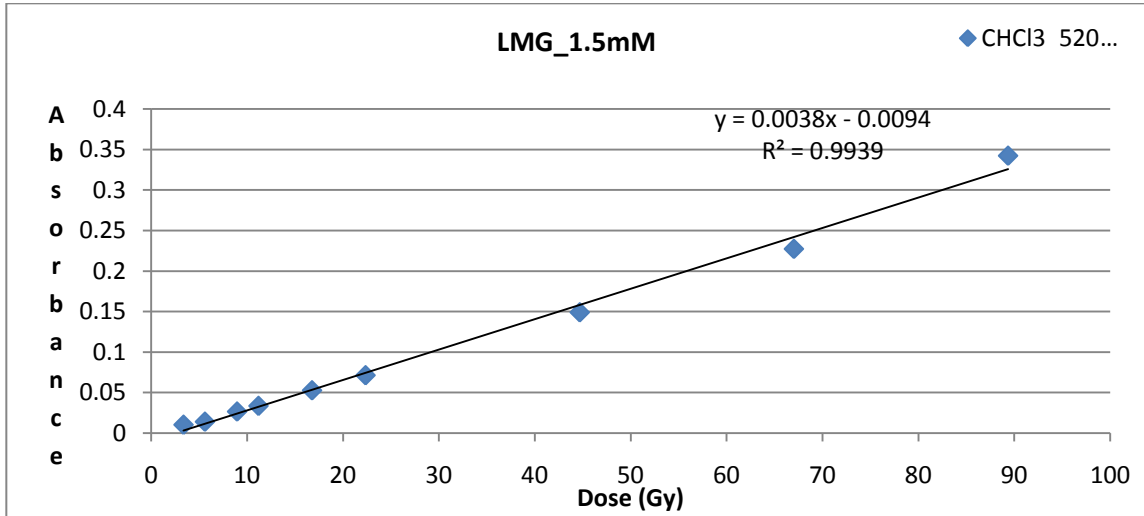
an exposure factor of 1.117. There was less than 5% error associated with the conversion of monitor units to Gray. Each of the polystyrene slabs used as build-up was assumed to be 2.5cm where there was 3% uncertainty in their thickness. Also there were some uncertainties on adjusting the source to surface distance (SSD). Hence, 5% error was associated with the conversion of monitor units to Gray.



(a)



(b)



(c)

Figure 3.11 Dose response of gelatin dosimeters with different concentrations of LMG: (a) 0.38 mM; (b) 1 mM; (c) 1.5mM

The effect of SDS concentration was also investigated. It was observed that as the concentration SDS increased the radiosensitivity decreased. Figure 3.12 shows this relationship.

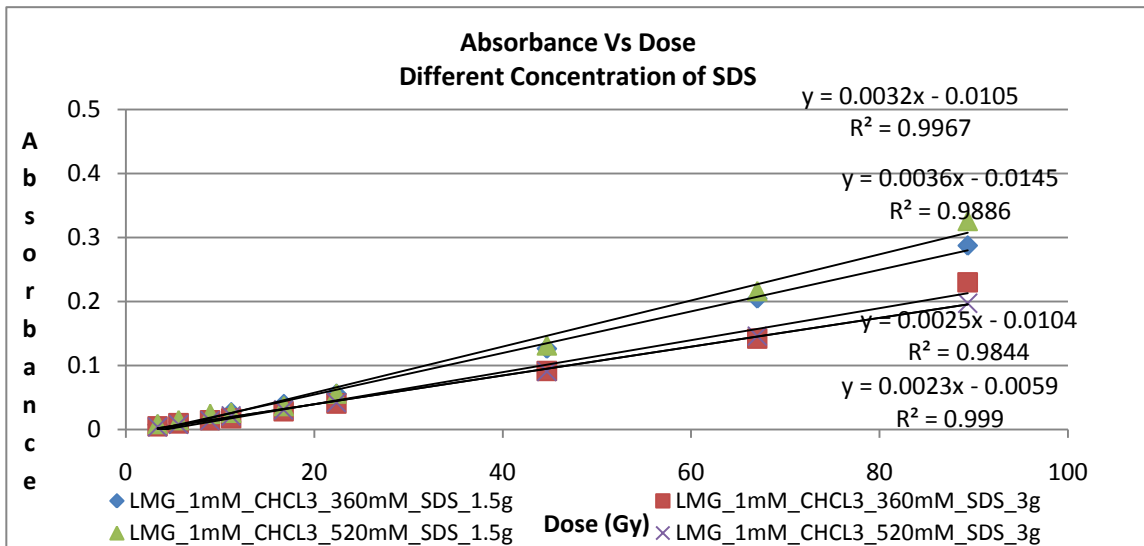


Figure 3.12 Effect of different concentrations of SDS on radiosensitivity

Table 3.3 summarizes the absorbance for different concentrations of LMG, CHCL3, and SDS.

LMG (mM)	CHCl3 (mM)	Optical Density per dose ($\times 10^{-5} \text{ cGy}^{-1}$)	
		SDS 50mM	SDS 100 mM
0.38	80	2.51	
	120	3.04	
	240	3.04	
	360	2.33	
1	240	2.95	
	360	3.22	2.51
	520	3.58	2.24
1.5	520	3.76	

Table 3.3 Optical density per unit dose for different chemical concentrations.

As shown in table 3.3, increasing the concentration of LMG led to greater sensitivity. Increasing the concentration of CHCl3 to a certain threshold also led to higher optical density; however, once the threshold was passed, increasing CHCl3 decreased the sensitivity. Even though higher concentrations of LMG and CHCl3 resulted in a larger sensitivity, it was decided to choose the lowest concentration of LMG and CHCl3 since they were more cost beneficial.

3.2.2 Dose Response

Once the desired chemical concentrations were chosen, the reproducibility of the dosimeter was investigated by repeating the irradiations 14 times, exposing the test samples to doses from 1000 MU, to 8000 MU. Figure 3.13 shows the reproducibility of the gel dosimeters over all 14 experiments.

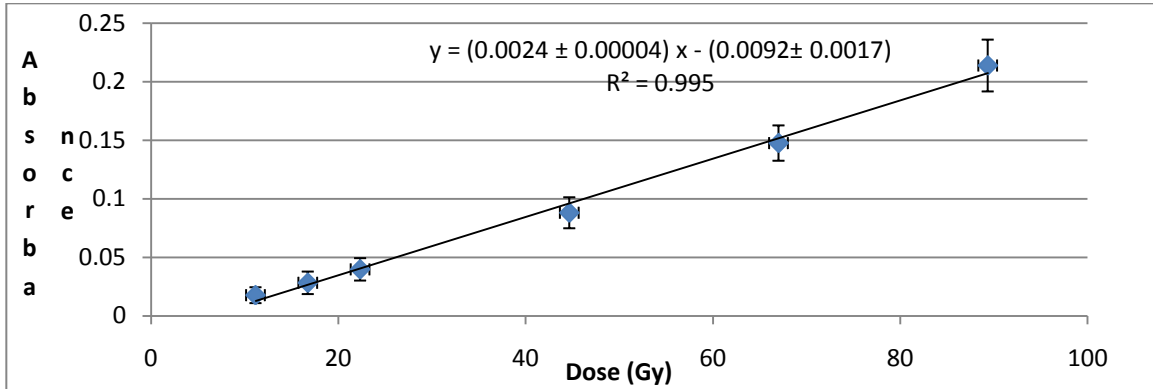


Figure 3.13 Absorbance Vs dose for 14 experiments. LMG 038mM, CHCl₃ 80mM, SDS 50mM, CCl₃COOH 5mM, gelatin 5.55% by weight and water 91.83% by weight, the error bars on the absorbance represent the standard deviation for 14 different experiments, the error bar on the absorbed dose is the error associated with conversion of monitor units to cGy, which is less than 5%.

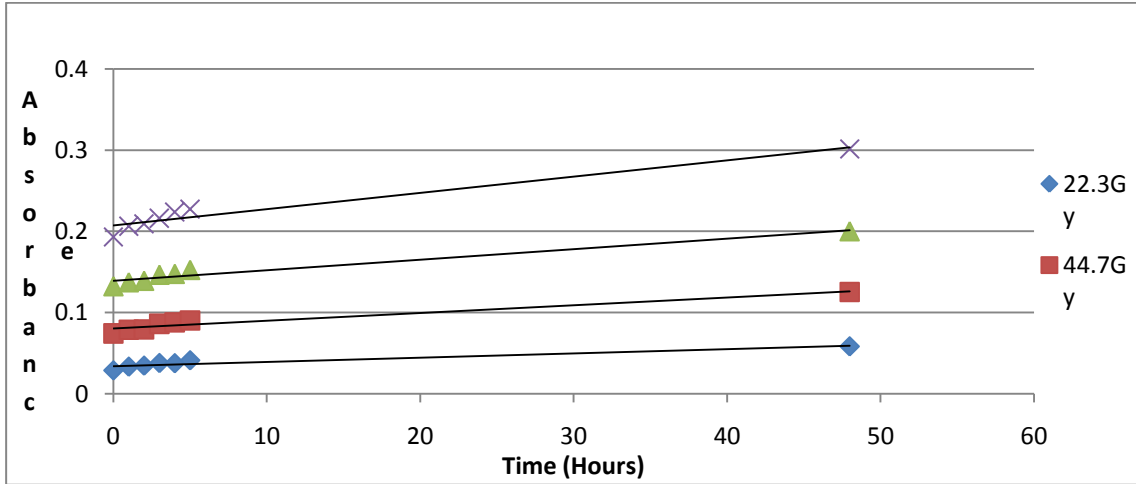
Table 3.4 summarizes the optical density of the combined data for 14 experiments.

	Optical Density per unit dose ($\times 10^{-5} \text{ cGy}^{-1}$)	y-intercept
01	2.33 ± 0.02	-0.006
02	2.42 ± 0.01	-0.016
03	2.33 ± 0.02	-0.012
04	2.33 ± 0.02	-0.014
05	2.69 ± 0.04	-0.003
06	2.51 ± 0.05	-0.011
07	2.69 ± 0.03	-0.011
08	2.51 ± 0.05	-0.010
09	2.51 ± 0.01	-0.011
10	2.60 ± 0.03	-0.006
11	2.33 ± 0.04	-0.019
12	2.24 ± 0.01	-0.020
13	2.24 ± 0.02	-0.019
14	2.42 ± 0.01	-0.023

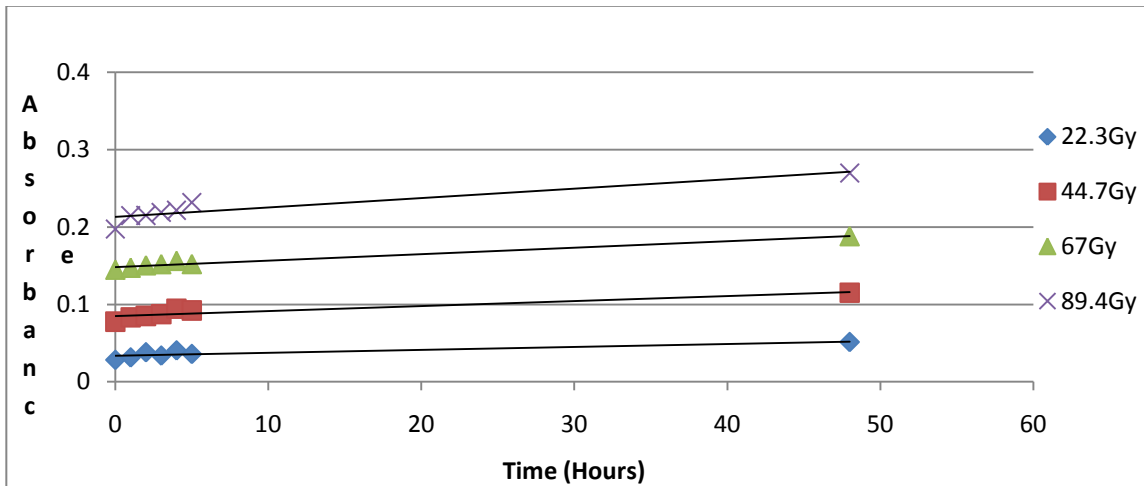
Table 3.4 Summary of optical Density for 14 experiments

As it is shown in figure 3.13 there is less than 2% uncertainty in the slope; however, there is 20% uncertainty on the y-intercept, similar to what was observed for PVA dosimeters.

The stability of the gelatin based radiochromic dosimeters over time was also investigated. Figure 3.14 shows the change in absorbance at different times post irradiation. The experiment was repeated two times to obtain a more accurate data.



(a)



(b)

Figure 3.14 Change in the optical density over time at different dose levels. The experiment was repeated two times and each graph represents different experiment. (a) experiment #1, (b) experiment #2

Table 3.5 summarizes the optical density data for the gel dosimeters over time.

	A		B	
	Optical Density per unit dose ($\times 10^{-5} \text{ cGy}^{-1}$)	y-intercept	Optical Density per unit dose ($\times 10^{-5} \text{ cGy}^{-1}$)	y-intercept
T = 0	2.33	-0.019	2.42	-0.020
T = 1 hour	2.42	-0.019	2.60	-0.021
T = 2 hours	2.51	-0.019	2.60	-0.019
T = 3 hours	2.51	-0.019	2.60	-0.019
T = 4 hours	2.60	-0.019	2.60	-0.017
T = 5 hours	2.69	-0.018	2.69	-0.017
T = 48 hours	3.40	-0.017	3.22	-0.022

Table 3.5 Summary of stability data over time

As shown in Table 3.5, the change in optical density is more stable 1 to 3 hours after irradiation ; 4 hours after irradiation the optical density increased slightly, and continued increasing. All of the measurements in this thesis were performed 1 - 2 hours post irradiation.

3.3 Discussion

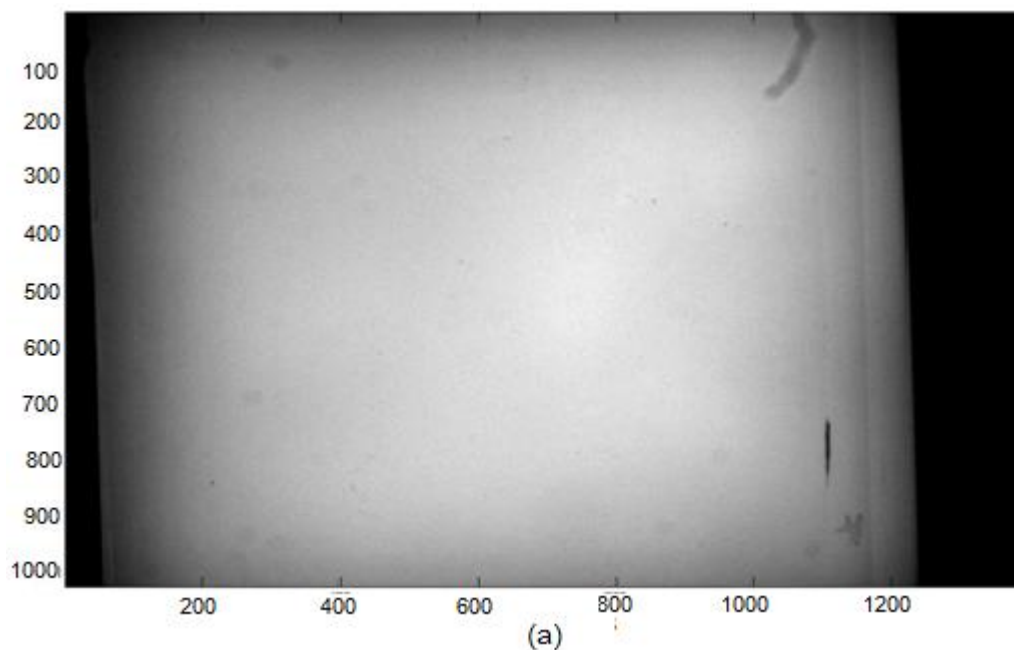
The sensitivity of the in-house radiochromic gel dosimeters was consistent over a wide range of radiation doses, as there was less than 2% uncertainty in the slope of the absorbance *versus* dose curves. The uncertainty was greater for the y-intercept of the curves, reaching 20% for the gelatin-based dosimeters. This suggests there was a large systematic error in the initial condition of the dosimeters. This uncertainty, which is the deviation of absorbance at no dose, may be due to different factors such as sensitivity of LMG to light and heat. Even though the samples were prepared under the same conditions, there may have been some differences in their production, such as how long they were kept in the refrigerator, the time between taking them out of cooling and

irradiation, the time to set up the samples for irradiation, and the light during treatment. Furthermore, the most significant issue during fabrication of the gels was controlling the temperature of the hot plate. Since the gels must go through different temperatures while being fabricated, this may be a source of uncertainty since LMG is sensitive to heat. The temperature likely changed at a different rate every time the gels were fabricated. These are all factors that may have affected the samples and caused the large systematic error.

In conclusion, the main source of uncertainty is introduced during the production of the gel dosimeters; this may be due to some combination of heat and light exposure. Even though these are difficult variables to control, especially the light exposure, future improvements in equipment and procedures may serve to reduce these sources of error.

4. 2D optical Measurements

In phase two of this research the gelatin based dosimeter was formed into thin two-dimensional films for 2D analysis. The 15X15 cm² films were 5mm thick to mimic human skin. The metal plates were refrigerated overnight and taken out one hour prior to irradiation. The fully transparent gels were without bubbles, and were imaged pre- and post- irradiation using the CCD camera apparatus. Figure 4.1 shows a typical optical intensity transmitted through the 2D gels. The top left corner of the gel was irradiated. The irradiated region absorbs light at 629 nm, and as a result, the red light is attenuated in a well defined region. This region of attenuation is prominent in the top left corner of Figure 4.1(b). The absorbance was calculated using the Beer-Lambert equation pixel by pixel.



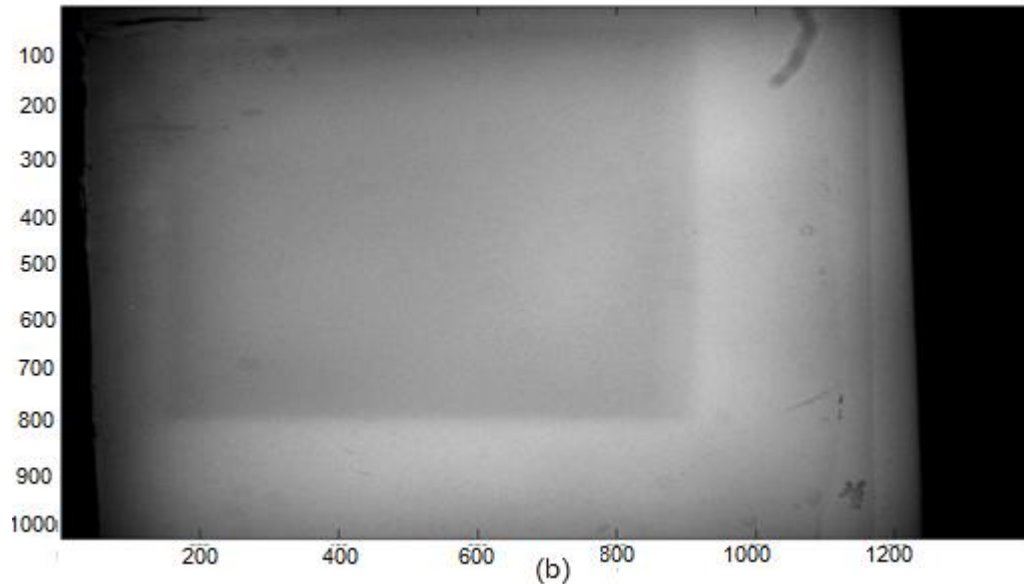
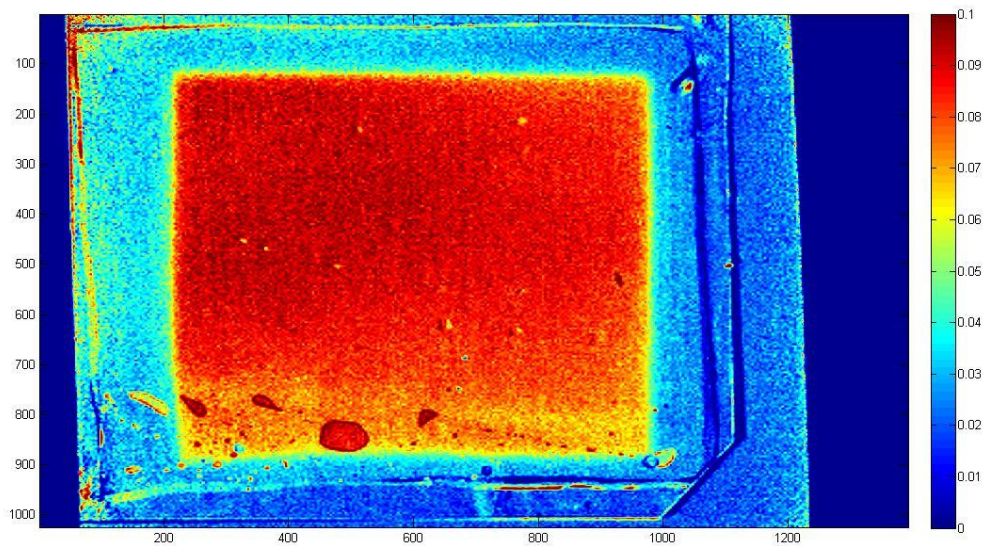


Figure 4.1 The Intensity of transmitted light (a) Pre-irradiation, and (b) Post-Irradiation at each pixel. The x- and y-axis are pixels.

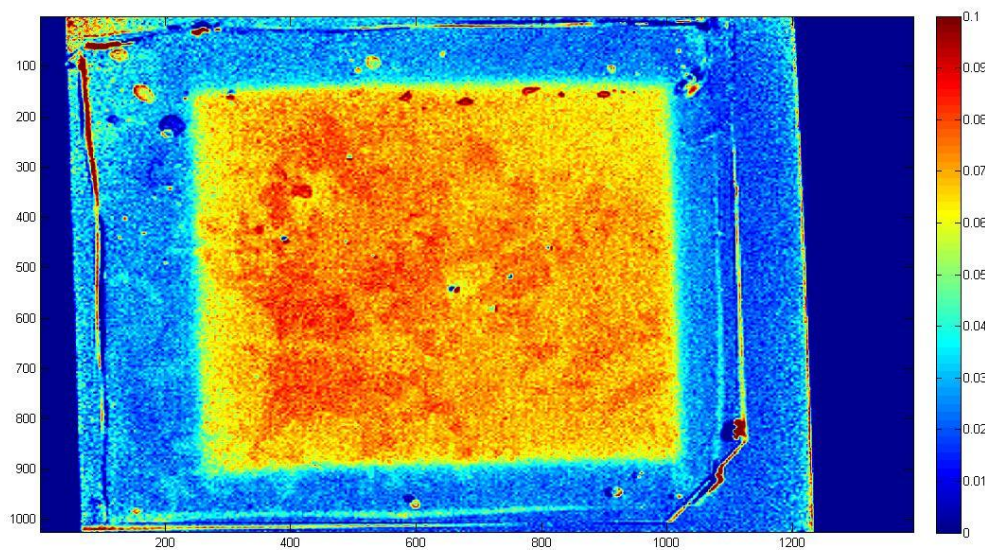
Studies on the 2D gels were performed in two stages. First, the gels were being exposed to known, uniform doses and their optical densities obtained. Second, the gels were exposed to complicated radiation fields. These IMRT fields exposed the gels to non-uniform dose levels and large gradients. These measured dose distributions were then compared to doses calculated using the Pinnacle 8.0m treatment planning system.

4.1 Dose Response Measurements

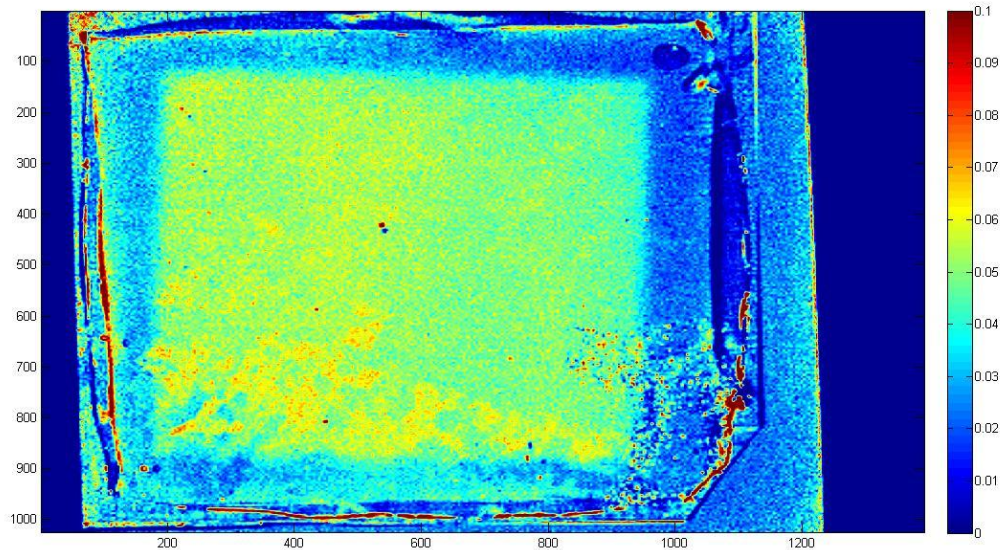
2D radiochromic gels were exposed to a uniform dose ranging from 20-80 Gy under reference conditions: the field size was set to be 10 X 10 cm², and 5cm polystyrene build-up was placed on top of the gels. Under these conditions, 100 monitor units is approximately equivalent to 100cGy when the source to surface distance is set to 95cm. Figure 4.2 shows examples of gels exposed to different dose levels.



(a) 80 Gy



(b) 60 Gy



(c) 40 Gy

Figure 4.2 2D maps of absorbance measured at each pixel(1024x1392) for (a)80Gy, (b)60Gy, and (c)40Gy.

As shown in Figure 4.2, the dose distribution is relatively uniform for the three different dose levels. However, some distortion can be seen. The circle at the bottom of image (a), for example, was caused by an air gap between the gel and the red light surface. The effect of this distortion may be reduced by choosing an appropriate region of interest. For the purpose of this analysis, the uniform regions were used to estimate the mean absorbance. Figure 4.3 shows the mean absorbance at each dose level; Table 4.1 also summarizes the standard deviation of absorbance seen in each image.

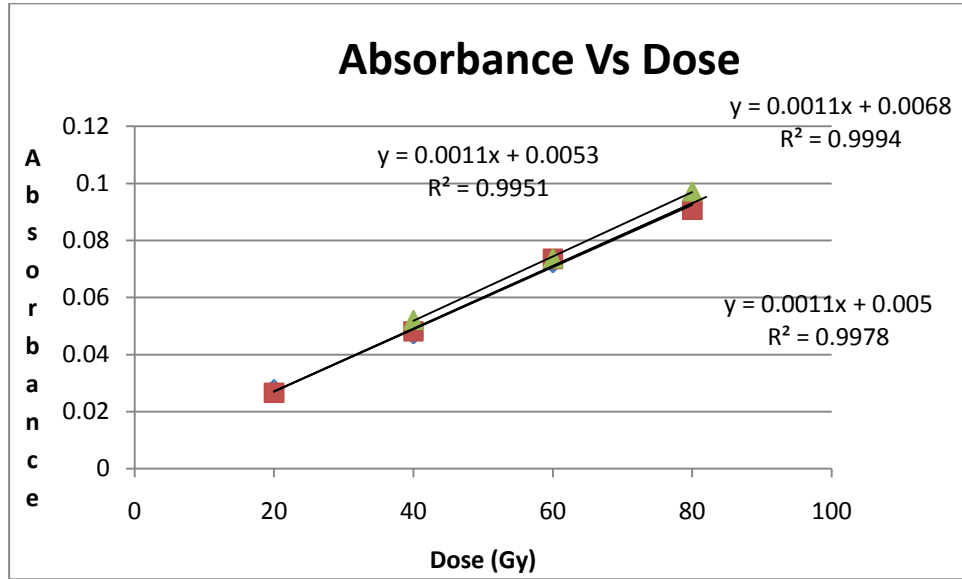


Figure 4.3 Average absorbance vs. dose for the 2D gels. The error bars are smaller than the plotted points and so are not shown

Dose (Gy)	Absorbance		
	Experiment 1	Experiment 2	Experiment 3
20	0.027 ± 0.006	0.026 ± 0.006	
40	0.047 ± 0.006	0.048 ± 0.006	0.052 ± 0.012
60	0.072 ± 0.006	0.073 ± 0.006	0.073 ± 0.015
80	0.092 ± 0.004	0.091 ± 0.005	0.097 ± 0.016

Table 4.1 Summary of mean absorbance and standard deviation at each dose level for multiple experiments

Combining the data from three different experiments, the dose response of the gel was obtained.

From the above data, the absorbance-dose relation is computed using equation (4.1).

$$Absorbance = (0.0011) \times Dose + (0.005 \pm 0.002) \quad (4.1)$$

4.2 IMRT field analysis

Six different IMRT fields were delivered to the 2D gels as a proof of principal test. The measured profiles were then compared to PCP dose maps. Figure 4.4 shows a sample calculated dose map of one of the IMRT fields.

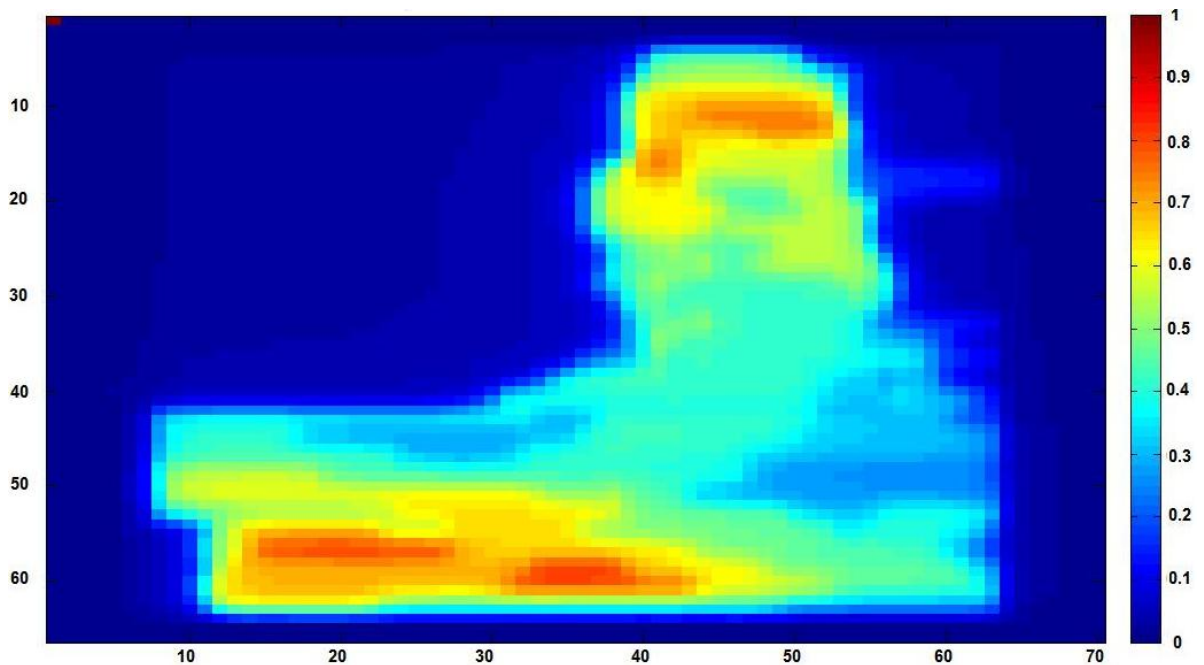


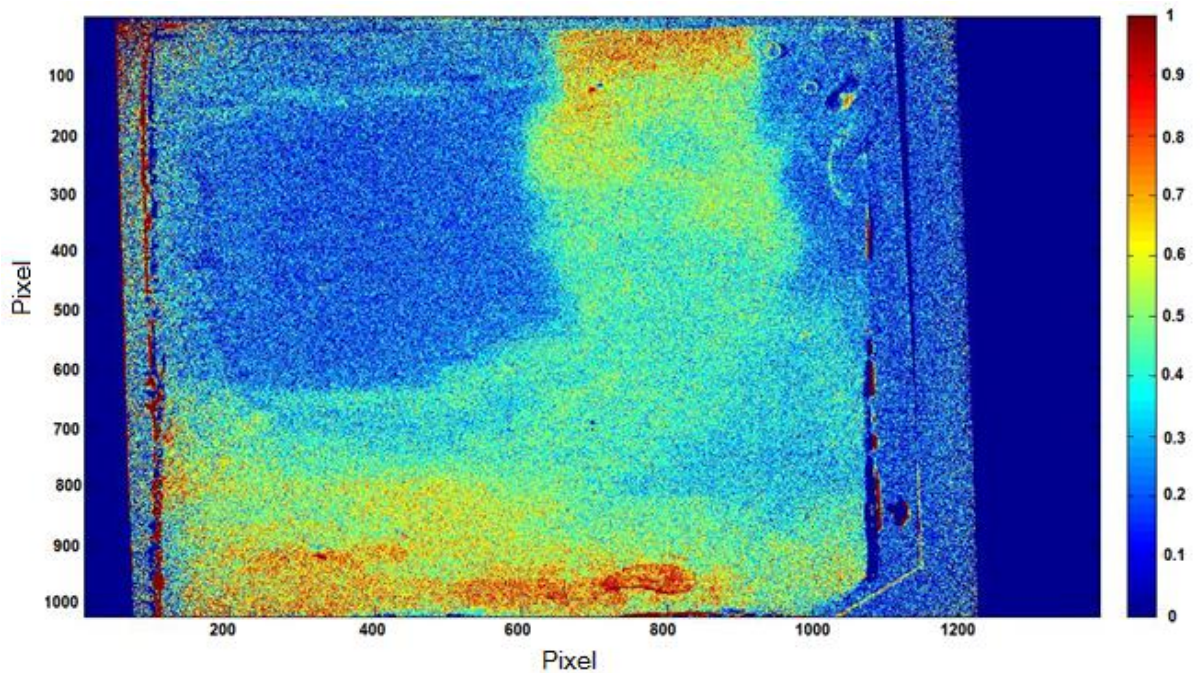
Figure 4.4 Planar dose map of Beam#6. The x- and y-axis represent the field size in mm

As shown in figure 4.4 the dose should be distributed non-uniformly on the gel. After irradiating the gels and calculating the absorbance at each pixel, the measured dose distribution image must be mapped onto the PCP image.

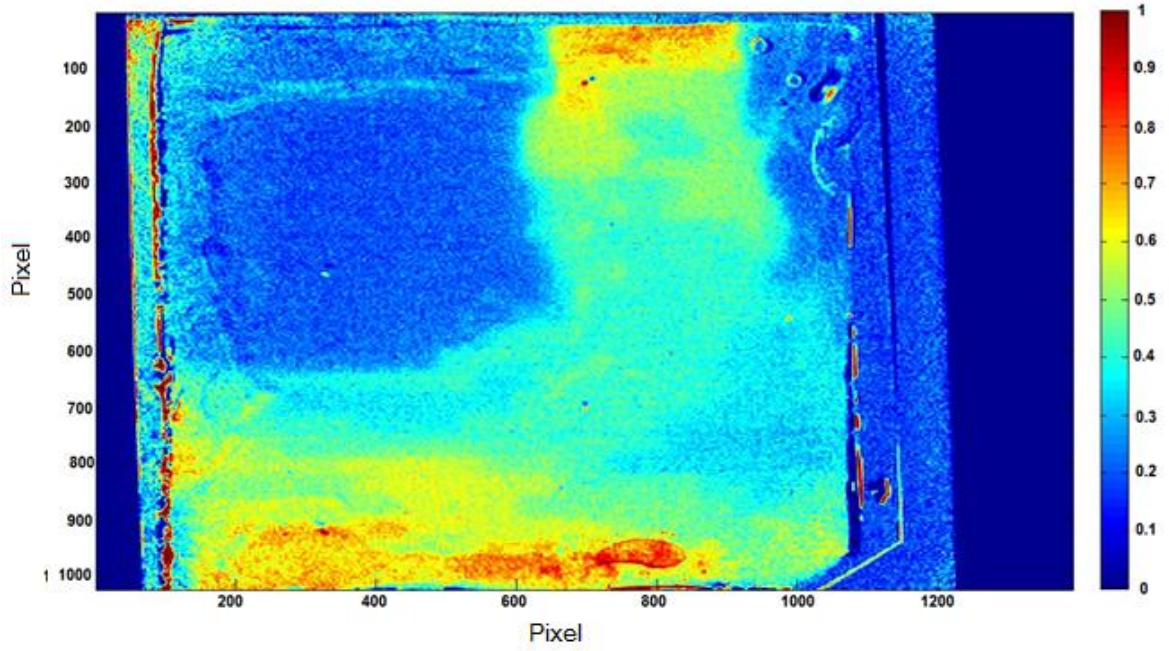
Before comparing the measured image with the PCP image, the measured image must undergo different stages of data processing. First, the obtained absorbance image was processed through a de-noising filter. The absorbance image was then shifted, stretched or compressed, and then rotated to fall exactly on the PCP image. Therefore the de-noised

image went through a complex image registering transfer function to transform the measured image into same coordinate system as the measured image. Subsequently, the resolution of the measured image was lowered to match exactly with the resolution of the PCP image. At this stage, the absorbance image went through bi-linear interpolation to interpolate the value of the measured image at the mapped coordinate.

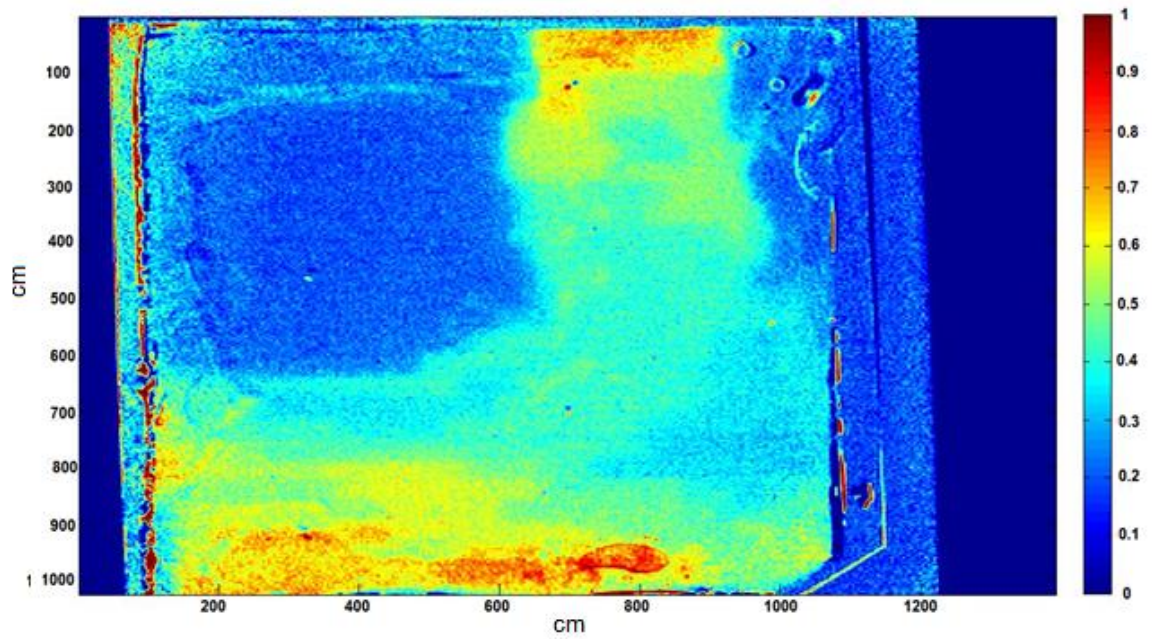
Figure 4.5 shows the steps involved in image registration. From figure 4.3, the absorbance value of 0.093 corresponds to 80Gy. Since 80Gy is the maximum exposed dose level, all the measured images were normalized to the absorbance value of 0.093, and the PCP images were all normalized to 80Gy.



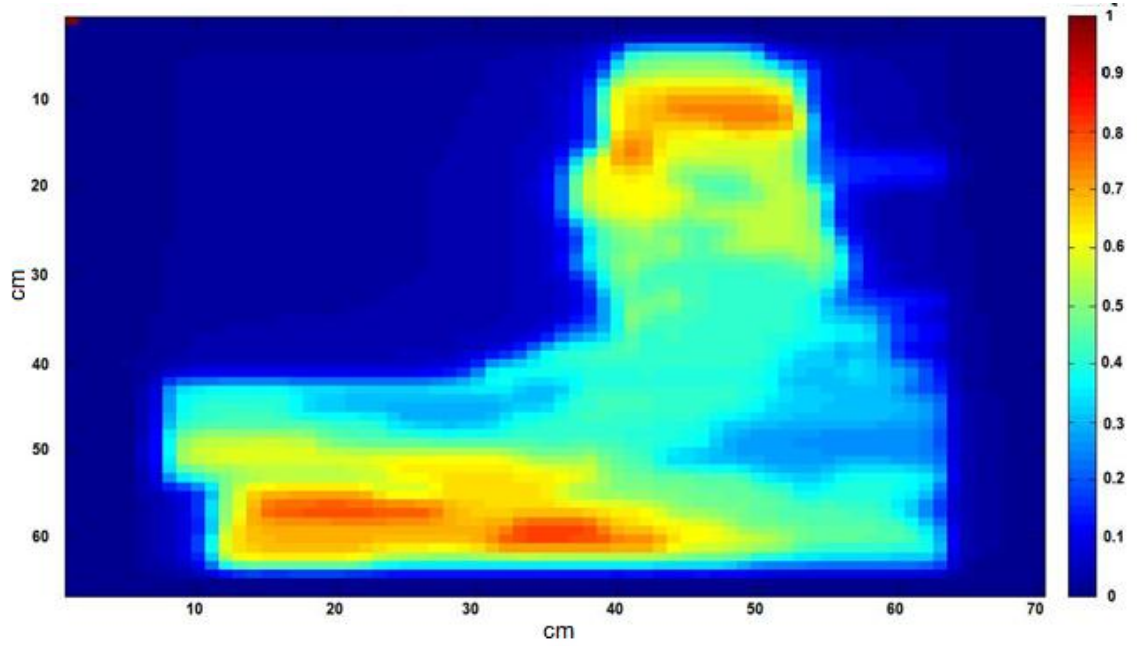
(a) Original



(b) De-Noise



(c) Mapped Image



(d) PCP image

Figure 4.5 Different stages of signal processing: (a) Measured absorbance normalized to 0.093, (b) Passage through the De-Noising filter; (c) The transformation matrix is applied and resolution adjusted; (d) Planar dose map normalized to 80Gy

In order to construct the transformation matrix, 10 points from the de-noised image were matched with the PCP image. Figure 4.6 illustrates how this matching was done.

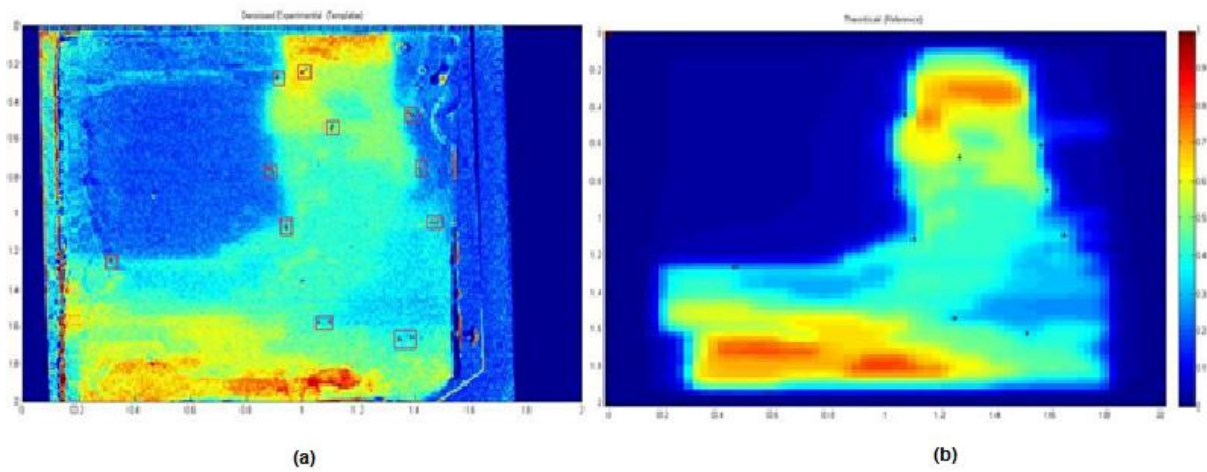


Figure 4.6 The selected points on the measured image (panel a), and the corresponding points on the PCP image (panel b). The points were chosen manually

Even though only three points are required to compute the transformation matrix, ten points were chosen to improve the accuracy of the transformation matrix. Image registration was performed in three stages: constructing of the transformation matrix; transformation of the PCP coordinate system onto the measured image, and interpolation of the pixel values from the measured data onto the transformed grid. Figure 4.7 shows the transformed grid superimposed on the measured image.

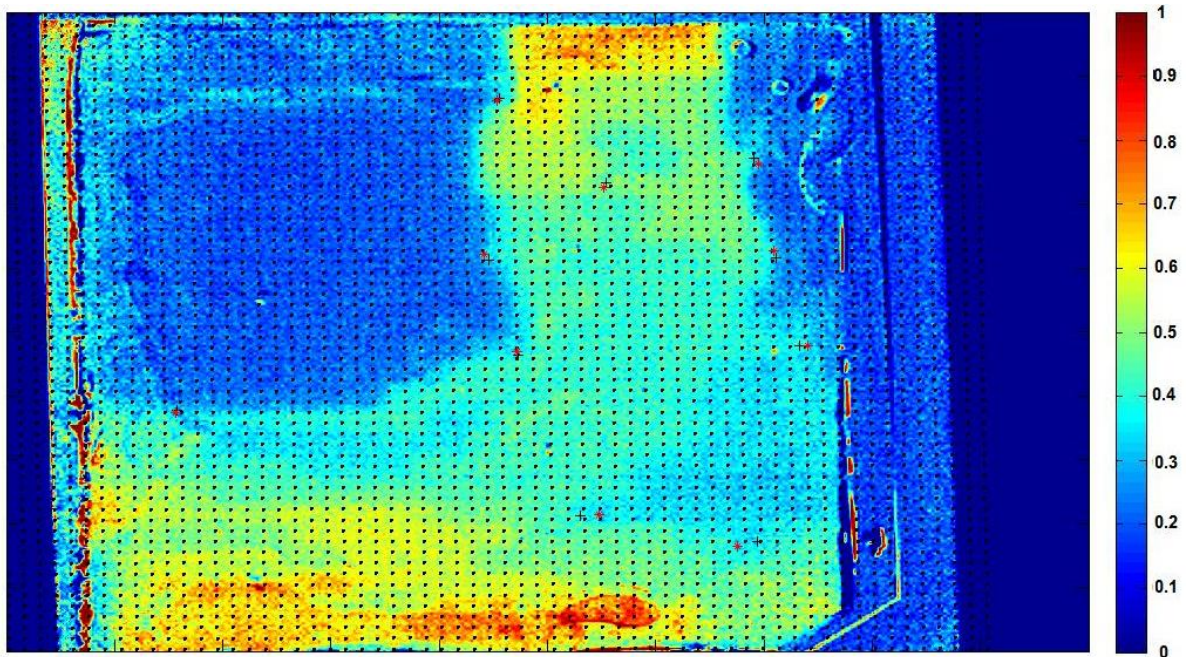


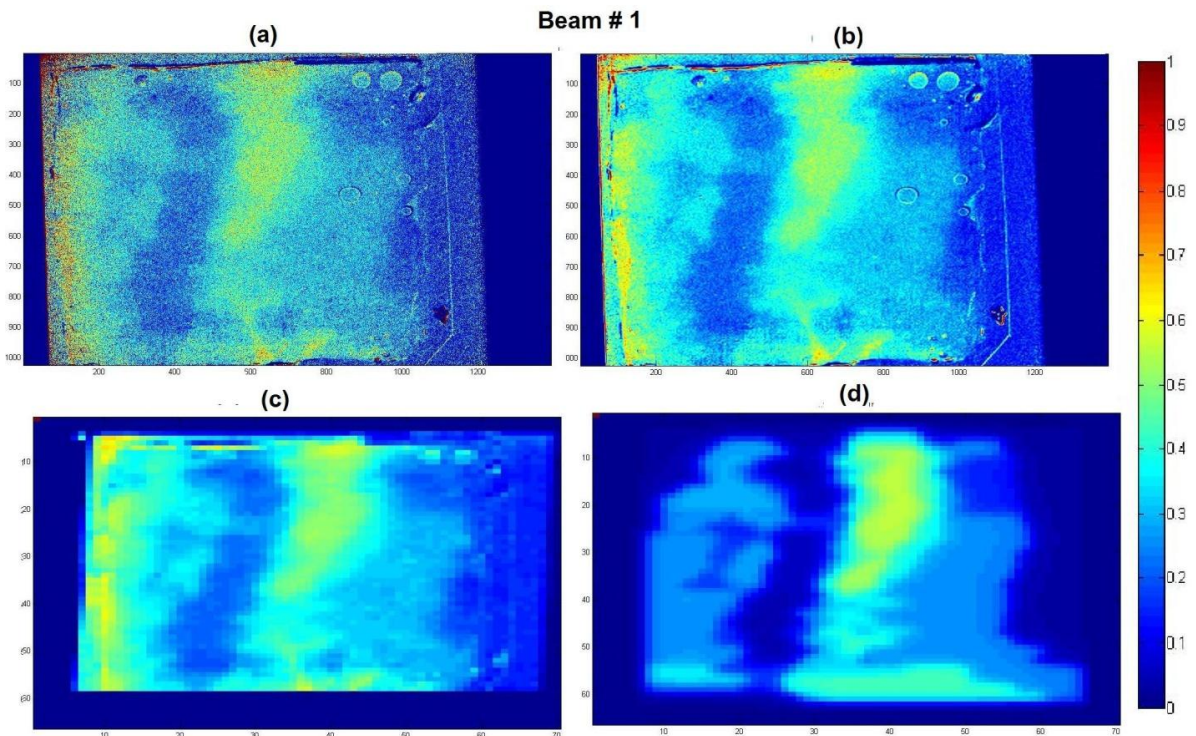
Figure 4.7 The transformed grid on the measured image

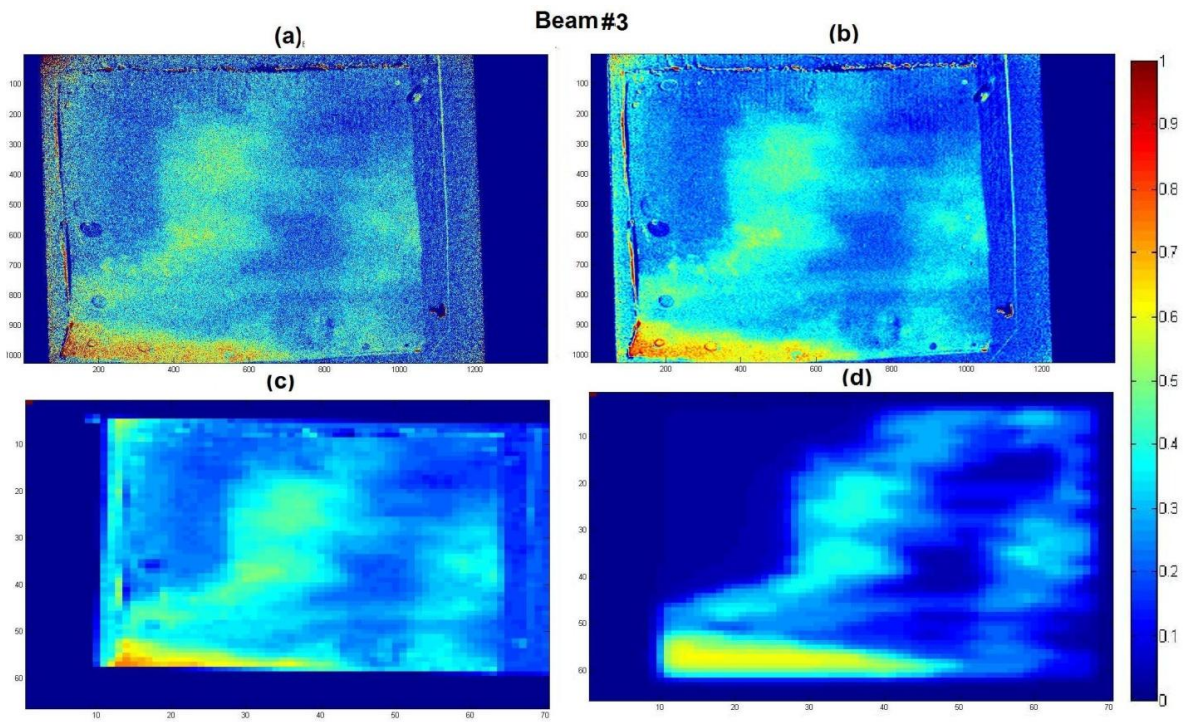
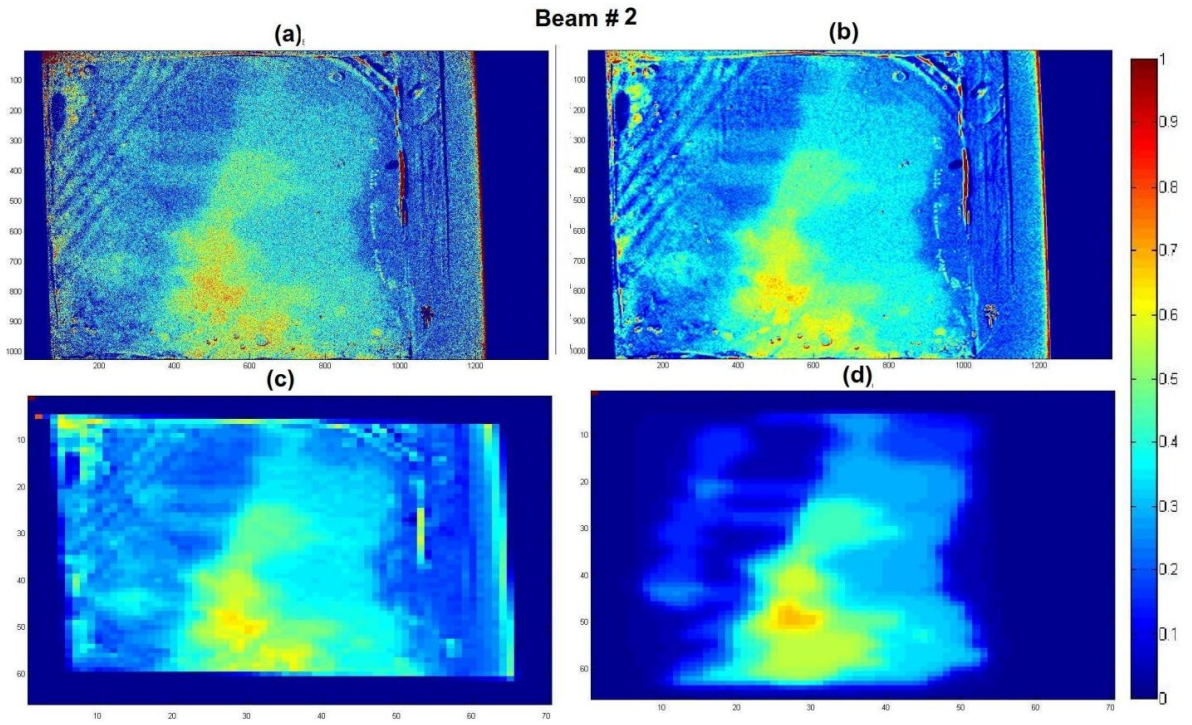
At this point, the colour information of each pixel was interpolated from the measured image.

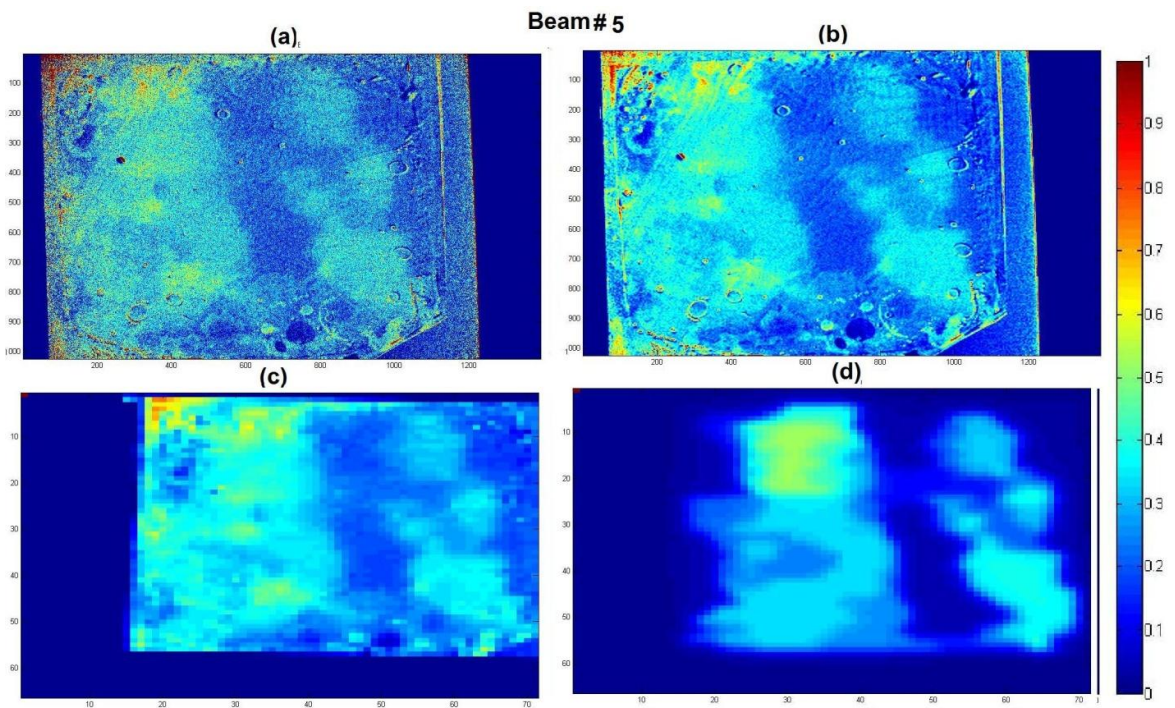
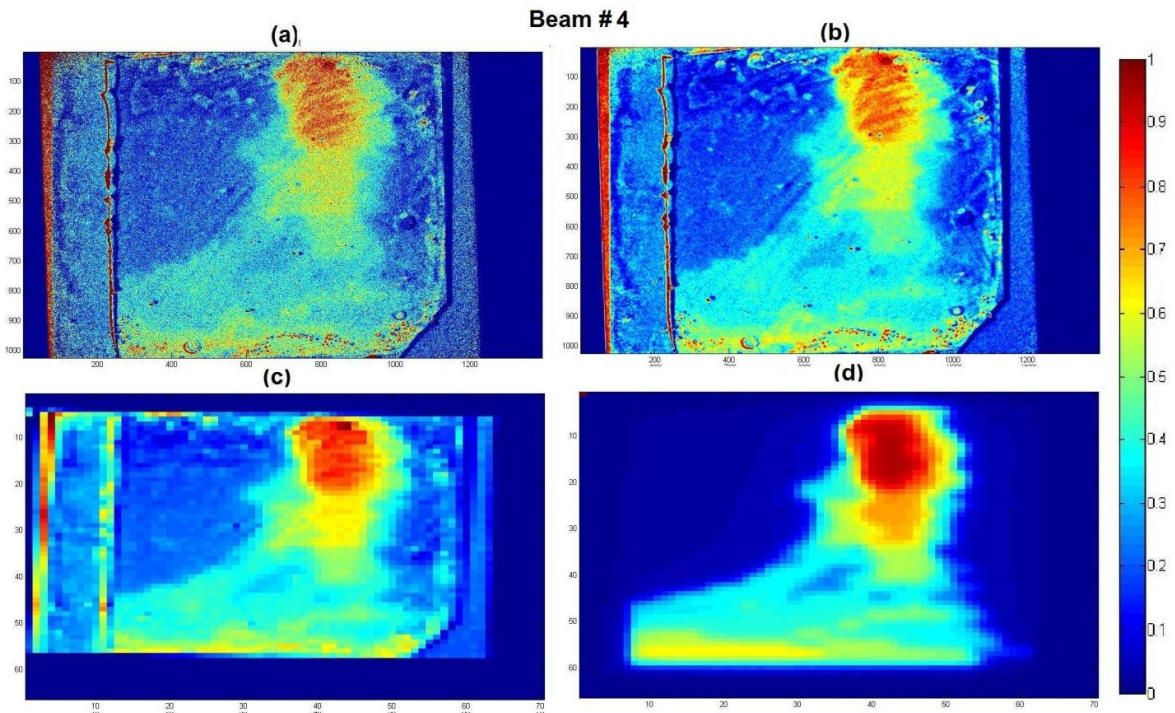
In Figure 4.8, the different stages of data processing are shown for all 6 beams. The images represented by panel (a) are the raw absorbance maps. The panel (b) images have been denoised. Panel(c) images have been mapped. Finally, the panel (d) images are the

planar dose maps. Image (c) was mapped onto image (d) for each beam, and a point by point comparison performed. In both measured and PCP images, the images were normalized to the maximum dose level; all the measured images were normalized to 0.093, and the PCP images are normalized to 80Gy.

The measured image has a much greater resolution than the PCP image. In order to simplify the comparison of the measured and PCP images, the measured image was down-sampled to match the resolution of the PCP image. The disadvantage of down-sampling is that potentially valuable information may be lost.







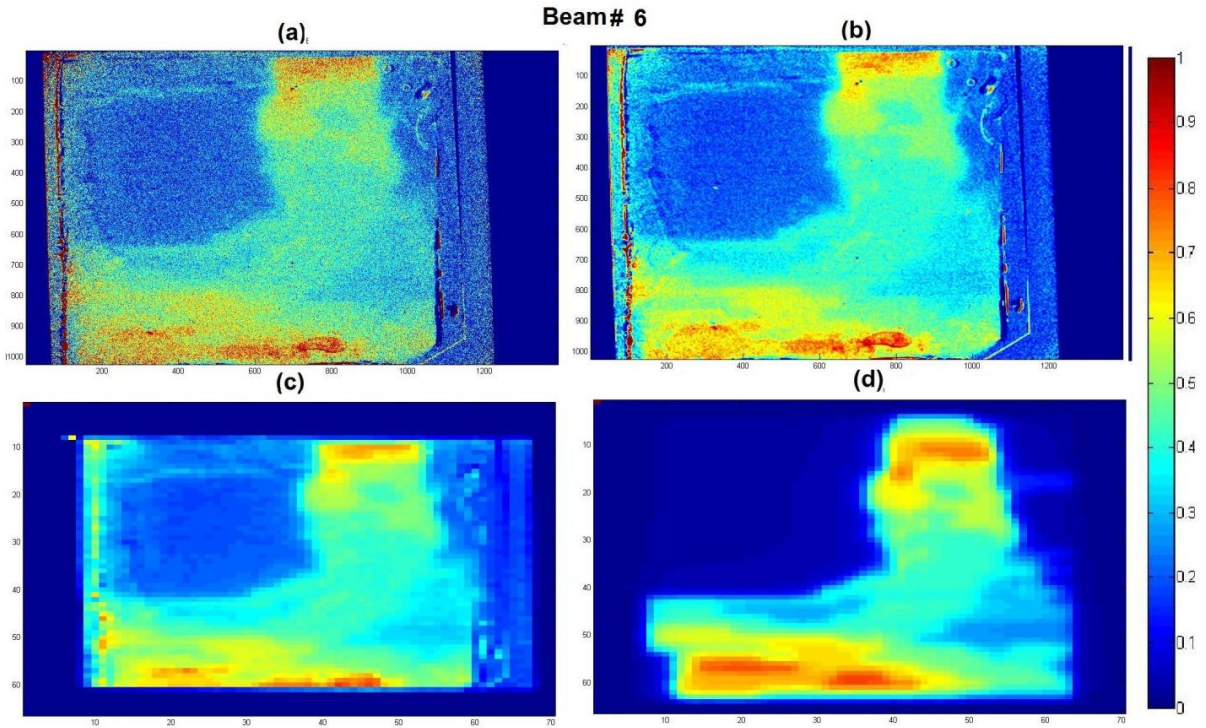
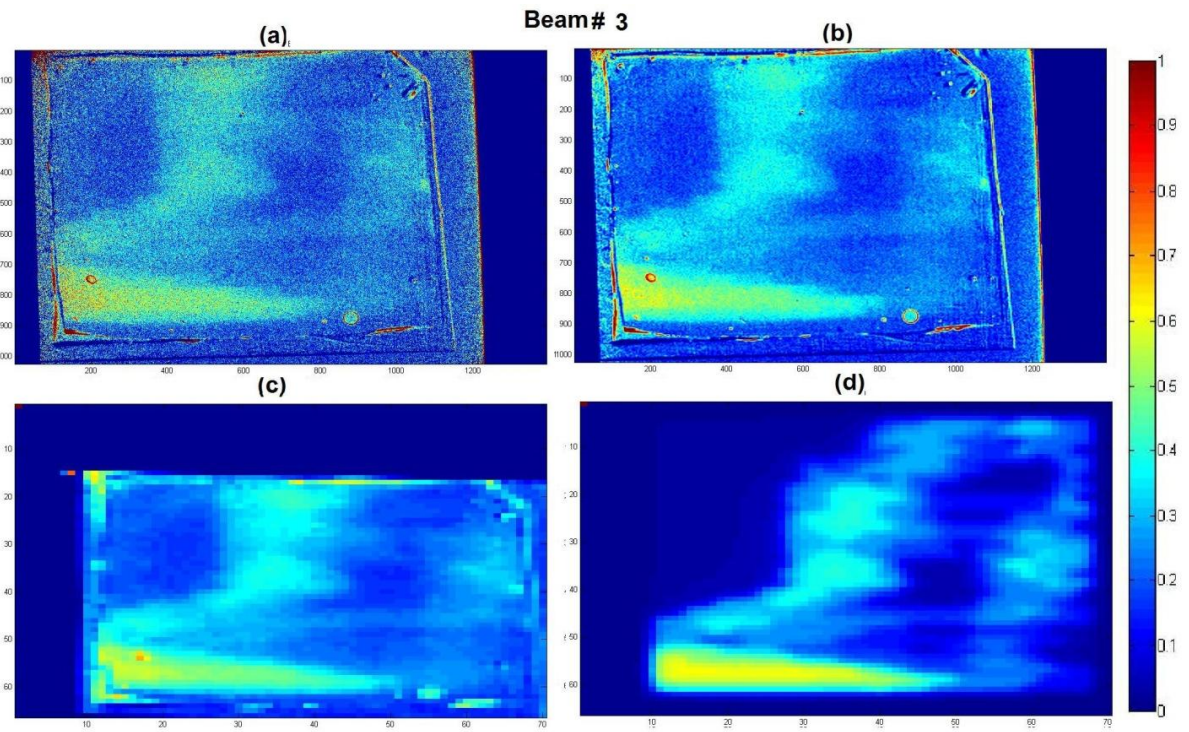
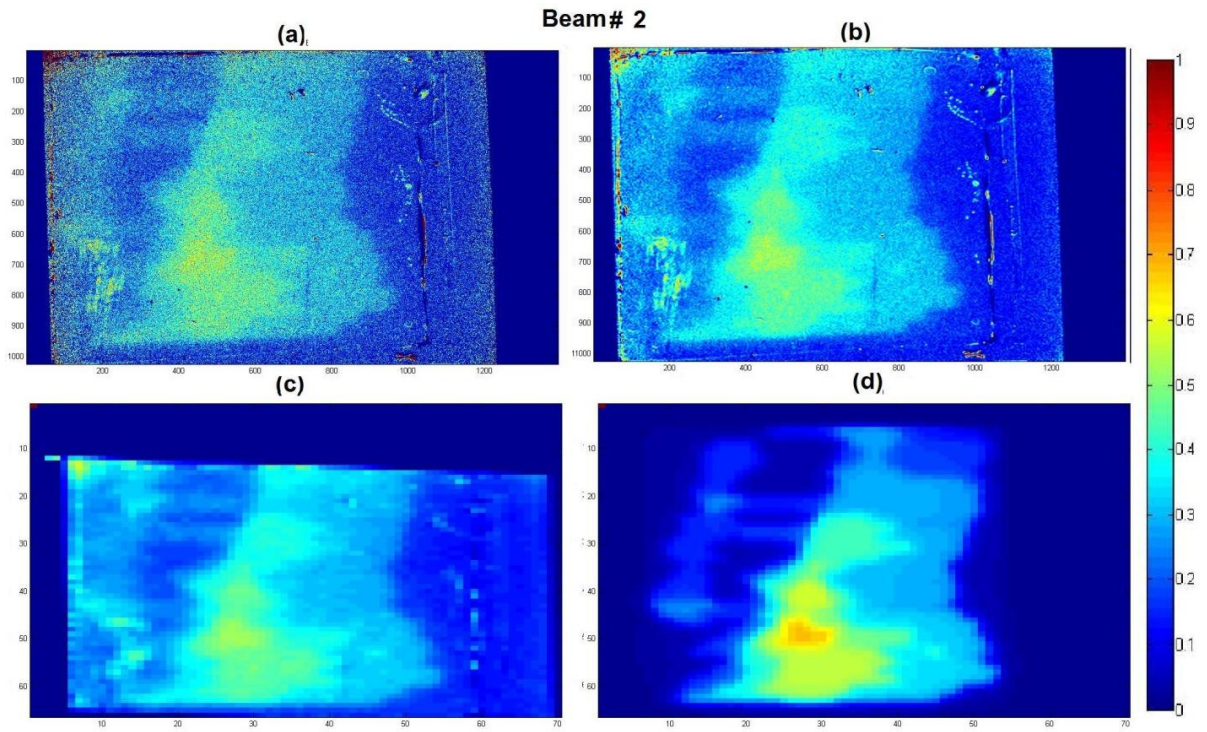


Figure 4.8 Different stages of data processing for six different IMRT fields. **(a)** Raw absorbance map, the absorbance was computed at each pixel. **(b)** The images were De-noised through wavelet transform and noise reduction, **(c)** The measured images were mapped onto the PCP image and down-sampled; **(d)** PCP image. X and y-axis for (a) and (b) are in pixels, for (c) and (d) are in cm

This experiment was repeated again for beams #2, #3, and #4 to check the reproducibility of the results. Figure 4.9 illustrates the repeated exposure.



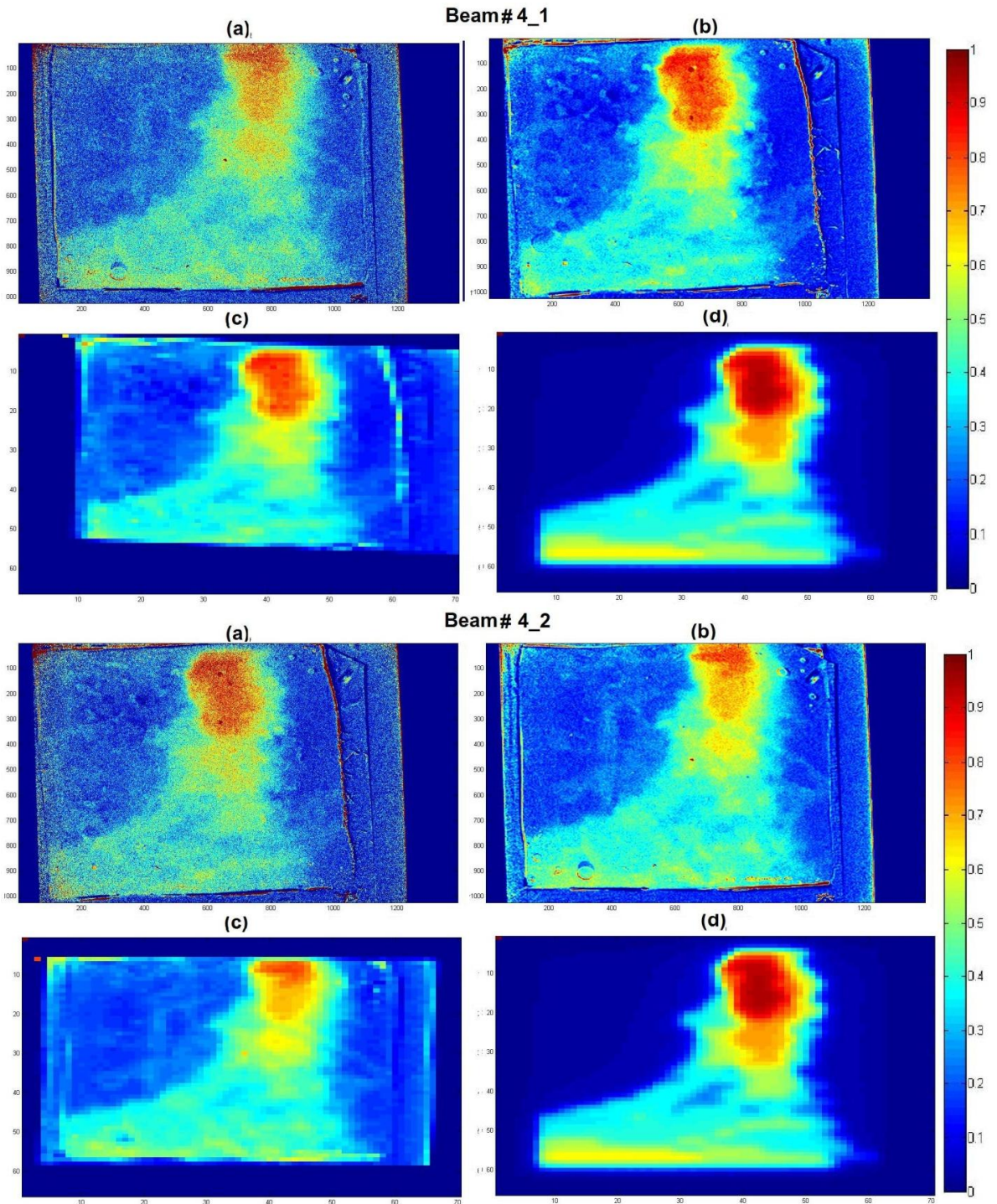


Figure 4.9 Repeated measurements for beam 2,3 and 4. **(a)** Raw absorbance map, the absorbance was computed at each pixel. **(b)** The images were De-noised through wavelet transform and noise reduction, **(c)** The measured images were mapped onto the PCP image and down-sampled; **(d)** PCP image. X and y-axis for (a) and (b) are in pixels, for (c) and (d) are in cm

Since the measured image was mapped onto the PCP image, the images were simply compared at each pixel.

Looking at the measured images, it was observed that at a dose level below a certain threshold, retrieving the correct information was nearly impossible. In order to find the threshold, the signal to noise ratio (SNR) was calculated for several dose ranges (eq. 4.6). Ideally, the pixel value of two images must be identical. For the purpose of this analysis, the error is referred to as the difference in the pixel value of the images. In order to obtain the threshold, we must find where the error surpasses the PCP pixel value. Therefore the ratio of the expected pixel value with the error was calculated.

$$SNR = \frac{Signal}{Error} = \frac{A_T}{|\Delta A|} \quad (4.6)$$

where A_T refers to the Pinnacle Calculated Planar dose, and $|\Delta A|$, which is the error, is the absolute difference in measured to the PCP absorbance.

$$|\Delta A| = |Normalized Value_{Pinnacle\ Calculated\ Planar} - Normalized Absorbance_{measured\ image}| \quad (4.7)$$

SNR was calculated for 10 different dose ranges. In each of the ten dose ranges the mean absorbance was calculated. Equation 4.8 shows how SNR is calculated for dose range 0 – 8 Gy, where the normalized absorbance value is between 0 – 0.1.

$$SNR = \frac{Signal}{Error} = \frac{A_T}{\|\Delta A\|}$$

$$SNR = \frac{\sum_{Normalized\ PCP\ value=0}^{0.1} A_T}{\sum_{Normalized\ Absorbance=0}^{0.1} |\Delta A|} \quad (4.8)$$

Usually, the ratio of signal power to the background noise is called signal to noise ratio. In this experiment this term was used to evaluate the agreement between the expected pixel value and the measured value. Greater “SNR” indicates the pixel difference is small and the images are more identical. As SNR approaches one, the pixel value differences are getting higher, to the extent that the error and the expected value are equal. If the value of SNR is smaller than one, the pixel difference is much greater than the expected value. This may be seen for pixels with relatively low signals. Therefore, when SNR is close or smaller than one, the measured data are unreliable. Table 4.2 represents the data SNR value for different dose levels.

Normalized value	0–0.1	0.1-0.2	0.2-0.3	0.3-0.4	0.4-0.5	0.5-0.6	0.6-0.7	0.7-0.8	0.8-0.9	0.9-1
Dose Level (Gy)	0 - 8	8 - 16	16 - 24	24 - 32	32- 40	40– 48	48-56	56-64	64-72	72 - 80
SNR Experiment # 1										
Beam1	0.257	1.182	2.436	4.334	4.797	12.889	-	-	-	-
Beam2	0.151	1.156	3.456	4.058	7.459	7.053	13.668	-	-	-
Beam3	0.223	1.384	2.741	3.811	1.756	2.116	2.144	-	-	-
Beam4	0.173	1.301	4.845	5.839	5.887	3.724	3.297	5.302	5.254	5.082

Beam5	0.259	1.116	3.581	9.746	8.015	5.822	-	-	-	-
Beam6	0.212	1.166	2.918	4.329	8.189	4.221	4.605	5.871	5.637	-
Beam2	0.181	1.144	4.200	22.14	8.7871	5.7722	4.5744	-	-	-
Beam3	0.270	1.487	2.829	12.176	8.039	6.731	7.041	-	-	-
Beam4_1	0.198	1.187	3.015	4.974	3.964	1.896	2.526	6.029	7.990	6.309
Beam4_2	0.195	1.209	3.713	5.361	7.678	4.460	3.436	4.839	4.237	4.149

Table 4.2 SNR values for different dose ranges

As shown in Table 4.2, the SNR value below 0.1 (8 Gy), the lowest dose range, is always less than 1. At 0.1- 0.2 (8 -16 Gy), the next highest range, the SNR is close to one. In 0.2- 0.3 (16-24Gy), the signal is stronger and the SNR is more than 1. Above 0.25 (20Gy) the SNR is large enough to have confidence in the measured data. Therefore, a threshold of 20Gy was chosen.

Table 4.3 summarizes the overall SNR value above 0.25(20Gy).

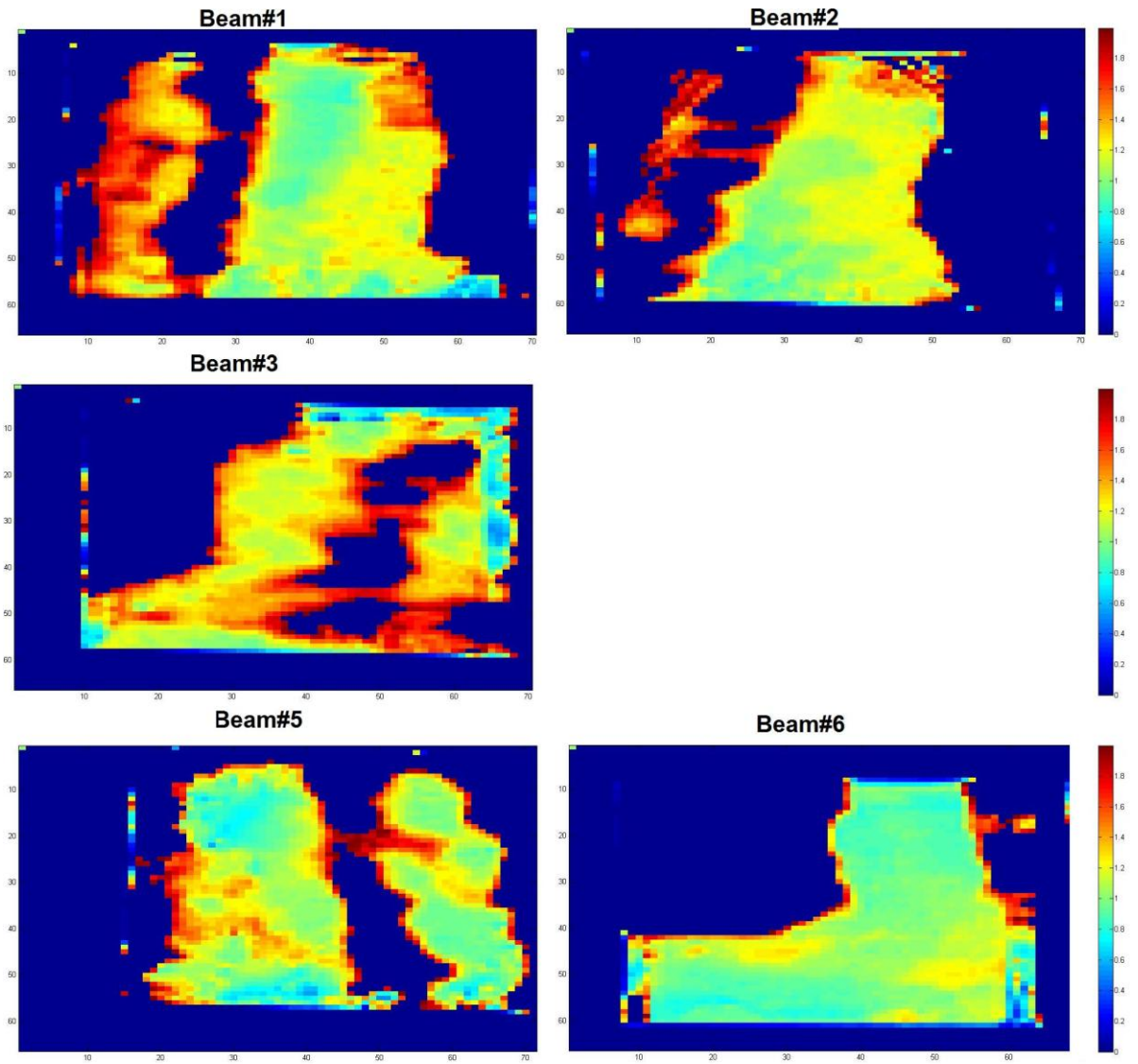
Exp#1	SNR	Exp#2	SNR
Beam1	3.71	Beam2	8.02
Beam2	5.28	Beam3	5.46
Beam3	2.89	Beam4_1	3.53
Beam4	4.79	Beam4_2	4.85
Beam5	7.57		
Beam6	5.12		

Table 4.3 Overall SNR value for measured dose maps

The measured value was also compared directly with the expected value at each pixel using the ratio of the pixel values (eq. 4.9). In another word, the measured value is being normalized to the PCP value.

$$Ratio = \frac{I_{Measured}}{I_{PCP Dose}} \quad (4.9)$$

Figures 4.10 and 4.11 show the ratio of measured image to PCP at each pixel, above the threshold value. As it may be seen the ratio is relatively high on the edges. Around the edges, the dose level is very close to the threshold level. These are also regions of very steep gradients. Any registration or down-sampling errors would be magnified in these areas. As the dose level increases slightly above the threshold, ratio ranges from 0.8 – 1.2. The mean ratios are summarized in Table 4.4.



(a)

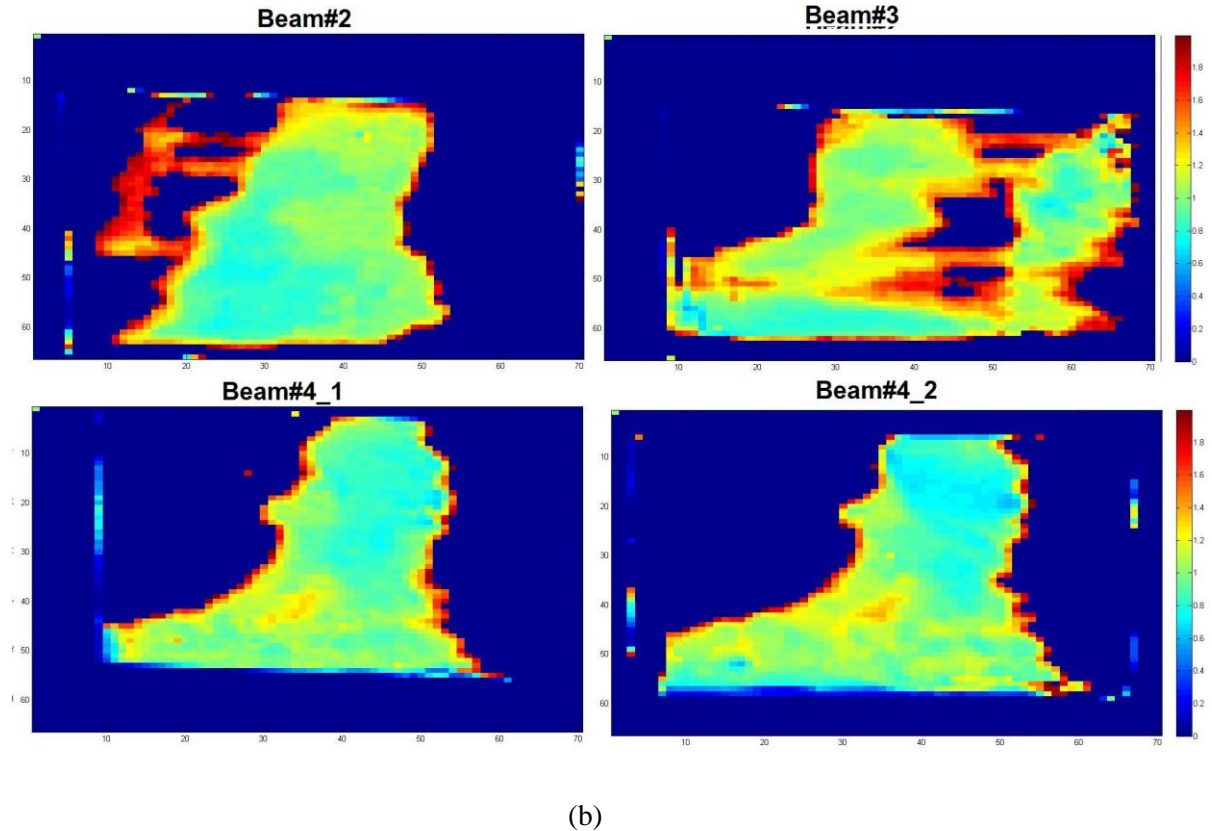


Figure 4.10 (a) The ratio of the measured to the PCP image at each pixel (Experiment 1) (b) The ratio of the measured to PCP images at each pixel for replicate measurements of beams 2,3 and 4. X and y-axis are in cm

Exp#1	Mean	Exp#2	Mean
Beam1	1.24 ± 0.36	Beam2	1.12 ± 0.38
Beam2	1.18 ± 0.39	Beam3	1.17 ± 0.34
Beam3	1.26 ± 0.39	Beam4_1	0.96 ± 0.33
Beam4	0.93 ± 0.32	Beam4_2	0.94 ± 0.34
Beam5	1.13 ± 0.36		
Beam6	0.95 ± 0.34		

Table 4.4 Mean ratio of the measured image to the PCP image. The associated error represents the standard deviation

As it is shown in table 4.4, the mean ratio of the images is close to unity; however there is an uncertainty of approximately 0.35, which is relatively high. The source of this uncertainty is likely from down-sampling the image, and losing some information. Image registration may also cause some error. In order to construct the transformation matrix,

ten random points are chosen by eye; therefore, human error also introduced some uncertainty. In order to reduce this error, a better a data processing method should be developed. Even though the comparison was performed between the normalized planar and measured images, the calibration curve obtained earlier may be used to compare the absolute dose maps.

4.3 Discussion

During this phase of research, 5mm thick transparent films were characterized and evaluated for potential use as quality assurance tool. Some of findings and complications associated with 2D gel dosimetry and discussed below.

The dose response was found to be linear above 20Gy, although variations in response were observed between batches. When the gels were used as quality assurance tools, it was seen that the measured images were qualitatively and quantitatively very similar to the associated PCP images. Even though the sensitivity of the gel was relatively low (i.e. they are responsive to high dose levels), the fabricated gels may be used as a quality assurance tool. The measured image computed from the absorbance of the gel was similar to the PCP designed beams above the threshold dose of 20 Gy. Even though the dose distributions matched well, the sensitivity of the gels must be improved. Better data processing techniques are also required to improve the accuracy of the technique. In order to use the gels as an accurate quality assurance tool, the error associated with fabrication, irradiation, read-out, and data processing must be minimized.

Consistent fabrication has been a challenge throughout this research, especially the control of temperature and light conditions. A slight change in the fabrication process may lead to change in the response of the gels. To produce perfectly transparent gels, the bubbles must be scrapped off the gel before it reaches room temperature. Clear films were also attached to the metal plates to minimize the effect of stretches and imperfections due to the metal plates. Even though all these were taken into consideration, it is unlikely that each batch of gels was identical. Some fabricated gels have slightly different colours due to some variation in different stages of fabrication. One of the major sources of these variations was the rate at which the temperature of the hot plate was changed. Since LMG is very sensitive to temperature, and different chemicals were added to the gel at different temperatures, the rate of change of the hot surface may have affected the colour of the pre-irradiated gels. Furthermore, light is another source that may introduce some uncertainties. Although the gels are kept under dark conditions, they may have been exposed to fluorescent light at different stages during transport. Bubbles are another source of error that must be reduced. Even though their presence was minimized, small bubbles sometimes appeared on the surface of the gels. Also, some bubbles appeared due to air gaps between the gel and the transparency sheet. Therefore, there are some complications involved in fabrication of the gels that may cause errors. In order to have more accurate results, these must be taken into consideration. In this experiment, all the mentioned sources of uncertainties were reduced as much as possible, but there is always room for improvement by utilizing more accurate laboratory equipment and techniques.

There were also some potential sources of error during radiation delivery. One potential complication arises since the gels were sandwiched between up to 5cm of polystyrene during the radiation process. Due to their low mechanical strength, the weight of the slabs may affect their shape, which may lead to complications during the readout. In order to obtain more accurate results, the same slabs were used every time, and also their weights were not directed toward the gels. This was done by placing spacers between the slabs. Dose rate was also kept the same for all rounds of irradiation. Even though all these potential sources of uncertainty were minimized, they were not fully diminished. In order to reduce this uncertainty further, a container should be designed to hold the gels in a dark environment, and also prevent them from losing their shape under stress. Having a polystyrene slab designed for the purpose of supporting the gels may lead to a better result.

The most significant source of uncertainty associated with the read-out was the registration of the pre and post-irradiated gels. Since the absorbance must be calculated at each pixel, the gels must be placed exactly on the same locations of the red light surface. Any variation in the gel's appearances, pre and post irradiation, would also lead to some errors (e.g. bubbles). As it was mentioned earlier, the gels have relatively low mechanical strength; as a result, they may lose their shape easily. Any change in the shape of the gel due to any sources of stress may lead to misregistration of the gels.

The 2D dose distributions of the measured and calculated IMRT gels were similar by the crude metrics used in this study. A more sophisticated technique should be implemented to compare the two images more accurately. Since the measured image has a much

higher resolution than the PCP image, the measured images were down-sampled, and therefore a large amount of data was lost; every 400 points in the measured image were translated to one theoretical point. This was done by averaging the 400 point in a specific pixel. Since there are some regions with relatively high dose gradients, averaging 400 points is certainly not the best method for the purpose of down-sampling.

A more sophisticated method of analysis, such as gamma test could take advantage of the additional measured data. This should be incorporated into future data processing software.

Unfortunately there was almost 35% difference comparing the measured images to the PCP images as demonstrated by the SNR and ratio data. However, considerable improvements may be achievable utilizing a more accurate data processing method.

In conclusion, the in-house 2D radiochromic gel dosimeters have a linear dose response. However, they require relatively high doses. Their production, in principle, is relatively easy. Furthermore, they do not have the oxidation problem associated with other dosimeters. Therefore, gelatin based radiochromic dosimeters doped with LMG may be used as quality assurance tools in any cancer center. There was a relatively large error associated with the gels in these experiments, but the error could be minimized by utilizing more accurate laboratory equipment for fabrication, and also utilizing a more accurate data processing technique. Even though the dosimeters have a linear dose response over a wide range of dose levels, increasing the sensitivity of the dosimeters should be the focus of future research in this field.

5. Summary

5.1 Conclusion

Radiotherapy is one of the major cancer therapy methods in most clinics. Radiotherapy is used to deliver an adequate and uniform dose to the cancerous tumours while minimizing the dose to normal tissues. Development of three dimensional conformal radiation therapy techniques has led to improved tumour control in some disease sites such as prostate, by aiming the dose of radiation to a specific targeted volume. The possibility of missing the target volume increases due to patient set up/motion errors, or any fluctuation in treatment delivery. Therefore, accurate dose verification tools are essential to evaluate the delivered dose distribution of the designed treatment plan under realistic treatment conditions.

Gel dosimeters extend the capability of dose measurement to three dimensional space. Consequently, various studies have been conducted to develop 3D dose verification tools to record the dose distribution in 3D for quality assurance purposes. The main focus of gel dosimetry is to develop gels that may be fabricated in clinics easily and can be analyzed using very simple and conventional readout techniques. The gels should also be tissue-equivalent and have the ability to be shaped into any desired organ or tissue. The objective of this research was to fabricate a transparent, tissue-equivalent, radiochromic gel dosimeter that could be used as a 2D quality assurance tool, and also be analyzed utilizing a simple optical readout technique.

In order to read the gels optically, they must be fully transparent. A colourless dye that is responsive to radiation was dissolved in the transparent gels. Leucomalachite green (LMG) is a radiosensitive agent that changes colour upon irradiation via oxidation by free radicals. The radiated gels have an absorbance band at 629nm when LMG is transformed into its chromatic structure (MG⁺). Therefore, the analysis was simple: the absorbance was calculated from pre- and post-irradiation transmission measurements, something that can be implemented in most hospitals.

Two different agents were tested as the matrix materials. First, poly(vinyl alcohol) was investigated followed by gelatin. PVA was studied as the primary agent due to its adjustable mechanical strength and high transparency. Being able to adjust the mechanical strength would lead to fabricating 3D dosimeters that could be formed into any desired organ or tissue. Even though PVA had all the desired characteristics such as high transparency and adjustable mechanical strength, fabricating a PVA based radiochromic dosimeter was not successful. Consequently, gelatin was used as the matrix material. Contrary to their advantage of being more tissue equivalent and equally transparent, gelatin based dosimeters have low mechanical strength. Nevertheless, fabricating a gelatin-based dosimeter was a success.

In PVA based gels, it was observed that crystallization of PVA at a low temperature prevented LMG oxidization upon irradiation. In order to fabricate a transparent gel, PVA must be dissolved in dimethyl sulfoxide (DMSO), which is a polar solvent. The effect of DMSO was examined and it was observed that, in the absence of DMSO, the PVA gels

were radiosensitive, even after they have been kept at a very low temperature (-80 °C) for the purpose of crystallization. Although three other clarifying agents (acetone, ethylene glycol, and glycerine) were studied to replace DMSO, none of them led to a suitable PVA based dosimeter.

Replacing PVA with gelatin, highly transparent radiosensitive gels were successfully fabricated; however, the gels were only responsive at relatively high doses. Even though there was a non-linear response below 10Gy (for 1D cuvettes with depth of 1cm), and 20Gy (for 2D films with depth of 0.5cm) they have a linear dose response above these thresholds. The dose-repose of the gelatin based dosimeters was obtained by performing 1D optical transmission measurements. Transmitting white light through the gel-containing cuvettes, the optical density over a narrow wavelength band was calculated. After, the gels were formed into 5mm thick films for 2D optical measurement. The relationship between absorbance and absorbed dose for 1D measurement is obtained to be $0.00241 \pm 0.00004 \text{Gy}^{-1}$ for 1 cm cuvettes. The measured response for the 5mm thick 2D gels was $0.0011 \pm 0.00003 \text{Gy}^{-1}$; the absorbance is equivalent to $0.0022 \pm 0.00007 \text{Gy}^{-1}$ for 1cm thick gels. This compared very well with the dose response measured in the cuvettes. In all of the experiments the absorbance-dose relationships were similar in slopes, but there was an offset between different batches. It was observed that this offset was 20% between the different experiments. Investigating both physical and chemical sources of error, it was shown that there was less than 5% error associated with the physical set up. Therefore the major source of error was due to the production and

handling of the mixture, possibly due to the effects of inconsistent heating and UV light exposure.

After characterizing the gelatin based dosimeters, 2D gels with thickness of 0.5cm were fabricated. The 2D gels were used to verify the dose distribution for the purpose of quality assurance. Six different complicated beams were delivered to the gels and their dose distributions were compared to their respective PCP dose maps. After extensive processing of the measured dose maps, the difference was found to be about 35% at worst. Utilizing more sophisticated data processing methods may reduce the magnitude of these errors. Nevertheless, the images were quite similar above 20Gy; the fabricated gel dosimeters show some promise as future tools for quality assurance purposes. Even though the dosimeter used in this study was reliable and consistent, the sensitivity must be improved in order to use this gel routinely.

In conclusion, the in-house 2D radiochromic gel dosimeters hold promise for use as quality assurance tools in the cancer clinics. Even though the gels operate at relatively high doses of radiation, above 20Gy, there is a relatively linear dose response. Furthermore, the dose distributions recorded by the gels are qualitatively and quantitatively similar to the Pinnacle Calculated Planar designed dose maps. Although it was observed that the fabricated gel dosimeters could be used for quality assurance purposes, they must go through many more stages of research to be used clinically.

5.2 Future Research

There is an absolute need for robust and convenient dosimetry tools to record complex 3D dose distributions [22]. There are two major areas of research for such 3D dosimeters [30]: development of optical readout techniques, and development of accurate and precise 3D dosimeters. Recently, transparent radiochromic dosimeters were introduced in the literature. In a study by Chu K *et al.*[41], an MRI-read Fricke dosimeter was suspended in a PVA cryogel matrix. They found that their formulation led to a significantly lower diffusion of Fe^{3+} ions in comparison with any previously published preparation in gelatin or agarose. This suggests that PVA has a promising future in fabricating dosimeters with lower diffusion rates.

Since the PVA leads to a highly transparent gel whose mechanical strength is adjustable, it is also an excellent candidate to be used in fabricating radiochromic gel dosimeters. Future studies must be on finding alternative solvents to replace DMSO, or investigating other radiochromic formulations. Therefore, investigating a solvent that leads to a transparent gel, and also prevents LMG from losing its radiosensitivity after PVA has gone through crystallization, should be a priority for future studies in PVA-based gel dosimeters.

Since the gelatin-based dosimeters were transparent, tissue-equivalent, easy to fabricate, and have a linear dose response over a wide range of dose levels, they are promising candidates for dosimetric quality assurance of complex radiation treatments. However, their sensitivity must be improved. Therefore, increasing the sensitivity of the gels to

operate at lower doses should be a priority for future studies in gelatin-based dosimeters. Also, using these dosimeters to record and verify 3D dose distributions must be investigated.

References

- [1] Schreiner L.J., “Where does gel dosimetry fit in the clinic?”, *Journal of Physics*, 5th International Conference on Radiotherapy Gel Dosimetry(DOSGEL 2008), Conference series 164, 2009.
- [2] Mclaughlin W. L, Miller A, Fidan S, Peltersen K, “Radiochromic Plastic Films for Accurate Measurement of Radiation Absorbed Dose And Dose Distribution” *Radia. Phys. Chem*, Vol. 10, PP. 119-127, 1997.
- [3] Kron T. “What do we expect from gel dosimetry”, DOSGEL, 2nd international conference of gel dosimetry, 2001.
- [4] M. Oldham, H Sakhalkar, Adamovics, A Molineau and G Ibbott, “The feasibility of comprehensive IMRT verification using Novel 3D Dosimetry Techniques Compatible with the PRC Head and Neck Phantom”, *Int. J. Radiat Oncol Biol Phys*, 72 S145, 2008.
- [5] Camphausen KA, Lawrence RC, "Principles of Radiation Therapy" in Pazdur R, Wagman LD, Camphausen KA, Hoskins WJ (Eds) *Cancer Management: A Multidisciplinary Approach*. 11 ed, 2008.
- [6] Day and Stein), “Chemical Effects of Ionizing Radiation in Some Gels”. *Nature*, 166, 146 – 147, 1950.
- [7] Andrew H L. Murphy R E and LeBrun E J, “Gel dosimeter for depth dose measurements”, *Sci. Instrum*, 28 329 – 332, 1957.
- [8] Gore J C, Kang Y S and Schulz R J, “Measurement of radiation dose distributions by nuclear magnetic resonance (NMR) imaging”, *Phys. Med. Bio.* 29, 1189 – 97, 1984.
- [9] Schreiner L.J. “Review of Fricke Gel Dosimeter” *Journal of Physics*, Conf. Ser. 3 9, 2004.
- [10] Baldock C, “Historical overview of the development of gel dosimetry: Another personal perspective”, 2009 *J. Phys.: Conf. Ser.* 164 012002, 2009.
- [11] Baldock C, De Deene Y, Doran S, Ibbot G, Jirasek A, Lepage M, McAuley K. B, Oldham M, Schreiner L. J, “Polymer Gel Dosimetry: Topical Review”, *Phys. Med. Biol.* 55, R1 – R63, 2010.
- [12] Alexander P, Charlesby A and Ross M, “ The degradation of solid polymethymethacrylate by ionizing radiations” , *Proc. R. Soc. A* 223 292, 1954.
- [13] Hoecker F E and Watkins I W, “Radiation polymerization dosimeter”, *Int. J. Appl. Radiat. Iso.* 3 31 – 5, 1958.

- [14] Boni A L, “A polyacrylamide gamma dosimeter”, *Radiat. Res.* 14 374-80, 1961.
- [15] Kennan R P, Maryanski M J, Zhong J and Gore J C, “Hydrodynamic effects and cross relaxation in cross linked polymer gels”, *Proc. Intl. Soc. Mag. Reson. Med (New York)*, 1992.
- [16] Maryanski M J, Gore J C and Schulz R J), “3-D radiation dosimetry by MRI: solvent proton relaxation enhancement by radiation-controlled polymerisation and cross-linking in gels”, *Proc. Intl. Soc. Mag. Reson. Med. (New York)*, 1992.
- [17] Maryanski M J, Schulz R J, Ibbot G S, Gatenby J C , Xie J, Horton D and Gore J C “Magnetic Resonance Imaging of radiation dose distribution using a polymer-gel dosimeter”, *Phys. Med. Biol.* 39 1437-55, 1994.
- [18] De Deene Y, De Wagter C, Van Duyse B, Derycke S, Mersseman B, De Gersem W, Voet T, Achten E and De Neve W, “Validation of MR-based polymer gel dosimetry as a preclinical three-dimensional verification tool in conformal radiotherapy), *Magn. Reson. Med.* 43 116–25, 2000.
- [19] Fong P M, keil D C, Does M D and Gore J C, “Polymer gels for magnetic resonance imaging of radiation dose distributions at normal room atmosphere”, *Phys. Med. Bio*, 46, 3105 – 3113, 2001.
- [20] Maryanski M j, Gore J C, Kennan R P, Schulz R J, “MMR relaxation enhancement in gels polymerized cross-linked by ionization radiation: a new approach to 3d dosimetry by MRI”, *Magn. Reson, Imageing* 11 253-8, 1993.
- [21] Gore J C, Ranade M, Maryanski M J and Scultz R J, “Radiation dose distributions in three dimensions from tomographic optical density scanning of polymer gels: I. Development of an optical scanner”, *Phys. Med. Biol.* 41, 2695 – 2704, 1996.
- [22] Guo P.Y, Adamovics J.A, Oldham M, “Characterization of a new radiochromic three-dimensional dosimeter”, *Med. Phys.* 33, P1338 – 1345, May 2006.
- [23] Bero M A, Gilboy W B, Glover P M, “An optical method for three-dimensional dosimetry”, *J. Radiol. Prot.* 20, 287–294, 2000.
- [24] Armstrong W A, Grant G A, “Radiation Chemistry of Solutions: I. Use of Leuco Triarylmethane Compounds for Chemical Dosimetry”, *Radiation Research: Vol. 8, No. 5*, pp. 375-387, May 1958.
- [25] Gupta B L and Narayan G R, “G(Fe³⁺) values in the FBX dosemeter”, *Phys. Med. Biol.*, Vol. 30, No. 4, 337-340, 1985.

- [26] Adamovics J and Maryanski M, “New 3D radiochromic solid polymer dosimeter from leuco dyes and a transparent polymeric matrix”, *Med. Phys.* 30 1349, 2003.
- [27] Adamovics J, “Three-dimensional dosimeter for penetrating radiation and method of use”, US Patent 7098463, 2006.
- [28] Senjabi Z, Zahmatkesh M.H, Kamali Asl A.R. , Bagheri S, “Sensitivity optimization of PRESAGE polyurethane based dosimeter”, *Radi. Measur.* 45 (1) 89-91, 2008.
- [29] Jordan K, Avvakumove N, “Radiochromic leuco dye micelle hydrogel: I. Initial investigation”. *Phys. Med. Biol.* 54 6773 – 6789, 2009.
- [30] Vandescastele J, Ghysel S, Baete S H, Deene Y De, “ Radio-physica properties of micelle leucodye 3D integrating gel dosimeters”, *Phys. Med. Biol.* 56 (2011) 627 – 651, 2010.
- [31] Hoang H. M, Solomon H. M, Taguchi M, Kojima T, “Polyvinyl butyral films containing Leuco-malachite green as low-dose dosimeters”, *Rad. Phys. Chem.* 77, 457-462, 2008.
- [32] Hyon S, H , Cha W.I , Ikada Y, “Preparation of transparent poly vinyl alcohol hydrogel”, *Polymer Bulletin* 22, 119 – 122, 1989.
- [33] Griffiths P, Stilbs P, Howe A and Cosgrove T, “ A self-diffusion study of the complex formed by sodium dodecyl sulphate and gelatin in aqueous solutions”, *Langmuir* 12 2884-93, 1996.
- [34] Babic S, Battista B, Jordan K, “Radiochromic leuco-dye micelle hydrogel: II. Low diffusion rate leuco crystal violet gel”, *Phys, Med, Biol.* 54, 6791 -6808, 2009.
- [35] Bielska M, Sobczynska A and Prochaska K, “Dye-surfactant interactions in aqueous solutions”, *J. Dye. Pig.* 80, 201–5, 2009.
- [36]Zahmatkesh M, Healy B, Nitschke K, Murry P, Baldock C, “Proceedings of the 1st International Workshop on Radiation Therapy Gel Dosimetry”, Lexington, KY, Queen_s University Printing Service, Kingston, Ontario, , p. 160, 1999.
- [37] Amara G, 1995 “An introduction to Wavelets”, *Computational Science & Engineering*, IEEE, Volume 2, P50- 61, summer 1995.
- [38] Salesnick I, “Wavelet Transform – A quick study”, *Polytechnic University Brooklyn NY, Physics Today Magazine*, 2007.

[39] Modersitzki J, “Numerical Methods for Image Registration”, Oxford University Press, 2004.

[40] Suong-Hyu Hyon; Yoshito Ikada, “Porous and transparent poly(vinyl alcohol) gel and method of manufacturing the same”, United states patents, Patent Number: 4 663 358, 1987.

[41] Chu K. C, Jordan K. J, Battista J. J, Van Dyk J, Rutt B. K, “Polyvinyl alcohol-Fricke hydrogel and cryogel: two new gel dosimetry systems with low Fe^{3+} diffusion”, Phys. Med. Biol. 45, 955- 969, 2000.